Utrecht University

The Influence of the TiO_2 Structure on the Formation of Gold Nanoparticles

Author: S.M.C. (Sanne) de Jong, BSc

January 17, 2018

Daily supervisor: M.J. (Mark) Meijerink, MSc
First supervisor: dr. J. (Jovana) Zečević
Second supervisor: prof. dr. P.E. (Petra) de Jongh

Faculty of Science
Department of Chemistry
Inorganic Chemistry and Catalysis

Abstract

Supported gold nanoparticles have been of interest in the catalytic industry for decades, since Au particles (< 5 nm) supported on metal oxides exhibit a high catalytic activity under mild or even ambient conditions for catalytic reactions such as CO oxidation. Yet, the exact formation of gold nanoparticles on support material remains unclear. In this thesis the influence of titania supports, with distinctive crystal structures, internal pore-structure and porosity including specific surface areas, on the formation of gold nanoparticles is investigated. Titania structures were successfully synthesized by using modified sol-gel procedures based on methods from literature. First, supports with both a pure rutile and anatase crystal structure, as well as an amorphous phase are investigated. Additionally, the commercially available Degussa P25, containing a mix of the anatase and rutile crystal structure is used as a support. Furthermore, in order to investigate the influence of the support porosity and surface area, three titania aerogels containing a range of low, intermediate and high surface area are used. At last, two mesoporous titania supports with an ordered and disordered internal pore-structure are investigated. The gold loading on these titania supports is carried out with ion-adsorption of a cationic gold precursor. The results indicated that the specific crystal structure of the support is an important factor in the formation of gold nanoparticles. Moreover, gold deposited on titania aerogels containing a low, intermediate and high surface area resulted in a few striking differences, including differently shaped gold particles on the low surface area aerogel, and more similar size distributions on the intermediate and high surface area aerogels. At last, the organization of the internal pore-structure did not significantly influence the gold nanoparticles, since a similar gold particle size distribution was observed on both titania structures. Thus, the crystal structure of titania supports influences the formation of gold nanoparticles, while the organization of the internal pore-structure is not of significant influence. Further, titania aerogels containing a low porosity and surface area contain differently shaped gold nanoparticles compared to aerogels with higher porosities and surface areas.

Table of Contents

List of Abbreviations

The following abbreviations are used throughout this thesis.

2θ	Bragg angle (°)
λ	Wavelength (nm)
A_N	Nucleophilic Addition
App.	Appendix
Au/TiO_2	Gold on titania
BET	Brunauer-Emmett-Teller
BJH	Barrett-Joyner-Halenda
CPD	Critical Point Drying
d	Interplanar distance (nm)
EISA	Evaporation-Induced Self Assembly
en	Ethylene diamine
HAADF	High-Angle Annular Dark Field
ICP-AES	Inductively Coupled Plasma Atomic Emmision Spectroscopy
M	Molar concentration (mol/L)
m/z ratio	Mass-to-charge ratio
n.d.	Not determined
NP	Nanoparticle
OMT	Ordered Mesoporous Titania
PEO	Poly ethylene oxide
PPO	Poly propylene oxide
PZC	Point of Zero Charge
rpm	Rounds per minute
RT	Room temperature
SDA	Structure-directing agent
S_N	Nucleophilic Substitution
STEM	Scanning Transmission Electron Microscopy

STP	Standard Temperature and Pressure
T_C, P_C	Critical point Temperature and Pressure
TEM	Transmission Electron Microscopy
TGA-MS	Thermogravimetric Analysis and Mass Spectroscopy
TTIP	Titanium(IV) isopropoxide
wt%	Weight percentage
XRD	X-Ray Diffraction

Chapter 1 Introduction

Catalysis is an important and developing field in the chemical industry and for the economy nowadays. The demands for catalysts on the market account for billions of dollars on a global level. Chemical processes generate a wide range of important compounds which can be used even in daily life or as building blocks in following reactions. Catalysts optimize these processes by lowering the activation energy of the desired reactions. New or improved materials can accelerate developments in the chemical industry, but also in modern technology, medicine, environment and others.

Solid catalysts, for heterogeneous catalysis, are generally more dominant in large-scale industrial applications. The expenses are significantly less than for catalysts used in homogeneous catalytic application due to easier separation of the catalyst from the reactants and products. Heterogeneous catalysts are therefore easier retrieved from reactions. One of the most important classes of heterogeneous catalysts is the supported catalyst. The support material carries the active metallic nanoparticles and provides stability (**Figure 1**).[1] The use of a support improves the activity and efficiency of the catalysts in some cases. There are three advantages of using support material for the manufacturing of catalysts. The support provides an increased mechanical stability by anchoring the metal on the support surface. Also, thermal stability of the catalyst particles is an important advantage, since it prevents sintering of the nanoparticles. It is highly important that sintering is prevented so that the metal particles refrain from growing larger and remain catalytically active.[2] Furthermore, supports contain a large surface to volume ratio, so by distributing catalyst particles over a support the catalytic surface area becomes large as well. Support material usually consists of porous zeolites, carbon, silica or metal oxides. Especially the latter has shown to dramatically change the chemical nature of the deposited nanoparticles.

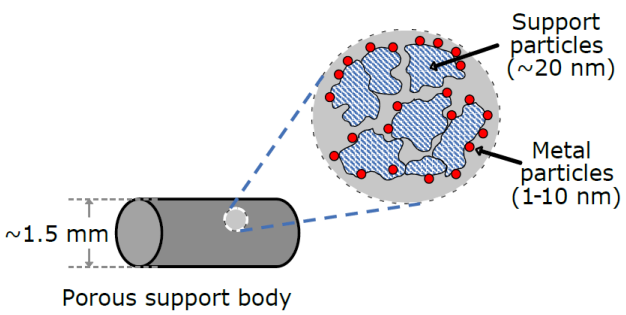

Figure 1: *A representation of supported nanoparticles on a porous support body.*[1]

It was long thought that gold had no significant catalytic properties. However, Haruta et al.[3] and Hutchings et al.[4] proved that gold was in fact a good catalyst. Experimental research was done by Haruta and Hutchings separately on the catalytic activity of supported gold nanoparticles on metal oxide supports. An enhanced catalytic activity towards the CO oxidation reaction was reported by Haruta et al.,[5,6] which were even active at temperatures below 0 °C. Furthermore, Hutchings showed that gold was active in the hydrochlorination of acetylene to vinyl chloride.[7, 8] Gold nanoparticles became more and more of interest since supported gold particles were considered the best catalysts for these reactions, with extraordinary high activities. The highest

activity was obtained when the gold nanoparticles, with sizes lower than 5 nm, were deposited on metal oxides including TiO_2, Fe_2O_3 and Co_3O_4. Moreover, the contact between the gold nanoparticle and the support surface is important for the nucleation and growth of gold. [11, 12]

A metal oxide support that is very promising is titanium dioxide, as it is an affordable, non-toxic and robust material. It is mostly used as a photocatalyst and as a pigment in products such as sunscreen, toothpaste, and paint to add whiteness. Titania is simple to manufacture and its structure can be manipulated. As a result, titania can be prepared with different crystal structures, particle sizes and porosity. When gold is deposited on the TiO_2 support, the ability to catalyze oxidation reactions increases significantly. It was determined by the group of Haruta that gold on titania had a very high selectivity for the epoxidation of propylene to propylene oxide and for the oxidation reaction of CO to CO_2, which are industrially relevant reactions.[9] For this reason, gold nanoparticles supported by titania is a highly promising research topic.

Furthermore, recent work involving the liquid phase TEM analysis on gold nanoparticles obtained more insight on the stability of several metal oxide supports. The liquid cell environment allows imaging of samples in liquid and can also be combined with heating of the sample. The liquid phase TEM is therefore a promising technique for in situ studies of gold nanoparticle formation.[13] However, most observed supports, such as SiO_2, are destabilized by the high-energy electron beam in these environments. Titania, on the other hand, remained stable during liquid phase TEM analysis, making it a perfect candidate for supported gold nanoparticle studies.

Research Objectives

The exact mechanism of gold nanoparticle formation remains poorly understood. Therefore, the aim of this research is to investigate the influence of the support on the synthesis and growth of supported gold nanoparticles. To accomplish this, gold precursors are adsorbed on various TiO_2 supports. The research is divided into two parts: the synthesis of titania supports and the gold loading with ion-adsorption on titania. Therefore, the focus of this thesis is on the following research questions:

1. How does the TiO_2 support influence the formation and growth of gold nanoparticles?
2. Which synthesis strategies should be followed to obtain titania structures with the required properties?

To answer the first question, the spatial and size distribution of the gold nanoparticles on the various titania supports is investigated by conducting the gold loading procedure similarly on each support. The titania supports are exposed to a solution containing 2.0 wt% gold precursor, which is adsorbed on the surface via ion-adsorption. The gold precursor used in this study is the cationic $Au(en)_2Cl_3$, where 'en' represents ethylene diamine, and adsorbs on the titania supports in an alkaline environment.

Support characteristics that are likely able to influence the formation and growth of Au nanoparticles are the crystal structure, the internal pore-structure, and the surface area. To investigate the influence of the crystal structure, supports are synthesized with anatase and rutile phases of colloidal titania, as well as an amorphous support. The gold nanoparticle formation influenced by the internal pore-structure of the support is investigated by synthesizing ordered mesoporous titania and disordered mesoporous titania aerogel. The influence of the

surface area is studied by synthesizing a series of three titania aerogels, ranging from low to high surface areas. The synthesis procedures of these titania materials are adapted from literature and optimized to acquire titania with the desired characteristics. Furthermore, it is essential that the Au/TiO_2 structures are comparable, so the structural characteristics on titania are similar, except for the studied property. Hence, when investigating the effect of the crystal structure, different properties like the crystallite sizes, porosity and surface area should remain similar. Moreover, when the influence of the pore-structure is studied, the crystal structure and surface area should be similar, except for the organization of the pores. Lastly, the crystal structure, crystallite sizes and pore-structure are similar when comparing the gold on series of titania aerogels with modified surface areas.

1.1 Titania Supports

1.1.1 Synthesis of TiO_2 Support

There are numerous approaches to manufacture titanium dioxide as a material. Common routes to obtain TiO_2 are flame synthesis of titanium tetrachloride (the chloride process), inert gas condensation, chemical vapor deposition and the sol-gel procedure. In this study, the sol-gel procedure is of particular interest, as it allows easy tailoring of the TiO_2 structure by merely changing reaction conditions.[14, 15a] Furthermore, unique structures can only be made using this technique and have not been reported by any other method (**Figure 2**).

Nowadays, the sol-gel technique is used in numerous applications, for instance for the production of silica and titania, but also thin films, protective coatings, and nanoscale powders which can be used in biomedical purposes. The technique has also been interesting for early transition metals, which are distinguished from non-metals by greater reactivity.[16] In this section the reaction mechanism of the sol-gel method is discussed. The reaction consists of several steps described in sections I-V.

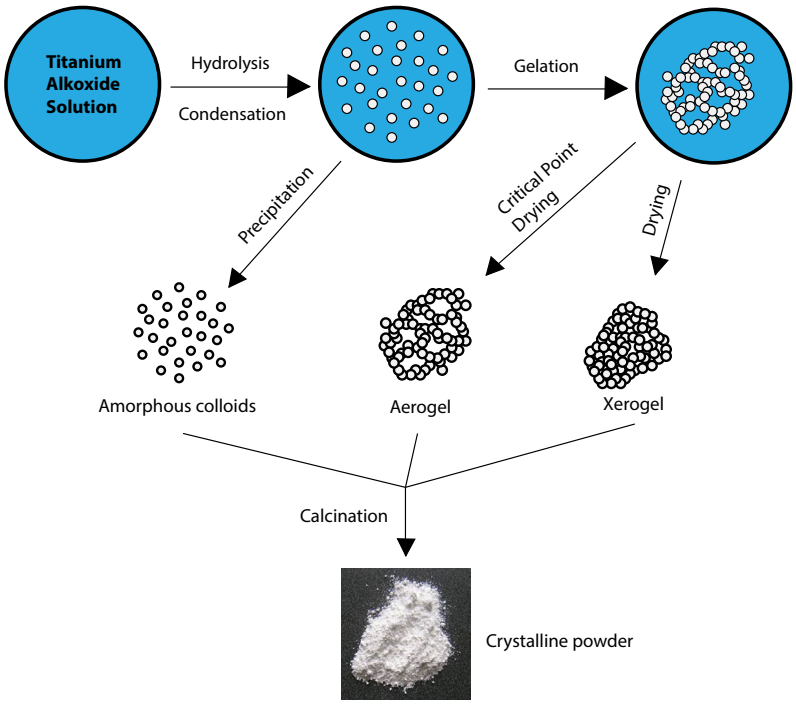

Figure 2: *A schematic representation of the sol-gel procedure.* [Based on 15b]

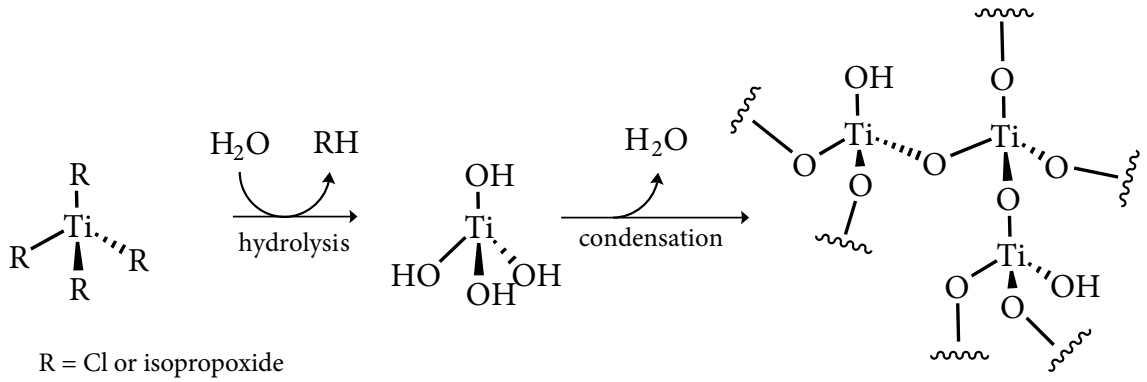

Figure 3: *The reaction equations for hydrolysis and condensation with either titanium(IV) isopropoxide (TTIP) or $TiCl_4$ as titanium precursor. Isopropanol or HCl is formed respectively during the hydrolysis step and water is formed after condensation.*

(I) Hydrolysis and condensation of the precursor. These two reactions occur almost simultaneously. The precursor for titania is often titanium alkoxide or chloride. It is hydrolyzed upon addition of water. Nucleophilic attack of water on the titanium atom releases alcoholic groups. (**Figure 3**)

This reaction is influenced by several factors in the reaction mixture. The titanium alkoxide to water ratio and the velocity of these reactants determine the amount of collisions and the rate of the reaction. This reaction is slowed down due to steric hindrances originating from the organic groups on titanium. So, the reaction rate can also be manipulated by changing the alkyl groups of the precursor. Another manner to influence the reaction is either by acid or base catalysis, which depends on the pH of the reaction mixture. The kind of solvent that is used influences the pH. The solvent is involved in the mixing process and is directly in contact with the reactants. Solvents can donate or accept H^+ ions to form hydronium or hydroxyl ions respectively depending on their nature. For instance, ethanol is a polar protic solvent with labile H^+ ions which can be donated to form more acidic conditions in contrast to aprotic solvents.

In the following condensation step the monomers polymerize to create a 3D network. This is achieved by creating either hydroxy-bridges *(Olation),* or oxo-bridges *(Oxolation)*. In general, olation most commonly occurs via the nucleophilic substitution mechanism (S_N), whereas oxolation takes place by nucleophilic addition (A_N). Both reactions are followed by elimination of H_2O. The formation of hydroxy- or oxo-bridged bonds is thermodynamically more favorable than the initial Ti-OH bonds. Eventually, a solution of colloidal particles, or sol, is formed. The sol can grow further into a gel with cross-linking. [14,16–19]

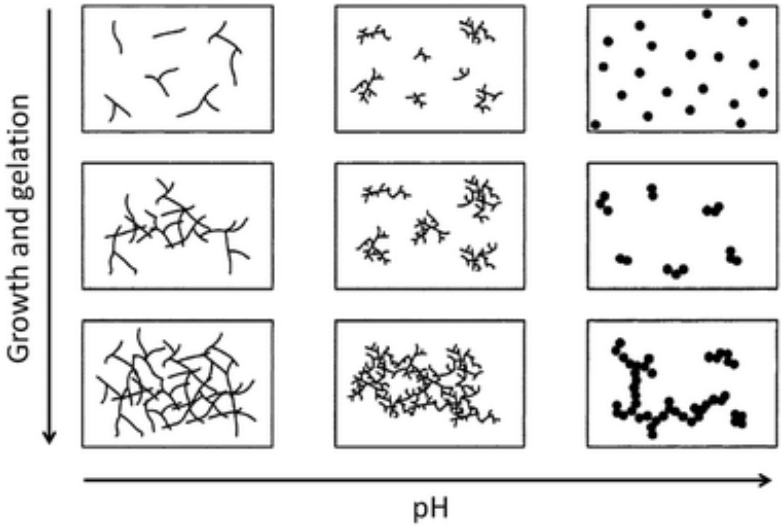

Figure 4: *The diagram shows the influence of pH on the growth of sol-gel structures during the gelation step.[17] When the solution has a low pH more chain-like polymers are formed, whereas branched polymers are formed at high pH.*

(II) Gelation by continued condensation of the sol solution. The inner network continues to grow by polycondensation and can either contain a chain- or branch-like structure. The formation of either chains or branches depends on the pH of the mother liquor. Under acidic conditions the condensation often proceeds on the terminal sites, resulting in the formation of more chain-like structures. The opposite is true for more alkaline conditions, where multiple sites undergo condensation at the same time which allows the formation of branched polymers or even agglomerated colloidal particles (**Figure 4**). The viscosity of the solution increases and eventually an elastic solid is formed.[17]

(III) Aging of the gel (Syneresis). The reactions from the gelation step can continue during the aging of the gel to increase the gel's stiffness and strength which reduces the risk of fracture. This is often accompanied by evaporation of the solvent and contraction of the gel network. The contraction rate of the network can be manipulated by changing the temperature or by changing the mother liquor during the syneresis. The reactions that induce this shrinkage are (**Figure 5**), corresponding with equations (1) and (2).

$$\equiv Ti\text{-}OH + HO\text{-}Ti\equiv \rightarrow \equiv Ti\text{-}O\text{-}Ti\equiv + H_2O \quad \textbf{(1)}$$

$$\equiv Ti\text{-}OR + HO\text{-}Ti\equiv \rightarrow \equiv Ti\text{-}O\text{-}Ti\equiv + ROH \quad \textbf{(2)}$$

Aging can also induce further hydrolysis or re-esterification, which is the reverse reaction. Re-esterification is prevented when an excess of water is used. The strength and stiffness of the network is increased due to coarsening of the structure. Growth of the necks between particles is induced by dissolution and reprecipitation, which is driven by the difference in solubility at curvatures. The gel network is less likely to collapse in the drying step due to capillary forces when it is aged at high solubility conditions (**Figure 6**).[16]

(IV) Drying of the gel forms a dense xerogel. Drying introduces stress that causes shrinkage of the network. This stress is induced by osmotic, disjoining and capillary forces. The capillary force is usually the dominant force, since it is caused by difference of energy when the solid-liquid interface changes to solid-vapor. When the liquid is slowly being evaporated from the gel, the liquid left in the pores produces compressive stress on the structure. As a result, the network collapses and the solvent is squeezed out of the pore-system. This phenomenon is separated in three stages: initial condition, constant rate period and falling rate period. In the initial condition the meniscus of the liquid-vapor interface inside the gel remains flat (App. A).

Critical Point Drying (CPD) is used to manufacture titania aerogels by drying the material with CO_2 at a temperature and pressure around the critical point (T_C and P_C) of CO_2. As seen in the phase diagram (App. D) after the critical point the distinction between gas and liquid disappears. Due to the disappearance of the

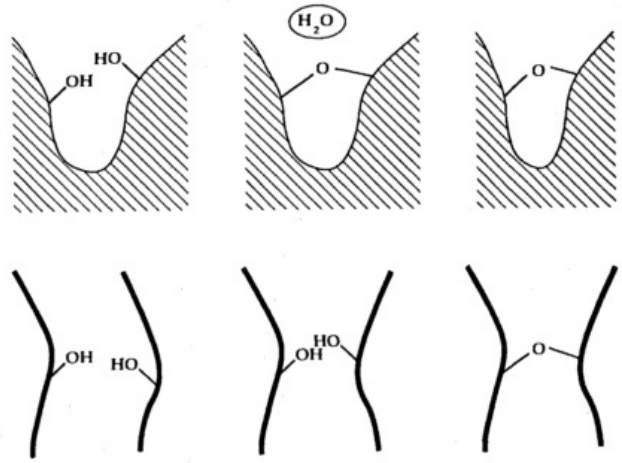

Figure 5: *Illustration of shrinkage caused by condensation.*[16]

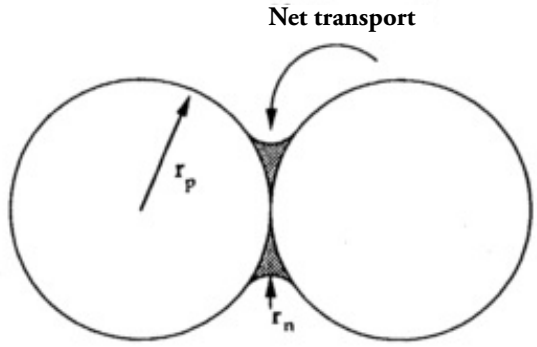

Figure 6: *Coarsening of the structure. The necks between particles grow at high solubility conditions.*[16]

liquid-vapor interface as well as the capillary force, since the surface tension becomes negligible, shrinkage of the network is avoided. As a result, the solvent inside the pores of the aerogel is removed with a minimal collapse of the titania walls.

(V) Calcination of the gel to remove organic compounds inside the pore network and to acquire crystalline material. Organic templates are removed around a temperature of 350 °C. The raise in temperature induces mesophase transition. Crystallization can be initiated at various temperatures, depending on the synthesis procedure of the material. The heating rate during this step is of great importance, since the structure may change or collapse upon a sudden removal of the organic molecules. Moreover, the amount of Ti-OH surface groups may also decrease upon calcination.[17]

1.1.2 The Influence of Reaction Conditions

It is well known form literature that synthesis conditions can be tuned to modify the morphology of TiO_2. For instance, research by Barbé et al.[20] described the influences of synthesis parameters on the final microstructure of TiO_2 film. The autoclave temperature, hydrolysis rate and pH during hydrothermal treatment are of influence on the crystallinity, surface area and sizes of the TiO_2 nanoparticles.

Synthesis of crystalline and amorphous titania It is possible to synthesize titania materials with different crystal structures, but similar morphology. The most common crystal phases of titania are the anatase, rutile and brookite phase (**Figure 7**), where the rutile phase is the only thermodynamically stable phase.[21] The research of Wang et al.[14] showed the formation of amorphous, anatase and rutile nanocrystalline TiO_2 particles by altering reaction conditions using the sol-gel hydrolysis precipitation technique. In this technique, white titania precipitate is formed directly upon dropwise addition of the titanium precursor to a water-ethanol medium. The sizes of the titania grains are controlled by changing the water:alkoxide ratio. In a series of increasing ratios (3.3 - 165), the TiO_2 particles decreased in size. Furthermore, the addition of HCl during the synthesis also resulted in a reduction of particle size.

Hydrothermal treatment, conducted in steel autoclave vessels, is a heterogeneous process for the development of mesoscopic regularity. In the presence of certain solvents, materials dissolve, reorganize and recrystallize due to the high temperature and pressure of the closed environment. This process is not possible under normal conditions. Amorphous material was produced by Wang et al.[9] at very low water:alkoxide ratio's (3.3 < 10) and a mild hydrothermal treatment. In the same research, a phase transition was observed by hydrothermal treatment of amorphous titania precipitates in nitric acid at an elevated temperature. When this procedure was executed in one day, a mixture of the anatase and rutile phase was observed. However, when performed over a time span of seven days, a pure rutile TiO_2 phase was obtained.

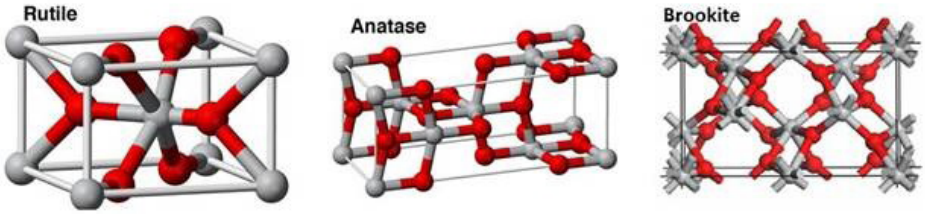

Figure 7: *The unit cells of the most common crystal structures of titania; rutile, anatase and brookite.[21] The red spheres represent oxygen atoms and the grey spheres are titanium atoms.*

Synthesis of titania aerogels Altering reaction conditions during the synthesis of titania aerogels can result in variations in surface area.[18, 22–25] For instance, titania aerogels possess a very high surface area due to the large, open porous network. Aerogels are manufactured using an acid-catalyzed sol-gel procedure and subsequent evacuation of the solvent with Critical Point Drying. Dagan et al.[26, 27] showed that the pore size and surface area can be changed significantly by modifying the molar ratio of water:Ti or ROH:Ti. The surface area and pore size is also influenced by washing the gels with water prior to washing with alcohol. The unreacted groups are removed upon washing with water and the skeletal density is improved, resulting in an increase of the surface area. Additionally, calcination of the aerogel resulted in significantly lower surface areas. Moreover, these titania aerogels contain a disordered internal pore structure, however the pores of titania supports can also possess an ordered structure. This is usually obtained by using so called template molecules. The next section describes the assembly of the ordered pore structure in detail.

1.1.3 Ordered Mesoporous Titania

Ordered mesoporous materials are commonly synthesized using the soft-templating. In the soft-templating method, organic surfactant molecules spontaneously self-assemble into micelles to form an organized array. Therefore, organic template molecules are considered structure-directing agents (SDA), since the structure is directed into a certain position.[28] The most popular technique to assemble an ordered structure is the Evaporation-Induced Self-Assembly (EISA) method, which was developed by Brinker et al.[29] This method is widely used to manufacture ordered porous materials.[30]

Templates that are often used for the synthesis of ordered mesoporous titania are amphiphilic triblock-copolymers of the Pluronic series.[28–39] These organic polymers contain ratios of hydrophilic and hydrophobic blocks (poly(ethylene oxide)-poly(propylene oxide)-poly(ethylene oxide) or PEO – PPO – PEO) and self-assemble into micelles. Their contribution in the sol-gel procedure is the separation of inorganic and organic molecules in the solution. The inorganic reactant molecules organize themselves to the hydrophilic exterior of the micelles, while the organic solvent is captured in the hydrophobic interior of the micelles (**Figure 8**).[29]

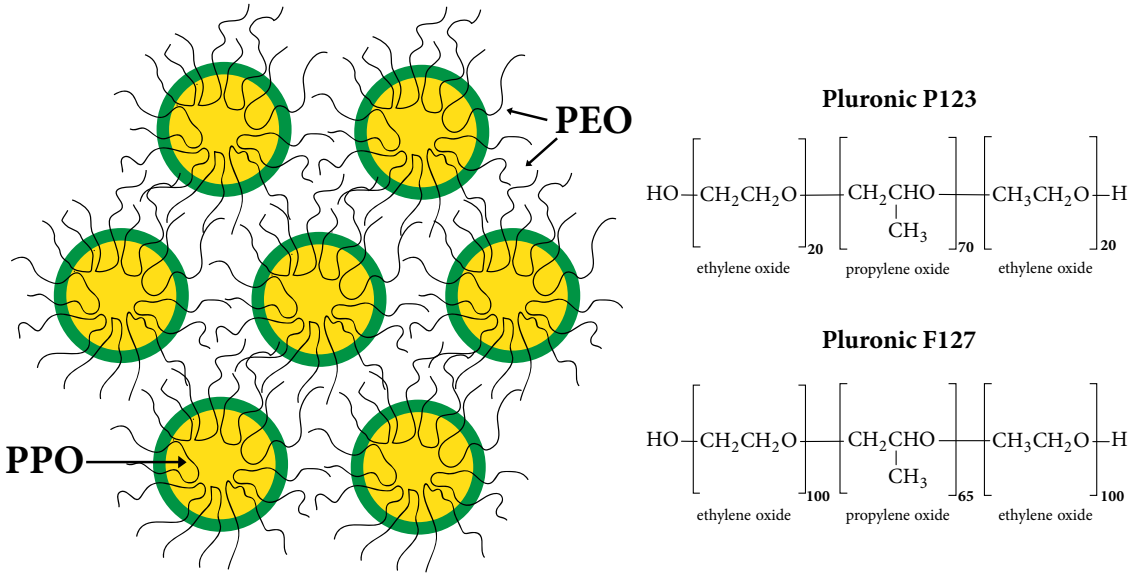

Figure 8: *A schematic representation of hexagonally ordered micelles with triblock-copolymers. The hydrophobic PPO blocks assemble in the center of the micelle, capturing the organic surfactant. The hydrophilic PEO blocks create the surface of the micelles and the inorganic molecules attach to EO groups to form an inorganic region. The organic surfactant and the amphiphilic block copolymers are removed upon calcination, leaving a hexagonal pore-structure.*

Stucky and co-workers were the first to successfully synthesize mesoporous titania with an ordered hexagonal, cubic or lamellar framework. In their procedure, various block-copolymers were used to give rise to the ordered structures. A worm-like two-dimensional hexagonal structure was obtained when using block-copolymer P123 ($EO_{20}PO_{70}EO_{20}$), but when they used PEG 1500 ($EO_{75}BO_{45}$) a cubic mesophase was obtained. However, the experimental procedure was very time-consuming and the structural organization was mostly localized.

Crepaldi et al.[30] proposed a modified EISA method that produces two-dimensional hexagonal and three-dimensional cubic thin film structures with triblock-copolymers Pluronic P123 and F127 ($EO_{100}PO_{65}EO_{100}$) respectively. In these methods, it was critical to stabilize the titania support to ensure minimal collapse of the titania wall structure during high-temperature calcinations. This was accomplished with a mild heat treatment over several days with a very slow heating and cooling rate (1 °C/min). They also stress the fact that the relative humidity is of great importance during the aging and drying steps in the EISA technique.

There have also been experiments in literature including fast preparations of ordered titania which undergo a slightly different procedure. Tian et al.[33] provided a fast and easy method to synthesize ordered mesoporous titania via mixed inorganic precursors. Titanium alkoxide was used as the main titanium source and $TiCl_4$ was added to maintain an acidic medium. The block-copolymers such as P123 was again used as the structure-directing agent. It was gelated around a temperature of 40 °C for only one day. A similar method using mixed inorganic precursors was performed by Zimny et al.[39] with immediate solvent evaporation under vacuum, followed by ammonia treatment.

1.2 Supported Gold Nanoparticles

There are various methods to prepare gold nanoparticles on a support, such as deposition-precipitation, co-precipitation or ion-adsorption. The influence of different preparation methods on gold catalysis have been a popular research subject. Other relevant studies showed that the nature of the support itself influences the size distribution and the particle size of the gold catalysts.[40] Interactions between the gold nanoparticles and the support have an enormous influence on the catalyst performance.[41] The most important factors are the gold nanoparticle size, the selected support material, and the contact structure of the gold on the support, since the interfaces around the gold nanoparticles act as active sites in reactions.[11] Both spherical and/or hemispherical Au particles are supported on TiO_2 (**Figure 10**).

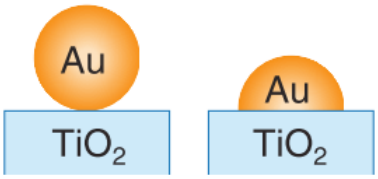

Figure 10: *A representation of a spherical and hemispherical contact structure.*[11]

1.2.1 Support Surface Chemistry

The surface chemistry of the TiO_2 support plays a significant role in the formation of gold nanoparticles, especially when ion-adsorption is used in the deposition of these nanoparticles. The ion-adsorption technique is sensitive to surface properties, such as ionic charges. The TiO_2 surface contains hydroxyl groups which can become negatively charged, neutral or positively charged, depending on the pH or the lattice structure and detailed bonding of the metal oxide. At a low pH, the hydroxyl groups become protonated, resulting in a positive charge on the support surface. However, when a high pH is used, the hydroxyl groups will donate hydrogen ions and the surface becomes negatively charged. These charges attract either an anionic or a cationic precursor, causing formation of an electrostatic double layer on the support surface (**Figure 9**).[42] The pH at which the net charge of the support is zero (or neutral) is the Point of Zero Charge (PZC). The total net charge is zero when an equal amount of positive and negative charge is present on the support surface. For TiO_2 the PZC is reported around a pH of 6.[43] The PZC of the support is of significant importance in the incorporation of the gold precursor on the titania surface.

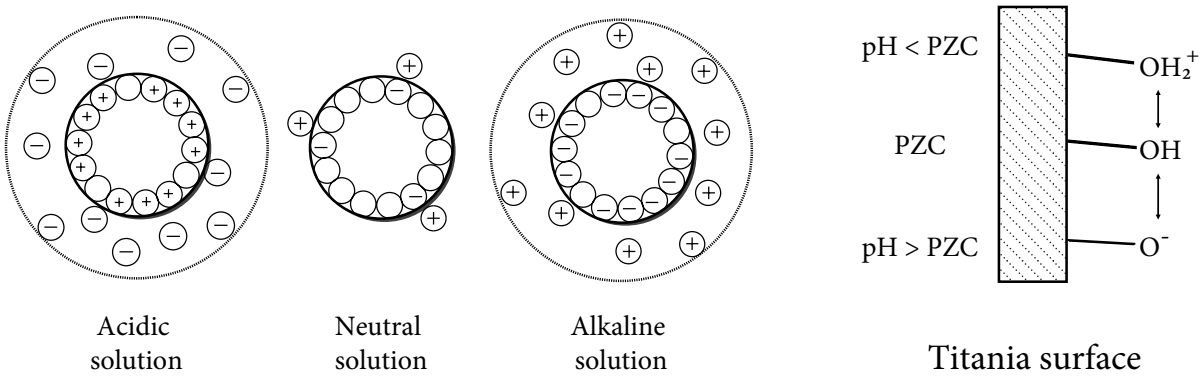

Figure 9: *A schematic representation of an electrostatic double layer on the titania support surface (left) and a section of a titania surface depicting the charge behaviour of the hydroxyl groups in accordance with the PZC (right).*[1]

1.2.2 Ion-adsorption

The gold loading with ion-adsorption is defined as the coordination of gold-containing complexes in solution on a solid surface support. The method is controlled by factors such as the nature of the complex, the Point of Zero Charge (PZC) combined with the acidity of the solution (pH). When these conditions are not optimized, proper attachment of the precursors to the surface of the support is hardly achieved. Moreover, the use of a specific support material for the formation of metallic nanoparticles by ion-adsorption is highly important (section 1.2.1).

In this thesis, the ion-adsorption method is of interest, since this method is well known in our group and provides clear inspection of the formation mechanism of gold catalysts. Additionally, ion-adsorption is preferable when noble metals, such as Au, are deposited on titania. At low loadings, high metal dispersions can be obtained, though a large amount of the gold remains unattached to the support and is discarded upon washing and centrifuging. Furthermore, the gold loading is easier to control and is often more homogeneously distributed on the support. Other methods, such as deposition-precipitation and co-precipitation have been presumed good methods for high dispersions of gold on titania. Though, high catalytic activity was not yet achieved.

Choice of the gold precursor In previous research on the deposition of gold nanoparticles supported by titania, Zanella et al.[44, 45] described preparations for Au/TiO_2 structures with ion-adsorption. In one of the methods, a cationic precursor bis(ethylenediamine)gold(III) trichloride ($[Au(en)_2]Cl_3$) is used to make the adsorption more favorable (**Figure 11**). The $Au(en)_2Cl_3$ precursor is a coordinated compound which consists of two ethyldiamine ligands. The ligands are connected to the Au(III) ion through dative bonds.[48] In alkaline solution, the $[Au(en)_2]^{3+}$ complex adsorbs on the surface support. This cation-adsorption led to small particles (~2 nm) and a gold loading was observed reaching 2 wt%. The precursor employed here, was first prepared by Block and Bailar in the early 50's.[46] It is known that ethylenediamine (en) forms stable cationic complexes in the presence of Au(III) by expelling the chloride ligands from the inner-sphere of $[AuCl_4]^-$. This complex was also successfully used by Guillemot et al.[47] to deposit gold nanoparticles on zeolite Y with ion-exchange, not to be confused with the ion-adsorption method. Zhu et al.[48,49] developed a novel, adept approach to synthesize highly active gold nanoparticles on a mesoporous silica support. This procedure utilizes the previously mentioned cationic gold precursor.

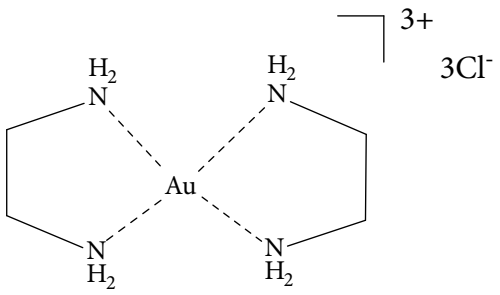

Figure 11: *The precursor $[Au(en)_2]Cl_3$*

It is also a possibility to use an anionic precursor in an acidic solution, since the titania support has a PZC of 6. Previous research used $HAuCl_4$ as the anionic precursor, but there are more complications to this method. For instance, $HAuCl_4$ leaves chloride ions during calcination which hinder the diffusion through the pores and promotes sintering. It is possible to remove the chloride ions by washing the titania with ammonia solution before calcination, however this adds extra steps in the synthesis procedures. Moreover, due to the experience in the group with the cationic precursor and the previously mentioned arguments, it was decided to use a cationic precursor in this research.

1.2.3 The Formation of Gold Nanoparticles

The formation of nanoparticles on titania support is illustrated in **Figure 12**. The titania surface becomes negatively charged upon addition of sodium hydroxide in solution. When the gold precursor is added in solution, the positively charged $[Au(en)_2]^{3+}$ complexes attach to the negatively charged oxide groups. The unattached gold complex cations are washed away with water. It was previously determined by McCafferty et al.[50] with quantitative XPS analysis found in literature that an average of 11 hydroxyl groups per nm^2 are present on a typical titania surface.

The composition of the gold precursor causes some drawbacks which diminish the strong metal-support interaction. For one, the Au^{3+} ions have no direct interaction with the titania surface. Moreover, large amounts of the organic functional groups originating from the ethyldiamine have to be removed and chloride ions are present during ion-adsorption, however the chloride ions are more easily removed compared to the anionic adsorption method with $HAuCl_4$.[48] The gold precursor can decompose from thermally unstable $[Au(en)_2]^{3+}$ to Au^0 due to exposure to light or heat, resulting in metallic gold particles in the samples. It is therefore essential that experiments performed with ion-adsorption are conducted in a dark environment without a heat source until the reduction-calcination step. Zanella et al.[45] reported that ion-adsorption conducted at room temperature gives rise to smaller gold particles on the titania support with a low gold loading after calcination. However, at temperatures of 80 °C the previous described decomposition of $[Au(en)_2]^{3+}$ results in larger gold particles. In another paper, the group showed that the adsorption time has a significant influence on the gold formation.[44] It was concluded that a longer contact time increases the Au loading and the particle size.

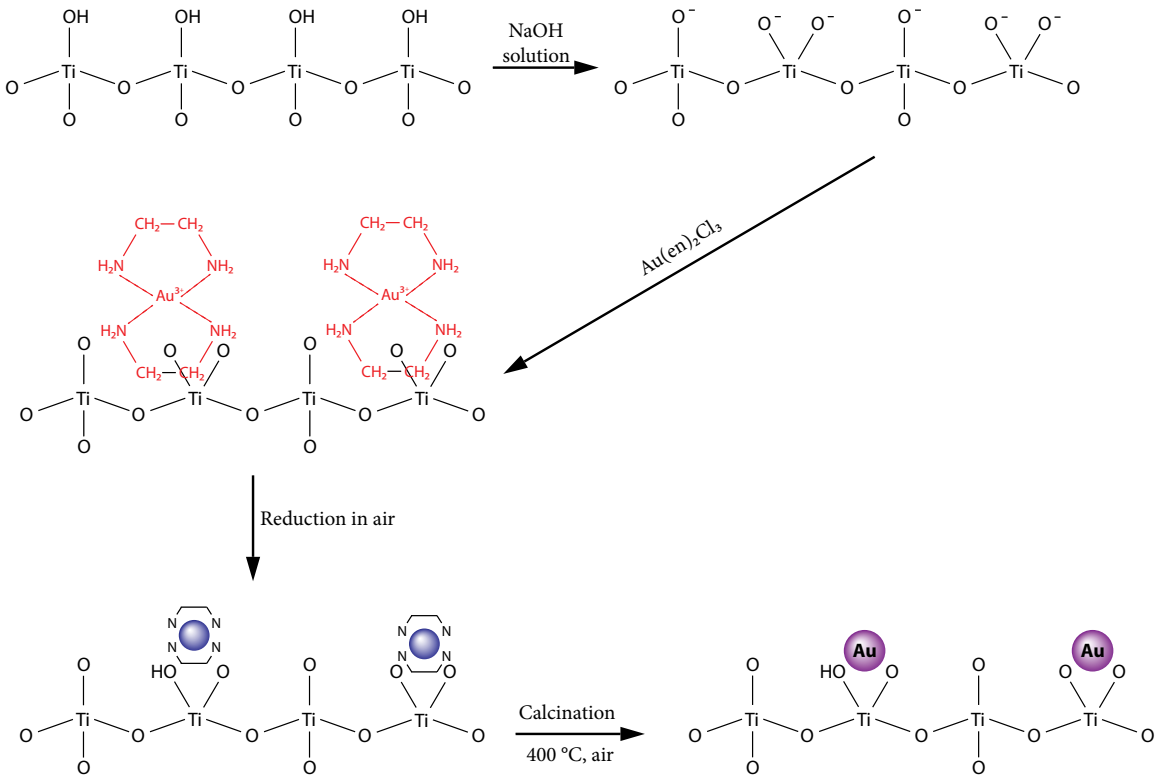

Figure 12: *The ion-adsorption mechanism of gold precursor $Au(en)_2Cl_3$ on titania surface in alkaline solution. Gold nanoparticles are formed after reduction and calcination.*[49]

Chapter 2 Experimental methods

This chapter presents the synthetic procedures of the titania supports, including an anatase and rutile titania support, as well as the amorphous titania support. Moreover, modified synthesis methods are followed for the synthesis of ordered mesoporous titania and several titania aerogels. Subsequently, the gold loading procedure on these supports is presented according to the cationic ion-adsorption method. At the end, the operation of the characterization techniques are described.

2.1 Synthesis of Titania Supports

2.1.1 Crystalline and Amorphous Titania

The manufacture of the anatase, rutile and amorphous titania support was based on the sol-gel precipitation procedure described by Wang et al.[14] The calculations before the procedures are described in App. B. An overview of the synthesized samples is presented in **Table 1**.

Synthesis of anatase titania In a typical synthesis, 4.05 g (14.4 mmol) titanium(IV) isopropoxide (TTIP) was dissolved in 6.5 g anhydrous ethanol (1:10). A solution of water and ethanol was made by mixing 25.8 g ethanol and 5.0 g demi-water. The TTIP solution was added dropwise to the ethanol-water solution whilst stirring and a white precipitate was formed instantly. Subsequently, the mixture was stirred for two hours with parafilm cover. Afterwards, the titania precipitate mixture was centrifuged using an Eppendorf Centrifuge 5804 at 5000 rpm for 10 minutes. The supernatant was decanted and the titania precipitate was washed with 15 mL ethanol before centrifuging. The mixture was then centrifuged and washed two more times while applying the same centrifuging conditions. The washed titania precipitate was transferred to a ceramic dish and was dried in air for five days. The precipitate was grinded to a fine powder and was put into a fluidized-bed reactor. Quartz wool was brought in the tube to prevent the powder from flowing out of the reactor. The powder was calcined at 450 °C in gaseous N_2/O_2 flow (340 mL/min N_2 and 30 mL O_2) for an hour. A heating rate of 10 °C/min was utilized.

Synthesis of rutile titania Pure rutile titania was made by adding 4.0 g TTIP to 6.48 g anhydrous ethanol. A water-ethanol (2:1) solution was made consisting of 41.81 g demi-water and 53.44 g ethanol. The TTIP solution was carefully added dropwise to the water-ethanol solution while stirring vigorously. The mixture was stirred for two hours with parafilm covering the beaker. After centrifuging the mixture for 10 minutes at 5000 rpm, the precipitate was dried in air. Subsequently, the powder was transferred to a round bottom flask and was further dried under vacuum for three days. A solution of approximately 100 mL (1 M) HNO_3 was made with 91 g demi-water and 9.66 mL HNO_3 in H_2O (≥ 65 %). Then the titania precipitate was brought

into a Teflon lined autoclave and the 100 mL (1 M) HNO_3 was added. The autoclave was put in an oven. The precipitate was hydrothermally treated at 180 °C for three days. Afterwards, the heat was turned off and the autoclave was retrieved around a temperature of 50 °C. The autoclave was cooled inside a fume hood before opening carefully. The precipitate was centrifuged at 5000 rpm for 10 minutes and washed with MilliQ water two times. The precipitate was dried at room temperature for six days.

Synthesis of amorphous titania Initially, 2.0 g of TTIP was added to 4.2 mL anhydrous ethanol. This solution was added dropwise to a solution of water-ethanol (1:2) consisting of 0.63 g water and 3.20 g ethanol. The mixture was stirred for two hours. This procedure was repeated a second time, with 2.0 g TTIP and 4.1 mL anhydrous ethanol which was added to a solution of water-ethanol (0.63 g H_2O and 4.06 g ethanol). The two batches were brought together in an autoclave. The autoclave was heated around a temperature of 80 °C for one day. The solution was then centrifuged three times at 5000 rpm for 10 minutes while washing with MilliQ water. The precipitate was dried at room temperature for a week.

Table 1: *The table shows the molar ratio's of TTIP, ethanol, water and the water-ethanol mixture for the synthesis of highly crystalline anatase and rutile titania phase and for amorphous titania.[9] Several entries were executed to obtain a sufficient support for gold ion-adsorption.*

Crystalline phase Entry	Ratio TTIP:Ethanol:water (water-ethanol)	Treatment	Oven (T)
Anatase 1	1:10:20 (1:2)	Calcination	Stagnant-air (450 °C)
Anatase 2			Fluidized-bed (450 °C)
Anatase 3			Fluidized-bed (450 °C)
Anatase 4			Fluidized-bed (450 °C)
Rutile 1	1:10:165 (2:1)	Hydrothermal treatment in acid	Autoclave (180 °C)
Rutile 2			
Amorphous 1	1:10:5 (1:2)	Hydrothermal treatment	Autoclave (80 °C)

2.1.2 Ordered Mesoporous Titania

Several attempts were carried out to acquire mesoporous titania with a highly ordered pore-structures with the use of structure-directing agents (SDA). One or more synthesis conditions were altered per entry (**Table 2**). The sol-gel procedures were derived from reported successful attempts.[30, 31, 33, 39]

A specific ratio between 0.005 - 0.03 of the SDA (either Pluronic P123 or F127) was dissolved in anhydrous ethanol in a glass beaker by swaying the mixture. Highly acidic $TiCl_4$ was added dropwise and with caution, where the ratio of the titanium precursor was 1. As a precaution, two layers of gloves were put over the gloves in the glovebox to prevent contamination. Subsequently, the mixture was retrieved from the glovebox.

The first three entries followed the EISA technique in which only moisture from the air provided H_2O, no additional water was added to the alkoxide mixtures. In entries 4 - 7 additional water was added. Moreover, entries 1 - 5 were transferred to petri dishes almost immediately. These first five attempts were then aged over a period longer than one week. In entry 6 and 7 an additional amount of TTIP was added dropwise. After

addition of water, the mixture was vigorously stirred for two hours. The clear solvent was transferred to glass petri dishes and were aged at different temperatures. Entries 3 - 7 underwent additional heat treatments (**Figure 13**) with increasing temperatures over a specific time period. Part of each sample was retrieved for TEM and XRD characterization. All entries were eventually calcined around 400 °C for four hours. The heat treatments and calcinations were carried out in a Nabertherm muffle furnace.

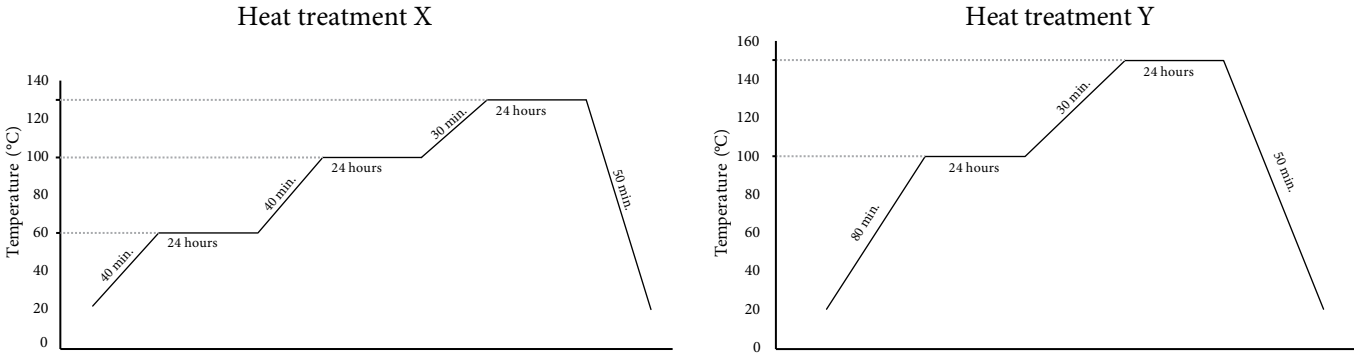

Figure 13: *Schematic illustration of the heat treatments X and Y, where X follows the temperatures 60 - 100 - 130 °C and Y follows 100 - 150 °C. Each temperature was sustained for 24 hours with heating rates of 1 °C/min between the temperatures.*

Table 2: *The table shows the reactions conditions during the several attempts to synthesize ordered mesoporous titania, where SDA stands for the molar ratio of template P123 or F127. Entries 3 - 7 are split over different petri dishes to investigate a specific parameter in the synthesis procedure.* [a] *The sample was dried additionally for six days* [b] *The petri dish was covered with a lid.* [c] *No lid was used.* [d] *Water was added until the solution became clear.* [e] *The sample was vacuum dried overnight and aged for about half a day at 40 °C.* [f] *n.d. not determined. (App. C)*

Entry	$TiCl_4$:Ethanol:SDA (:TTIP)	H_2O	Aging T. (°C)	Aging time	Heat treatment (°C)	Calcination heating ramp
1	*P123* 1:22: 0.02	EISA	60	[a]6 days	-	10 °C/min
2	*P123* 1:20: 0.02	EISA	RT	11 days	-	2 °C/min
3	*P123* 1:20: 0.02	EISA	RT 40	21 days	60 - 100 - 130	2 °C/min
4a	*F127* 1:40: 0.010	1.86 g	[b]RT [c]RT	11 days	60 - 100 - 130	2 °C/min
4b	*F127* 1:40: 0.005	1.79 g	[b]RT [c]RT	8 days	60 - 100 - 130	2 °C/min
5	*F127* 1:40: 0.005	0.9 g 1.83 g	40 RT	1 week	60 - 100 - 130	0.5 °C/min
6	*F127* 1:137: 0.03 (:2.78)	[d]0.63 g	40 [c]RT / 40	24 h 24 h	60 - 100 - 130	1 °C/min
7	*F127* 1:146: 0.03 (:1.85)	[d, f] n.d.	40 40 60	24 h	60 - 100 - 130 100 - 150 60 - 100 - 130	1 °C/min

2.1.3 Titania Aerogel

The disordered porous titania aerogels were synthesized with different surface areas according to the acid-catalyzed sol-gel procedure of Dagan et al.[26] Varying amounts of diluted HNO_3 concentrations were used in this preparation. A typical synthesis of titania aerogels is described here.

Initially, an alkoxide mixture was prepared of a certain amount of TTIP and anhydrous ethanol. Three stock-solutions, including 1.35 M, 1.57 M, and 1.95 M HNO_3, were made by diluting 2.15 mL, 2.50 mL and 3.10 mL of ≥65 % HNO_3 (remainder water) respectively in 50 mL measuring flasks. Specific amounts of these solutions were added to the alkoxide mixtures with a Finnpipette whilst simultaneously swaying the beaker (**Table 3**). The mixture became viscous and a solid gel was formed after a short moment. The gels were aged inside the mother liquor at room temperature for at least five days with parafilm cover. The gels were washed with 15 mL ethanol (≥ 99,5%) once a day for four consecutive days. Most gels were additionally washed with 15 mL demi-water prior to the alcohol washes, with exception of entries 3, D and 5. Afterwards the gels were aged in the mother liquor for at least 12 days to approximately a few months.

The gels were dried using the Critical Point Drying (CPD) technique where the first two gels were dried by using an autoclave and the other gels were dried inside an automated CPD machine (CPD300 AUTO Leica Microsystems). In the first method, dry ice was brought into an autoclave to cool it down for a few minutes. The aerogel sample was brought into the autoclave and a maximum of 26 g CO_2 (s) was added to the autoclave. The reactor was closed with one valve open and put in the heating setup. Subsequently, the valve was closed and the autoclave was heated to 45 °C, where the temperature was held for two hours. Afterwards, the pressure was released slowly and the autoclave was cooled down.

Table 3: *The above table shows an overview of the titania aerogel samples, where C_{HNO_3} (M) is the concentration of HNO_3 present in the mother liquor and H_2O: Ti is the ratio of water to TTIP that was added in the mother liqour. The molar ratio of TTIP:Ethanol was 1:20. [a]The solution was not swayed. [b]Entries 5 and 6 used 1.5 times more TTIP:Ethanol. [c]Entries 7 and 8 used 3 times more TTIP:Ethanol.*

Entry	TTIP (mmol)	C_{HNO3} (M)	H_2O: Ti	Gel appearance	Gelation time	Washes	Aging time
1	**7.04**	0.06	2.8	Clear, stable	5 days	2x water 4x ethanol	1 month
2	**7.04**	0.06	2.8	[a]Clear, cloudy	6 days	3x water 4x ethanol	1 month
3	**7.04**	0.04	1.8	Clear, soft	1 month, 16 days	6x ethanol	1 month
D	**7.04**	0.06	2.8	Clear, cracks	1 week	4x ethanol	4 months
4	**7.04**	0.05	3.0	Clear, cracks	1 week	4x water 4x ethanol	12 days
[b]5	**10.56**	0.05	3.0	White, opaque	10 days	4x ethanol	1 month
[b]6	**10.56**	0.05	2.0	Clear, cracks	10 days	4x water 4x ethanol	1 month
[c]7	**21.12**	0.04	2.1	White, opaque	5 days	4x water 4x ethanol	1 month, 20 days
[c]8	**21.12**	0.04	1.4	Clear, monolith	5 days	4x water 4x ethanol	1 month, 20 days

Inside the automated CPD machine, multiple filler compartments were used to dry two aerogels simultaneously. Thin filter papers (Mascotte Original) were used for encasing the gels inside the fillers to ensure minimal contamination of the gels and the machine. The compartments were filled with anhydrous ethanol before closing. A liquid stream of CO_2 was supplied from a gas cylinder attached to the machine and the automated program was started. The obtained gels were calcined at 400 °C for one hour in a Nabertherm muffle furnace with a heating rate of 2 °C/min. However, titania aerogel entry 2 was calcinated three hours at 400 °C.

2.4 Gold Ion-adsorption

The following gold ion-adsorption method is based on the procedure by Zhu et al.[48] Initially, a stock-solution of the $Au(en)_2Cl_3$ precursor was made. An amount of 0.865 g $HAuCl_4 \cdot 3H_2O$ and 5.0 mL H_2O was brought into a beaker and the yellow solution was stirred for 10 minutes covered with parafilm and aluminum foil. Then, 0.52 mL of ethylene diamine was added dropwise with a Finnpipette to the stirring solution. The solution gained a red-brown color and was likewise stirred for 30 minutes with cover. Afterwards, 50 mL of ethanol was added to the solution. The stirring was stopped and the now yellow dispersion was left overnight with cover. Later, the remaining liquid was decanted and the precipitate was dried in air. The $Au(en)_2Cl_3$ precipitate was dissolved in demineralized water in a 100 mL measuring flask.

The titania supports were all loaded with 2.0 wt% of the gold precursor according to **Table 4**. Typically, an amount of approximately 2-3 mL of the $Au(en)_2Cl_3$ solution was brought into a beaker and water was added while stirring. The pH was increased by adding 0.5 mL (1 M) NaOH with a Finnpippette. A pH of 12-13 was measured with indicator paper in all gold loading procedures. Subsequently, the corresponding amount of the titania support was added to the solution and a pH of around 11 was measured after titania addition. The mixture was stirred for two hours in the dark by covering the beaker with parafilm and aluminum foil. Afterwards, the mixture was washed with demineralized water and centrifuged three times at 5000 rpm for 5 or 10 minutes. The white or slightly yellowish precipitate was dried in the dark at 60 °C overnight. Later, the precipitates were dried under vacuum over a period of at least two days. The precipitates were reduced at 400 °C in a covered fluidized-bed reactor with gaseous N_2 (238 mL/min) and O_2 (60 mL/min), or synthetic air flow, from underneath. Quartz wool was used in the reactor to prevent powder from disappearing with the flow.

Table 4: *An overview of the amounts of titania supports: commercial Degussa P25, anatase titania, rutile titania, amorphous titania, ordered mesoporous titania and four titania aerogels. The supports were loaded with 2.0 wt% of the gold precursor dissolved in water. [a]OMT: Ordered mesoporous titania from entry 7, aged at 60 °C was used. [b] The numbers represent the titania aerogel entries with different surface areas which were specifically chosen.*

	Degussa P25	Anatase Titania	Rutile Titania	Amorphous Titania	[a] OMT	[b] Titania Aerogels			
						2	4	5	6
Amount (mg)	2500	599.6	599.7	599.7	489.9	400.2	415.3	500.6	500.1
$Au(en)_2Cl_3$ solution (mL)	13.1	3.15	3.14	3.15	2.62	2.11	2.18	2.62	2.62
Water (mL)	45.7	~11	~11	~11	9.1	7.4	7.6	9.1	9.1

2.5 Characterization Techniques

2.5.1 Powder X-ray Diffraction

The crystal structures of the titania supports and the Au/TiO_2 samples were investigated with powder X-ray diffraction (XRD) measurements at room temperature, which were acquired with a Brücker D2 Phaser diffractometer with Co $K\alpha_{1,2}$ radiation (λ =1.79 Å), and an X-ray source of 30 kV and 10 mA. High angle measurements were carried out between 2θ: 25° - 80° with an increment (I) of 0.02° - 1.2°, which were adjusted per individual measurement in order to acquire a sufficient amount of data points per peak diffraction and to obtain an acceptable resolution. Low angle measurements between 2θ: 0.8° - 10° (I = 0.02°) were carried out on the ordered mesoporous titania structures after the heat treatment and after calcination to investigate if the powders contained an ordered pore-structure. High energy photons (X-ray beam) penetrate deep into the solid. The X-rays are diffracted by the lattice planes inside the bulk material and the diffracted waves interfere constructively at specific angles, resulting in a peak. The angle in which the interference of the scattered X-ray beams is at its strongest is described in Bragg's law in equation (3).

$$n\lambda = 2d \sin \theta \quad \textbf{(3)}$$

where λ is the wavelength of the incident beam, d is the interplanar distance and n is a positive integer. The diameter of the titania crystallites can be estimated. Information is obtained from the peak broadening: larger crystallites are present when sharp peaks are seen, whereas small crystallites result in broad peaks. The line broadening is measured to give the average size of the particles with the Scherrer equation (4).

$$D = \frac{K \cdot \lambda}{b \cdot \cos \theta} \quad \textbf{(4)}$$

where the average diameter (nm) of the crystalline particles is D, the constant K depends on the shape of the crystal, λ represents the wavelength of the incident beam, b is the peak broadening at half the maximum intensity and θ is the Bragg angle.[51]

2.5.2 Nitrogen Physisorption

The morphology of the titania supports and Au/TiO_2 catalysts were analyzed with the N_2 physisorption technique, which were carried out by a Micromeritics TriStar 3000 V6.08 A instrument. The surface area and porosity of the titania structures were determined with adsorption and desorption measurements. With N_2 physisorption the pressure change is measured with simultaneous addition of the adsorbent (N_2) gas. The Brunauer-Emmett-Teller (BET) analysis models the adsorption and desorption of the gas on the solid surface, when the adsorption and desorption isotherms show a non-overlapping region a hysteresis is observed which corresponds with porosity. The technique has its roots in the Langmuir theory which describes monolayer adsorption, whereas the BET theory describes multilayer adsorption. From the information that is acquired with N_2 physisorption, the total surface area and the specific surface area with the equations (5) and (6): [52]

$$S_{(total)} = \frac{(v_m \cdot N \cdot s)}{V} \quad \textbf{(5)}$$

$$S_{(BET)} = \frac{S_{total}}{a} \quad \textbf{(6)}$$

where v_m is the monolayer volume of the adsorbate gas (at STP), N is the number of Avogadro, s is the adsorption cross section, V is the molar volume of the gas and a is the mass of the titania sample. Moreover, the pore size distribution is retrieved with Barrett-Joyner-Halenda (BJH) analysis. The microporosity is measured with the t-plot analysis based on the reference isotherm of Harkins and Jura shown in equation (7).[53]

$$t_{(nm)} = \sqrt{\frac{13.99}{0.034 - \log p/p_0}} \quad \textbf{(7)}$$

2.5.3 Electron Microscopy

Transmission Electron Microscopy (TEM) imaging was conducted with a FEI Talos™ F200X instrument. A spatula tip of the solid powder was ground in approximately 1 mL 2-propanol. Suitable samples for TEM characterization were obtained by depositing three drops of the 2-propanol suspension on thin film Formvar copper carbon grids (300 mesh) and were dried for at least 10 minutes in air.

Inside the instrument, a beam of electrons is transmitted through the thin sample grid. The electrons interfere with the various elements in the sample. From the transmitted electrons an image is acquired. The electron emission source emits electrons which travel through a vacuum system. Electrostatic plates inside the system allow for beam manipulation.

In the bright-field (BF) mode the contrast on the image is determined by the density and thickness of the material. Scanning Transmission Electron Microscopy (STEM) is a similar technique to TEM, however additional scanning of a narrow section on the sample is applied in a raster with the electron beam. The electrons are scattered over a larger angle after transmission. For the analysis, the High-Angle Annular Dark-Field (HAADF) technique is used to detect the electrons based on variations in the atomic number. Regions with a relatively high atomic number, such as gold, will appear bright, whereas regions with a relatively low atomic number, such as titania, will appear darker. It is also possible that a sample emits X-rays after the electrons collide on the sample. Compositional information of the sample were obtained by detecting the X-ray energies, which are characteristic for its elemental composition, with Energy-Dispersive X-ray (EDX) spectroscopy (**Figure 14**).[54]

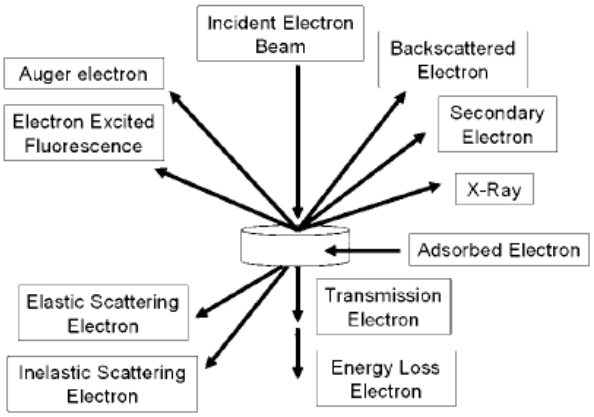

Figure 14: *Representation of an incident electron beam and the possible emission paths in different microscopy techniques.*[45]

The sizes of the titania supported gold nanoparticles were measured with iTEM software. At least 200 gold nanoparticles were counted per Au/TiO_2catalyst from 3 or 4 HAADF-STEM images. The size distributions of each Au/TiO_2 catalyst were plotted in histograms. The mean average catalyst particle sizes were also calculated, as well as the regarding standard deviations.

2.5.4 Thermogravimetric Analysis and Mass Spectroscopy

The thermogravimetric analysis and mass spectroscopy (TGA-MS) were recorded for the amorphous titania support by a PerkinElmer Pyris 1 TGA instrument with an Omnistar Pfeiffer Vacuum mass spectrometer. This technique determines the thermal behavior and stability of the material. Initially, the apparatus was flushed with N_2 20 mL/min. The drying step was hold for 10 min. at 30 °C, then the gass was switched to 10 mL O_2 per min and the titania support (7.674 mg) was heated to a temperature of 600 °C with a heating rate of 2 °C/min. The decomposition of the sample was monitored by weighing the sample continuously throughout the measurement. The released gas was analyzed with a Mass Spectrometer.[55] Several *m/z* ratio's were observed during thermogravimetric measurements in the MS data. A summary of the observed *m/z* ratio's is shown in **Table 5**. The ion-currents were normalized with equation (8).

Table 5: *The table below shows the detected compounds and their corresponding m/z value of the ion-currents.*

Analyzed compound	*m/z* ratio
CO_2	12, 44
CO	28
H_2O	17, 18
CH_4	15, 16
C	12

$$I_{current} = \frac{I_i - I_{min}}{I_{max} - I_{min}} \quad \textbf{(8)}$$

2.5.5 Inductively Coupled Plasma and Atomic Emission Spectroscopy (ICP-AES)

ICP-AES is an analytic technique for the detection of metals. The amount of gold present on the titania structures was determined with this technique. Specific amounts of the Au/TiO_2 samples (25 mg) were sent to Mikrolab Kolbe, where the samples are dried before the analysis. Subsequently, the solid sample is dissolved in water before the sample is pumped into the system and is exposed to very high temperatures of an argon plasma flame. The sample is decomposed into atoms and ionized resulting in excitation of the ions. When the excited electrons in these ions fall back to lower energy states, light is emitted which is detected by a CCD detector. The light that is emitted is characteristic for specific elements. For a full representation of the technique see **Figure 15**. From the detected wavelength of light an emission spectrum is plotted with the intensity of the radiation versus the wavelength.[55, 56]

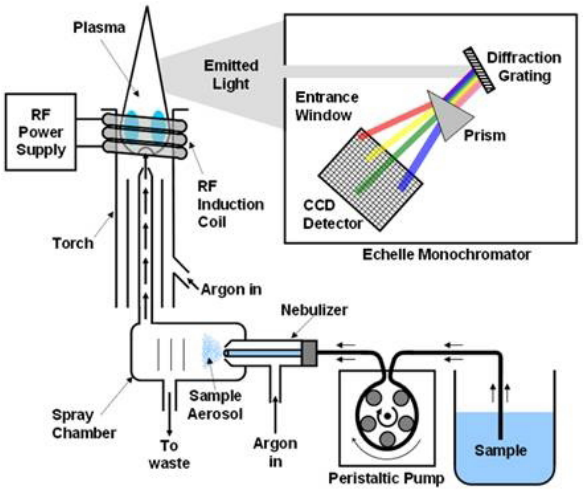

Figure 15: *Schematic representation of an ICP-AES apparatus.*[56]

Chapter 3 Results and Discussion

The results, including the synthesis and characterization of the titania supports and the supported gold particles, are explained and discussed in the following chapter. Each section starts with the results of the support, followed by the results of the gold ion-adsorption on the regarding supports. The results of the gold ion-adsorption on various titania supports are compared, including the influence of the crystallinity in section 3.1, the internal pore-structure in section 3.2, and the surface area in section 3.3. Furthermore, for the comparison of the internal pore-structures the ordered mesoporous titania and titania aerogel (entry 4) is used.

3.1 Crystalline and Amorphous Titania

3.1.1 Support Synthesis

The molar ratio's of 1:20 and 1:165 (TTIP: water) were chosen carefully to control the particle sizes of the anatase and rutile support respectively. The ratio's were chosen so that the particle sizes of the anatase and rutile phase supports were expected to be similar. A very low molar ratio of 1:5 (TTIP: water) was chosen for the amorphous support. The three supports were successfully obtained.

The synthesis of anatase titania was repeated four times to acquire the sufficient support for the gold loading procedure. The procedure was optimized by doing a fluidized-bed calcination in N_2/O_2 flow, instead of calcination in a Nabertherm muffle furnace. This procedure minimized the amount of agglomeration between the anatase particles. However, very small rutile peaks became visible in the third and fourth entry. This is likely caused by the formation of larger particles, since larger particles with critical nuclei sizes of 40 - 50 nm tend to initiate the anatase to rutile phase transformation.[14] In the fourth entry, more washing steps are added in attempt to diminish this particle growth and transformation. Furthermore, hydrothermal treatment in acid around 180 °C for three days was sufficient to obtain a pure rutile titania support.

3.1.2 Support Characterization

3.1.2.1 Powder X-ray Diffraction

The XRD measurements were used to investigate the crystal structure and the crystallite sizes of the crystalline supports. The results indicate that mostly pure crystalline anatase and rutile phases were reached in the supports as well as an amorphous XRD measurement of titania (**Figure 16**). In the amorphous measurement (a) very broad bands around 30° and 55° are observed. This may indicate that extremely small crystals are present in the amorphous support. Moreover, these positions correspond to the largest peaks of the anatase crystal structure (App. B).

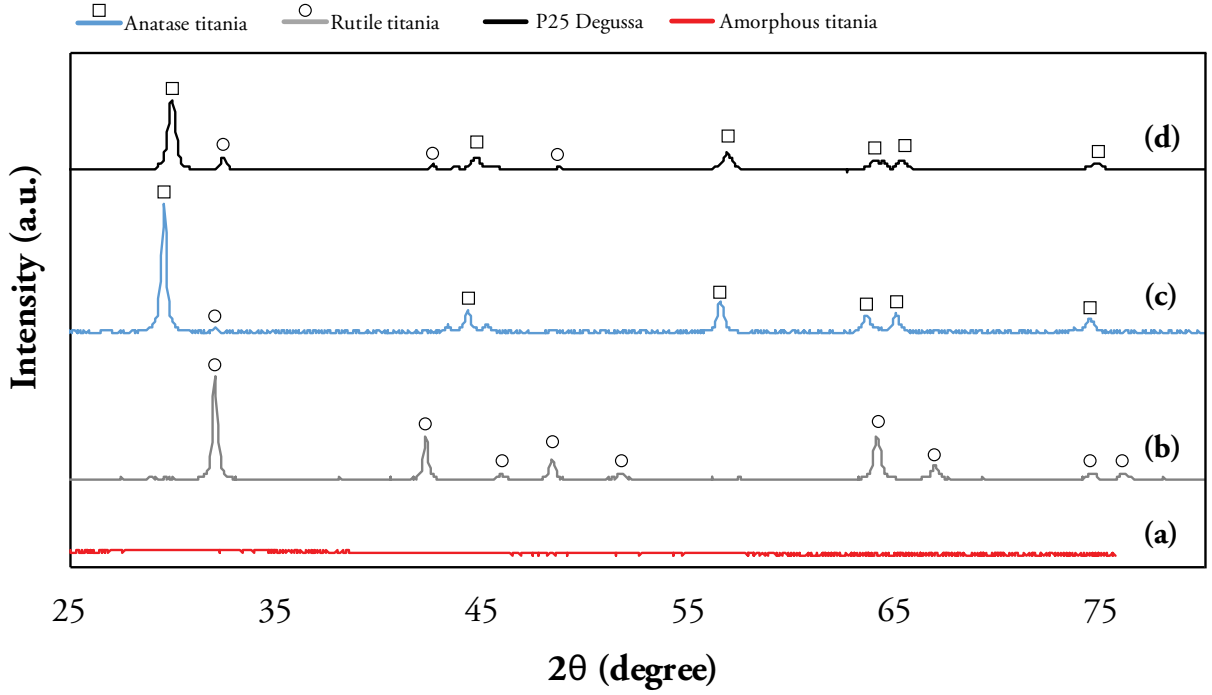

Figure 16: *Powder X-ray diffraction patterns of the supports (a) amorphous titania, (b) rutile titania, (c) anatase titania, and (d) commercial Degussa P25 are shown. The characteristic anatase peaks are shown in blue, while rutile peaks are depicted in gray. (App. B)*

The XRD measurement of the rutile support (**Figure 16b)** shows the largest sharp peaks at 32° (110), 42° and 64° which are characteristic peaks for the rutile phase. The sharp peaks correlate to crystallite sizes of around 36 - 39 nm, which were measured with the Scherrer equation, however the reliability of the Scherrer equation is questionable when measuring such large crystals. In the XRD measurement of the anatase titania, sharp peaks at 29.5° (101), a triplet at 44°, singlet at 56.5°, doublet at 64° and 74° are observed which are characteristic for the anatase crystal phase. Moreover, a very small peak at 32° is seen, originating from a rutile phase, indicating that the anatase phase was not purely acquired (**Figure 16c**). Crystallite sizes of around 30 nm were measured for the anatase titania support. The commercial Degussa P25 titania (as-recieved), contained a mixture of anatase and rutile peaks (**Figure 16d**). The peaks of the anatase phase are more prominent than the rutile peaks, which indicates that the anatase phase is dominant in this material. The crystallite sizes are approximately 20 nm and were determined from the largest peaks with the Scherrer equation.

3.1.2.2 Transmission Electron Microscopy

Bright-Field TEM and HAADF-STEM images of the three synthesized supports and the commercial Degussa P25 were made (**Figure 17**). Important differences are observed regarding the morphologies of the structure. The images of commercial Degussa P25 titania contain crystal sizes of around 20 nm, which are similar to the results obtained from powder x-ray diffraction (section 3.1.2.1). However, for the rutile and anatase support this is not the case. The image of the rutile titania support reveals that the crystals have a rod-like shape, containing a width of 30 - 50 nm and a length up to 100 nm. Furthermore, the images of the anatase titania support reveal that the crystalline nanoparticles have a spherical length of around 50 - 100 nm on both the BF-TEM and the HAADF-STEM images. However, some agglomeration of the crystalline nanoparticles is observed, which might be the result of this larger size. This difference between crystallite sizes could also originate from the Eva program, since the limit of the apparatus is reached. Moreover, all images indicate that

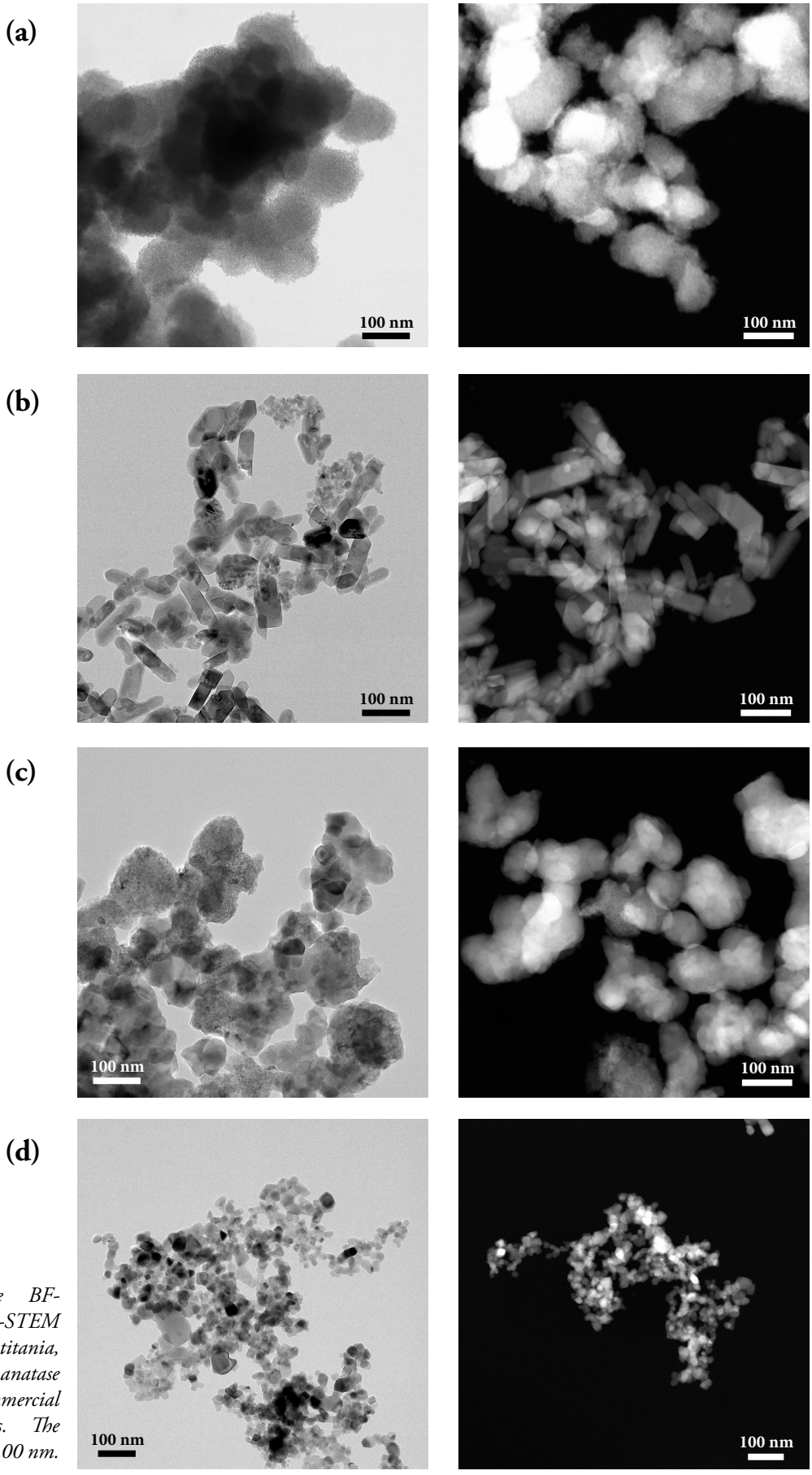

Figure 17: *Representative BF-TEM and HAADF-STEM images of (a) amorphous titania, (b) rutile titania, (c) anatase titania, and (d) commercial Degussa P25 supports. The images have scale bars of 100 nm.*

no significant pores are present in these supports. Still, there is some evidence in some HAADF-STEM images which could indicate very small pores. At last, the amorphous titania support appears to have a very dense structure, consisting of tiny crystallites inside the accumulated titania material which were formed during the hydrothermal treatment. This property gives rise to a significant amount of interparticle space between these tiny crystallites which gives the material a sponge-like appearance.

3.1.2.3 Nitrogen Physisorption

The Brunauer-Emmett-Teller (BET) surface areas and porosity of the anatase, rutile and amorphous titania support were measured with N_2 physisorption (**Figure 18**)(**Table 6**). The isotherm linear plots of the anatase and rutile titania supports contain a hysteresis, which is usually formed due to capillary condensation. Both hysteresises vertically approach 1.0 relative pressure (P/P_0) where the nitrogen gas behaves as a liquid. This suggests that the hysteresis originates from the presence of macropores. The result is confirmed by the BJH

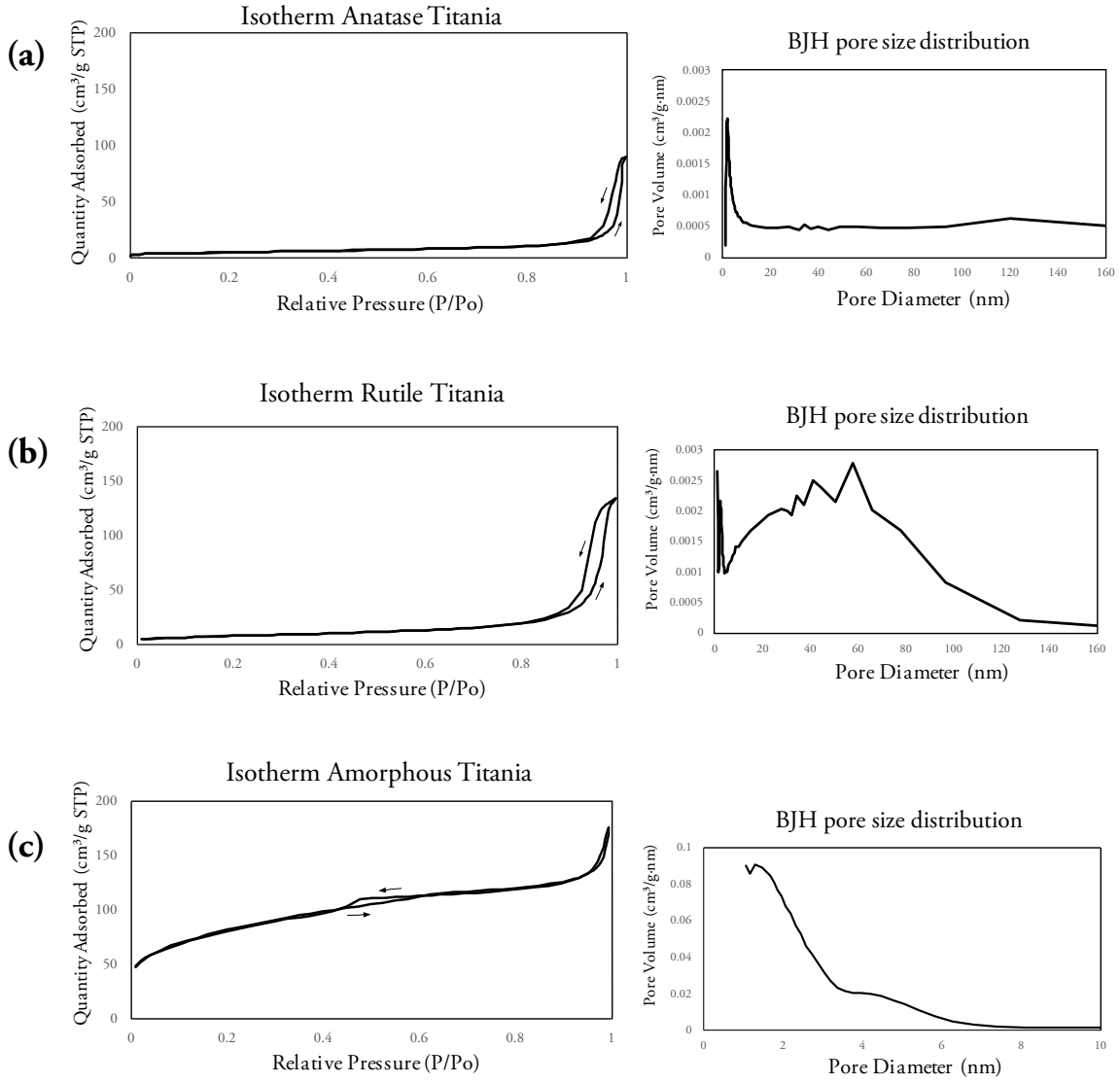

Figure 18: *The nitrogen adsorption - desorption isotherms are shown, accompanied with the corresponding BJH pore size distributions for (a) anatase titania, (b) rutile titania, and (c) amorphous titania. Note that the pore volume in the BJH plots of the anatase and rutile supports are considerably low compared to the amorphous support.*

Table 6: *The table shows the BET surface area's, total pore volumes, the micropore volume and the mean pore sizes of the crystalline and amorphous titania supports.*

Support	BET surface area (m^2/g)	Total pore volume (cm^3/g)	Micropore volume (cm^3/g)	Mean pore size (nm)
Anatase Titania	18.8	0.13	0.00	n.d.
Rutile Titania	29.6	0.21	0.00	n.d.
Amorphous Titania	292.5	0.28	0.01	3.0

adsorption plots, which both show a really broad pore size range. Thus, the measured pore volume most likely originates from interparticle spaces between the crystallite particles. However, in the BJH plots of the anatase and rutile titania a small increase is observed around 2 nm, which could suggest tiny pores or agglomeration between the titania particles. Still, the total pore volume most likely originates from the interparticle space, since the BJH plots of both the anatase and rutile support reveal a broad range from 0 - 160 nm. Furthermore, a specific BET surface area of 18.8 m^2/g and 29.6 m^2/g for the anatase and rutile titania support respectively was determined. The amorphous support contains a rather large BET surface area of 292.5 m^2/g, which was expected from literature.[14] The large surface area is caused by the large amount of tiny particles throughout the amorphous material and the interparticle space between these particles. This was also observed in the TEM images in section 3.1.2.2. The isotherm shows a broad section between 0.4 - 0.6 which suggests the presence of mesopores. The BJH plot shows two peaks at 2 nm and 5 nm, so mesoporosity is not negligible in this support.

The micropore volumes in all titania supports described above are negligible, since values of 0.0 cm^3/g are calculated. Thus, no micropores are present in the supports. The total pore volume is caused by either mesoporosity for the amorphous titania support and mostly macroporosity for the anatase and rutile titania supports, originating from interparticle space.

3.1.2.4 Thermogravimetric Analysis and Mass Spectroscopy

A thermogravimetric analysis (TGA-MS) combined with mass spectroscopy was performed in O_2 atmosphere from 30 °C to a temperature of 600 °C for the amorphous titania support (section 2.5.4). The thermal stability of the support and the composition of the various gasses is determined. The TGA plot shows that the weight loss of the sample starts immediately and ends at a temperature around 400 °C. At this temperature a relative mass of approximately 78 % is still present (**Figure 19**).

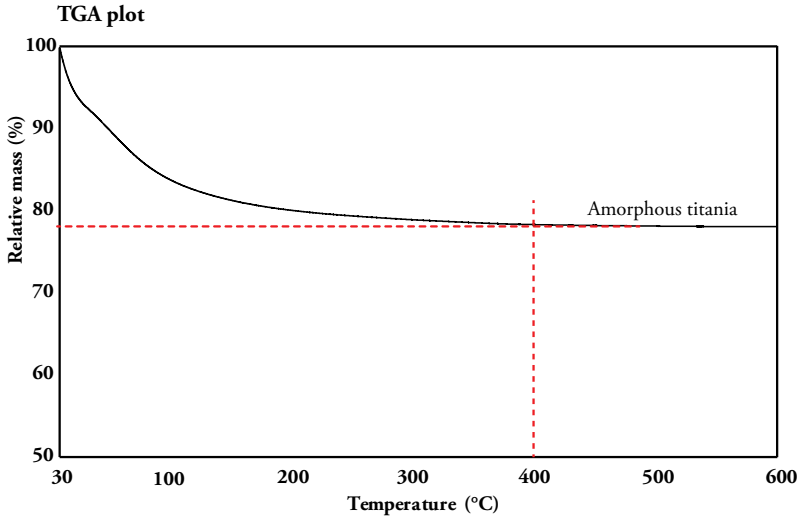

Figure 19: *The TGA plot of the amorphous titania support measured in O_2 from 30 - 600 °C. The relative mass is presented in percentages.*

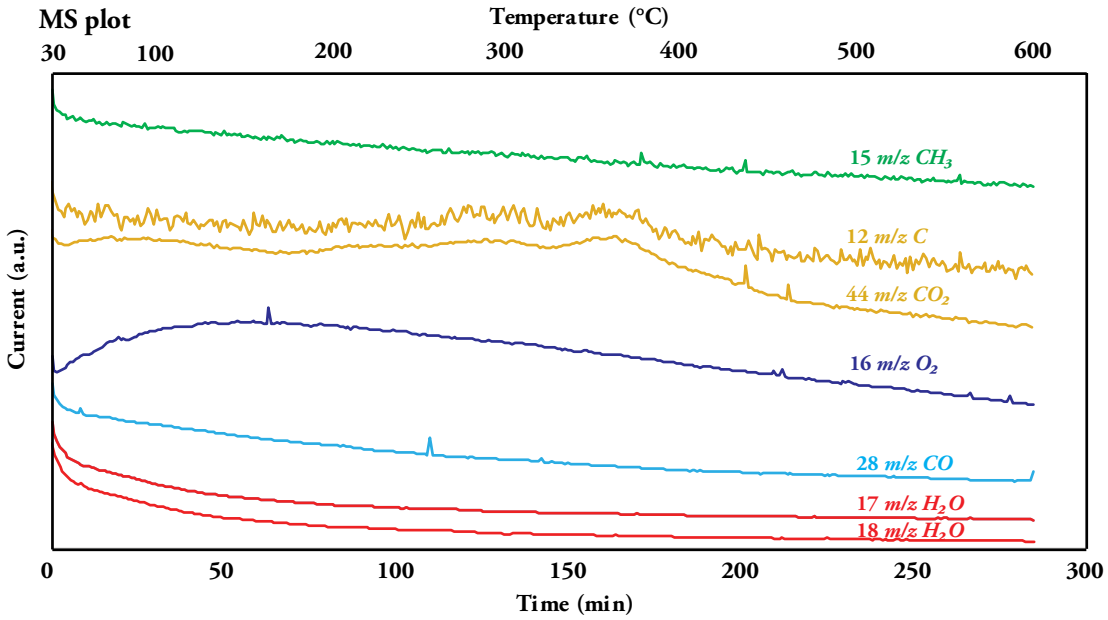

Figure 20: *The MS plot acquired during the TGA measurement of amorphous titania is shown. Most of the loss in relative mass takes place between 30 - 100 °C, which mostly corresponds with the loss of water.*

The mass spectrometer detected the emission of compounds, originating from water and ethanol being the reactant and solvent during the reaction of amorphous titania (**Figure 20**). Although the amorphous support was dried at room temperature (section 2.1.1), it could still be possible that some ethanol was present in the sample. The ion-current of 15 *m/z* corresponds to the detection of CH_3 which originates from the decomposition of ethanol. Ethanol also decomposes to CO and CO_2 (12, 28 and 44 *m/z*). The ion-currents of 12 and 44 *m/z* increase around a temperature between 300 - 400 °C, corresponding to the emission of CO_2. This also explains the slight weight loss around higher temperatures in **Figure 19**. Still, most of the weight loss occurs between 30 - 100 °C, as observed from the thermogravimetric analysis plot, and is caused by water and possibly some ethanol corresponding to the ion-currents of 15, 17 and 18 *m/z*. Moreover, the ion-current of 16 *m/z* corresponds to oxygen, which was flushing through the apparatus (section 2.5.4).

3.1.3 Gold on Crystalline and Amorphous Titania

3.1.3.1 Synthesis

Four Au/TiO_2 catalysts were obtained successfully, the synthesis went well on the supports. After the drying step, a color change was observed for two catalysts. The gold on rutile titania powder became light-brown and the gold on amorphous titania powder acquired a blue-ish hue. The gold on anatase and P25 support remained yellowish white. After the calcination, the rutile/Au powder acquired a purple color, the amorphous/Au a blue-purple color and the anatase/Au powder acquired a light-purple color.

3.1.3.2 Gold Characterization

The gold on the four titania supports was analyzed with powder x-ray diffraction (**Figure 21**). However, no significant gold peaks were observed with XRD, due to the low amount of gold loading on the support. Moreover, the most prominent peaks corresponding to gold generally diffract around the same bragg angle as the titania crystal structures, resulting in an overlap of the peaks in the diffractograms. Furthermore, the most significant difference observed in the XRD measurements occurs in the amorphous support. Simultaneous crystallization of the support took place during the reduction and calcination step of the gold loading synthesis.

Furthermore, the measurement of the amorphous titania suggests that the tiny crystallites have grown to sizes of approximately 5 - 6 nm. The XRD data on the gold on anatase, rutile and P25 remain similar to the measurements of the bare supports (**Table 7**). The small peaks of the rutile phase are slightly larger in the mostly anatase titania support. This is expected as anatase is a metastable phase, whereas the rutile phase is the most stable crystal structure of titania. Furthermore, rutile phase formation occurs from 400 - 1200 °C for this specific material.[14]

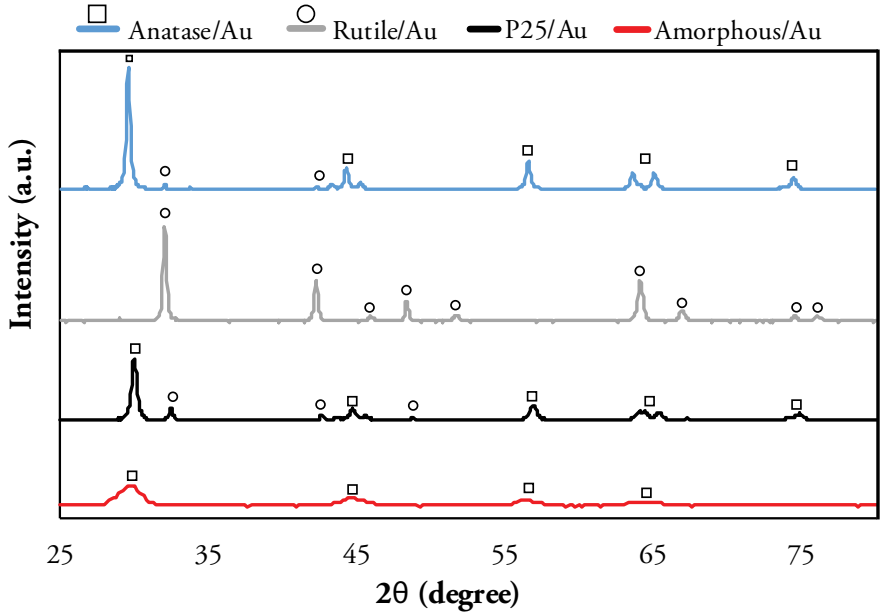

Table 7: *Crystallite sizes calculated with the Scherrer equation.*

Catalyst	Crystallite sizes (nm)
Anatase/Au	29 - 36
Rutile/Au	30 - 42
P25/Au	20 - 22
Amorphous/Au	5 - 6

Figure 21: *XRD diffractograms of the gold on anatase, rutile, Degussa P25 and amorphous titania supports. The amorphous titania crystallized to the anatase phase.*

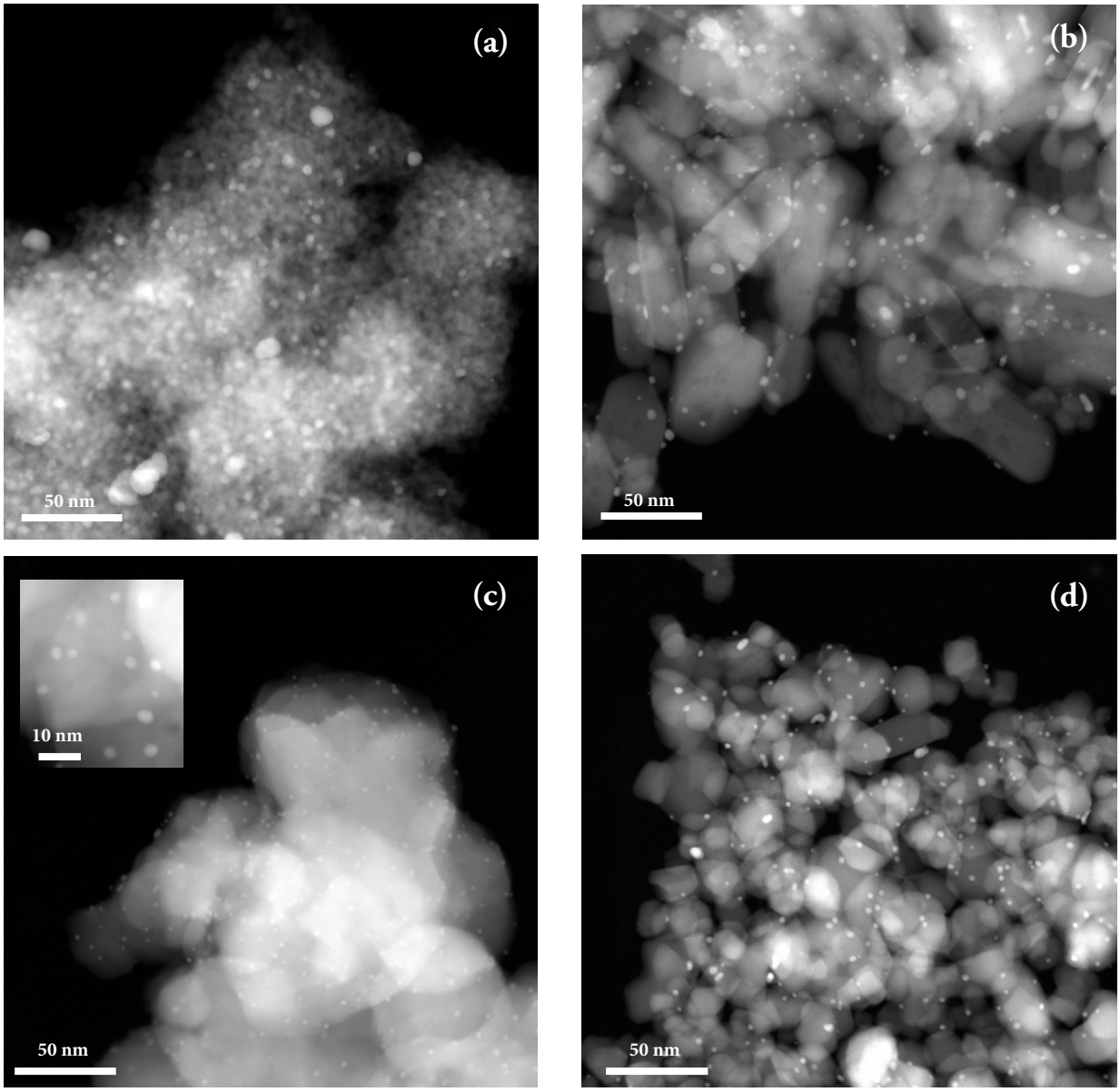

Figure 22: *HAADF-STEM images of gold on (a) amorphous titania, (b) rutile titania, (c) anatase titania, and (d) commercial Degussa P25 supports.*

HAADF-STEM images were acquired of the four supported gold catalysts (**Figure 22**). The gold nanoparticle sizes were measured with iTEM and the corresponding gold size distributions are depicted in histograms (**Figure 23)**. A striking difference is observed when examining the size and localization of the gold nanoparticles on the four titania supports. This difference is likely caused by the crystallinity of the supports.

The gold nanoparticles on the amorphous titania support appear in small sizes throughout the material. Moreover, a striking observation are the large chunks of gold material present on the surfaces (**Figure 22a**). The broad distribution of the gold sizes with a mean average of 3.8 ± 1.7 nm (**Figure 23a**) is likely caused by changes in the amorphous support structure. Initially, a large amount of gold is able to adsorb throughout the material, due to the large surface area of 292.5 m^2/g. During reduction and growth of the gold nanoparticles, further crystallization of the titania support occurs simultaneously, forming TiO_2 crystallites of around 5 nm. As a result, the gold nanoparticles which were located on the growing crystallites are likely confined, while larger chunks of gold nanoparticles are formed on the surfaces of the titania material. Furthermore, the formation of

the anatase crystal structure likely gives rise to electronic interactions between the titania support and the gold nanoparticles, since the titania-gold interactions on crystalline titania are generally strong.[43, 57]

The anatase titania support shows small, spherical gold particles with an average size of 2.4 ± 0.7 nm and a more uniform size distribution (**Figure 22c and 23c**). Especially in comparison with the gold nanoparticles supported by the rutile support, where also larger, spherical and elongated gold nanoparticles are seen. Moreover, a broader size distribution is observed on the rutile support according to the histograms with an average of 2.7 ± 1.7 nm (**Figure 22b and 23b**). This is likely caused by the different support-gold interaction between these crystal structures. It was found by Comotti et al.[58] that the support influenced the shape of the gold nanoparticles, which generally gives rise to faceting and even defect sites and resulted in different activities for the CO oxidation reaction.

The gold supported on commercial Degussa P25 shows both a significant uniformity and a somewhat broad size distribution compared to the gold supported by the rutile and anatase titania. Moreover, it is observed that the elongated rutile crystals contain somewhat fewer gold particles. These results are likely influenced by the mixture of the anatase and rutile crystals of the support (**Figure 22d and 23d**). However, the size distribution is more similar to the anatase titania, since the anatase crystal structure is dominating in the P25 support (section 3.1.2.1).

The color change during the synthesis can be explained by the difference in to the gold nanoparticle sizes. The only significant color changes were observed in the gold on amorphous titania and gold on rutile titania, which both contain generally larger gold nanoparticles. This could explain the hue of the material. The position of the nanoparticles could explain the color, where gold on the surfaces and in the material results in a more blue color and gold particles on the rutile titania surface results in a brown color.

Figure 23: *Size distribution histograms of gold nanoparticles supported on (a) amorphous titania, (b) rutile titania, (c) anatase titania, and (d) commercial Degussa P25.*

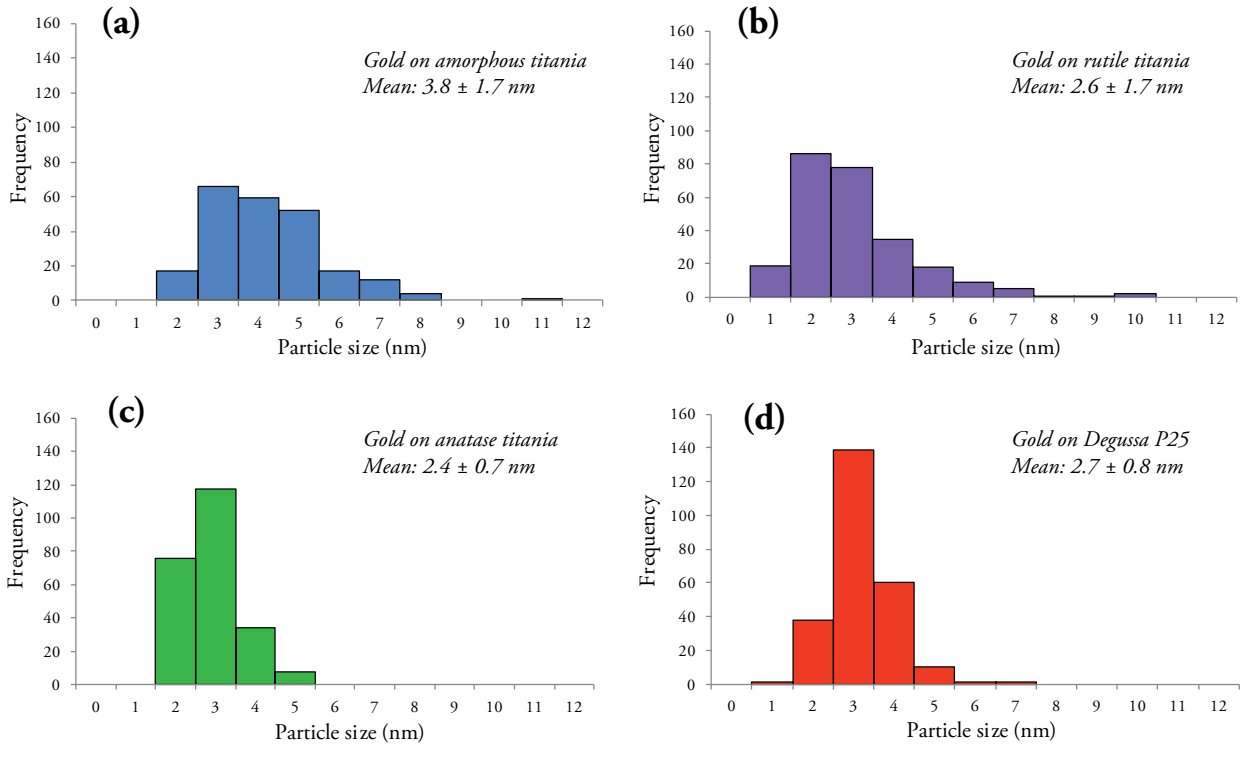

The inductively coupled plasma atomic emission spectroscopy (ICP-AES) results were obtained from Kolbe in Germany. The amount of gold present on the titania supports was analyzed (**Table 8**). Quite a difference is observed which correlates with the specific BET surface areas of the titania supports. The most gold is present on the amorphous titania support with 2.48 wt%. This is generally caused by the larger amount of hydroxyl groups per gram on the surface area of 292.5 m^2/g that this support posseses. Still, this high amount of adsorbed gold is peculiar, since a nominal amount of 2.00 wt% was supposed to be used during ion-adsorption. The higher weight percentage is most likely caused by the assumption that the weight of the support was 100% titania, however results from the TGA-MS analysis indicated that only 78% of the weight corresponded to dry TiO_2, since mostly water was still present in the support. This weight difference was not taken into account while calculating the theoretical gold weight percentage which was supposed to be added, so eventually a relatively higher gold weight percentage is used (App. E).

The anatase titania support had the lowest surface area of 18.8 m^2/g and also the lowest amount of gold was adsorbed on the structure (0.69 wt%). The rutile has a slightly higher amount of gold adsorbed on its structure (0.95 wt%). This is likely caused by the slightly larger surface area of 29.6 m^2/g, so the rutile support theoretically contains more hydroxyl groups than the anatase titania support. However, it is also possible that the difference in gold weight percentage is caused by the differences in gold sizes on the two supports, since the anatase support contains many small gold nanoparticles, whereas on the rutile support also larger gold nanoparticles are observed.

The commercial Degussa P25 support has a theoretically slightly larger BET surface area (35 - 65 m^2/g) compared to the rutile support and also a similar deposited gold amount of 0.90 wt%.[59] The relatively high amount of gold may also be caused by defects on P25, where gold is adsorbed more easily.

Table 8: *The amount of gold on the regarding titania supports presented in wt%.*

Catalyst	Gold (wt%)	Dry (wt%)
Au/amorphous	2.48	5.5
Au/anatase	0.69	0.3
Au/rutile	0.95	0.7
Au/P25	0.90	1.2

3.2 Titania Aerogels

3.2.1 Support Synthesis

Titania aerogel supports were acquired with different porosity and surface areas. However, it was quite difficult to acquire specifically very low and high surface areas by altering the synthesis procedure. The aerogels which were washed with water acquired relatively larger surface areas, as expected from literature.[26] The slight difference of HNO_3 (mol) added to the mixtures did not significantly influence the outcome of the aerogels, however the amount of water in the acidic concentrations most likely influenced the hydrolysis and condensation of the reaction. The critical point drying and calcination step appear to have a significant influence on the surface area as well. The first two entries were dried manually in an autoclave which is a difficult procedure, since a significant amount of the CO_2 is already lost before the drying step can initiate. This problem was resolved by using the automated CPD machine. The machine was also able to dry two gels at a time. Eventually, the titania aerogels were synthesized successfully. Four of the titania aerogels with different surface areas were used for gold ion-adsorption. Furthermore, the CPD machine was broken for a short period, this resulted that entry D had a relative longer aging time of 4 months.

3.2.2 Support Characterization

In this section, the titania aerogels 2, 4, 5, and 6 are discussed, since these supports are used to investigate the influences on the gold nanoparticle formation. Additional information on the other titania aerogels can be found in Appendix D. The influence of different surface areas of aerogels 2, 5 and 6 are investigated in section 3.2.3, whereas aerogel 4 is used as the disordered titania in comparison with the ordered mesoporous titania in section 3.3.

3.2.2.1 Powder X-ray Diffraction

The crystal structures of the calcined titania aerogels are analyzed with powder X-ray diffraction. The measurements were executed between 25° - 80° degrees (**Figure 24**). The XRD diffractogram shows peaks in similar areas for all four titania aerogels. It indicates that the supports have an anatase crystal structure, however

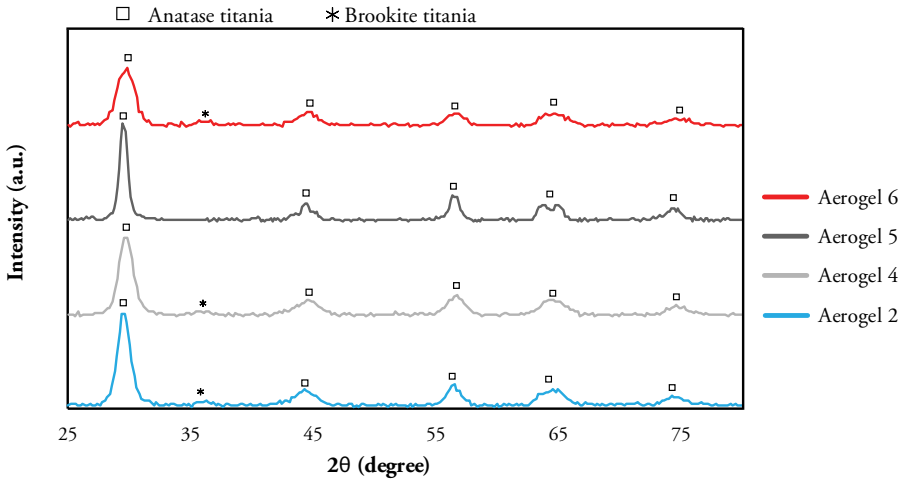

Figure 24: *The XRD diffractograms of the four titania aerogel supports. The diffractograms show anatase-characteristic peaks.*

not as dominant as in the anatase titania support from section 3.1. Moreover, a tiny broad peak around 36° degrees is observed in the diffractograms of aerogels 2, 4 and 6. This correlates with a brookite crystal structure and is only visible in the titania aerogels which were washed with water. The amount of acid added in all the alkoxide mixtures was similar, however the Water: Ti ratio differed due to the different acid concentrations. A large water: Ti ratio of 3 was used for titania aerogel 5, while a significantly lower water: Ti ratio of 2 was used for aerogel 6, since the concentrations 1.35 M and 1.95 M HNO_3 were used respectively (section 2.1.3).

The crystallite sizes are depicted in **Table 9** and were derived with the Scherrer equation. Titania aerogel 6 has much broader peaks compared to the other diffractograms, correlating with slightly smaller crystallite sizes of 6 nm. Aerogels 2 and 4 contain slightly larger crystal sizes of 7 - 8 nm. The slight difference between aerogel 6 and 2 is likely caused by the longer calcination time of three hours. Moreover, aerogel 5 contains the largest crystallite sizes of approximately 13 nm. This may be the consequence of only washing the aerogel with ethanol instead of the additional washes with water. The phenomenon was also observed for entry 3, with crystallite sizes of 15 nm (App. D). However, this explanation is contradicted by the findings of Dagan et al.[27], where an increase of the crystallite dimensions was observed upon additional water washes.

Table 9: *The crystallite sizes of the titania aerogels.*

Titania Aerogel	Crystallite size (nm)
Aerogel 2	8
Aerogel 4	7
Aerogel 5	13
Aerogel 6	6

Furthermore, a slight peak shift toward higher 2Theta (°) is observed, when the peaks are compared with the general anatase peak pattern. This is probably cuased by compression of the crystal structure induced by strain on the porous structure due to imperfections and local distortions of the lattice.[51a] Phase transition from brookite to anatase could possibly also be an explanation, however the evidence of a brookite crystal structure is merely based on one tiny peak. Another explanation would be that some organic species were chemisorbed on the internal titania walls, causing shrinkage of the titania aerogel due to drying (App. A). All in all, this phenomenon could be caused by multiple factors concerning the crystal structures of the titania aerogel and why or how this phenomenon occurs is not exactly clear.

3.2.2.2 Transmission Electron Microscopy

HAADF-STEM images of representative titania aerogels are shown (**Figure 25**). It is clearly seen that **Figure 25a** consists of larger titania particles compared to the other two entries. This confirms the findings of the XRD analysis regarding the crystallite sizes (section 3.3.2.1). Moreover, titania aerogel entries 2 and 6 have similar particle sizes.

The pore-structures of supports are disordered, as expected from the reported data by Dagan et al.[26] The titania aerogel in **Figure 25a** appears very dense compared to the other two, indicating that it most likely contains a lesser amount of total pore volume and also a smaller surface area. This is further analyzed with nitrogen physisorption in section 3.3.2.3. However, most of this information is based on representative images from other entries, since the TEM grids of the corresponding titania aerogels were contaminated with gold on alumina and not all titania aerogel supports were analyzed with TEM. For that reason, these images present only a visual aid and do not perfectly show the characteristics of the titania aerogel entries 2, 4, 5 and 6.

Figure 25: *Representative HAADF-STEM images are shown of (a) titania aerogel 5, (b) titania aerogel 2, (c) titania aerogel 6, and (d) titania aerogel 4. All images contain scale bars of 50 nm.*

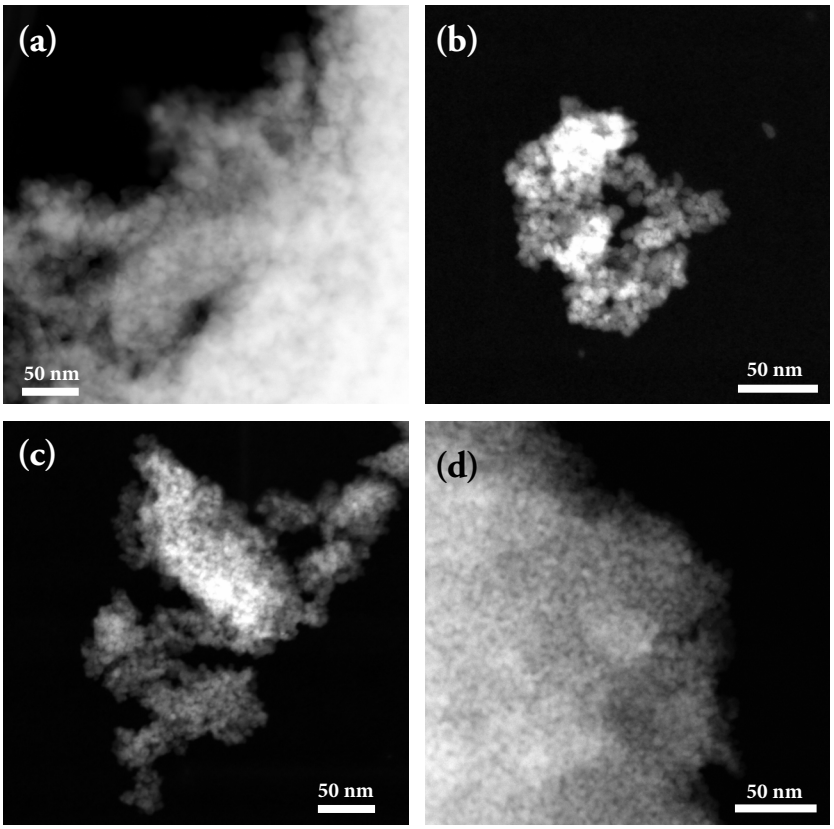

3.2.2.3 Nitrogen Physisorption

The titania aerogels were analyzed with N_2 physisorption and several distinctive surface areas and porosities were found (**Table 10**). The adsorption-desorption isotherms of the supports are shown in **Figure 26**.

Table 10: *An overview of the nitrogen physisorption data of the titania aerogels. The mean pore sizes were not determined.*

Titania Aerogel	BET surface area (m^2/g)	Pore size distribution (nm)	Total pore volume (cm^3/g)	Micropore volume (cm^3/g)
2	117.7	2 - 10	0.17	0.00
4	131.0	2 - 8	0.16	-0.01
5	27.8	1 - 5	0.02	0.00
6	168.7	2 - 8	0.21	-0.01

Titania aerogels 2 and 4 show a similar porosity and intermediate BET surface areas of 117.7 m^2/g and 131.0 m^2/g respectively. The latter titania aerogel support was sufficient for the comparison to the ordered mesoporous titania (section 3.3). A very low surface area of 27.8 m^2/g was observed in the results of aerogel 5, accompanied with a lower pore size distribution and a pore volume of 0.02 cm^3/g. This aerogel was merely washed with ethanol, which is the cause of its lower porosity and surface area. The other three aerogels were additionally washed with water. According to Dagan et al.[26] the water washes had a significant influence on the surface area and pore structure of the titania aerogels, since unreacted organic groups in the solvent are removed and the skeletal density of the aerogels increases.

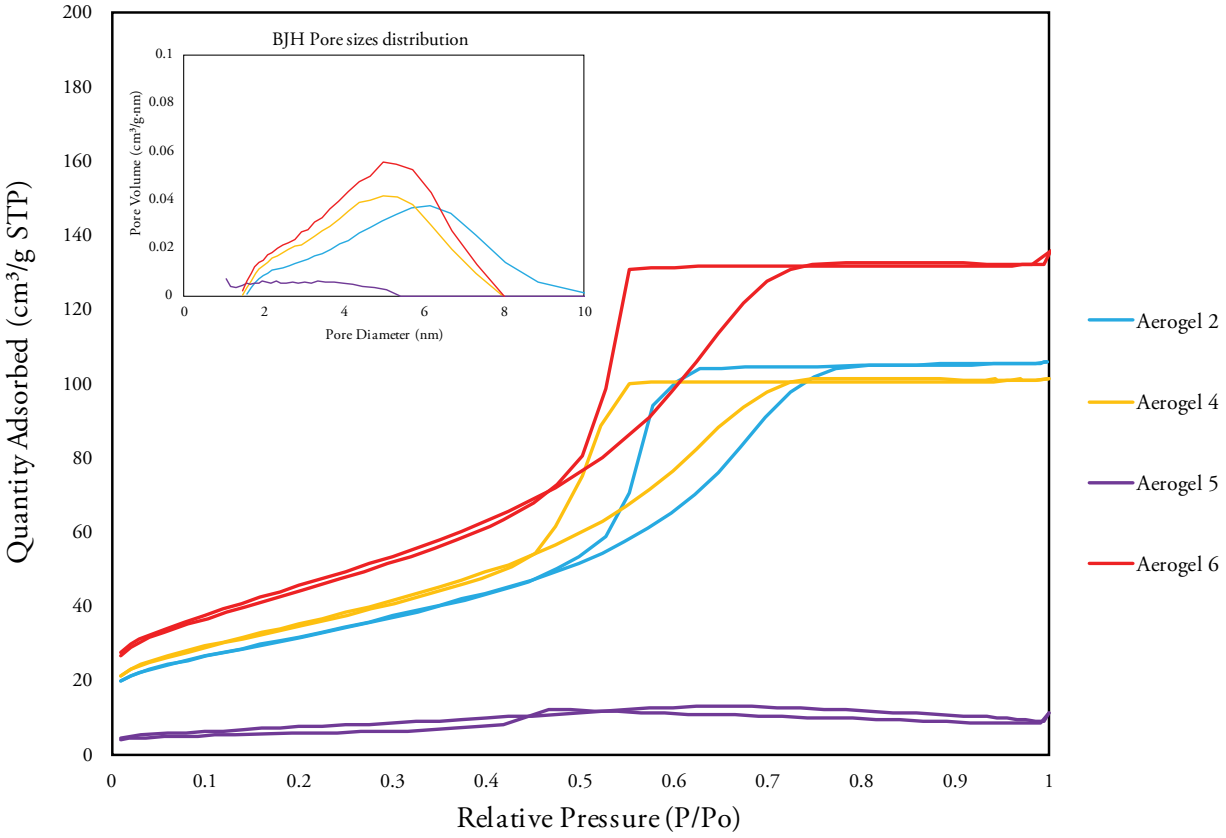

Figure 26: *The adsorption-desorption isotherms of the three titania aerogels.*

Aerogel 6 acquired a quite high surface area of 168.7 m^2/g and a high pore volume. This is caused by both the water washes and the addition of an ideal concentration of acid catalyst of 0.4 mL (1.95 M) HNO_3. This higher stability originates from the polarity and increased water content (H_2O:Ti = 2) where the hydrolysis and condensation rates are in balance. This results in clear and strong gels opposed to the white, cloudy opaque gels where the gel growth is incomplete due to a fast hydrolysis and slow condensation. The latter is the result of aggregation and instable gels with lower surface areas, as seen for entries 2, 5 and 7 (App. D).

The isotherms of aerogels 2, 4 and 6 have similar shapes, corresponding to the presence cylindrical mesopores with a larger central pore volume (bottle-neck). The pore distribution is also similar with average pore sizes of 5 or 6 nm. Furthermore, a small shoulder is observed around 2 nm, corresponding with the small 'tail' of the hysteresis around 0.5 relative pressure. Moreover, the three isotherms approach 1.0 relative pressure in a horizontal manner, indicating that no macropores are present. However, a slight increase is observed in the isotherm of aerogel 6, but this amount of adsorption is low and therefore negligible. The micropore volumes of the three aerogels are around 0.0 cm^3/g, so no micropores are present in the titania aerogels. This confirms that the total pore volume only originates from the presence of mesopores, this is also observed in the BJH pore size distribution plots (**Figure 26**).

Furthermore, the additional calcination causes the titania aerogels to collapse and decreases the porosity significantly. According to Dagan et al.[26] the surface areas of the gels prior to the calcination treatment could have reached 600 m^2/g. The reduction in surface area is caused by coalescence of very small pores. Simultaneously, the pore sizes increase, causing a change in the pore volume. Moreover, multiple calcinations causes a change is morphology, relevant for aerogel 2, which was calcined for three hours instead of one hour.

3.2.3 Gold on Titania Aerogels

In this section the gold on titania aerogels containing a range of increasing surface areas are compared, including aerogels 2, 5 and 6. The aerogels have surface areas of 27.8 m^2/g, 117.7 m^2/g and 168.7 m^2/g corresponding to aerogels 5, 2 and 6 respectively (section 3.2.2.3).

3.2.3.1 Synthesis

There were no significant complications during the gold ion-adsorption procedure on the three titania aerogels. Aerogels 2 and 5 contained a yellow/brownish color prior to the gold ion-adsorption. After the ion-adsorption and reduction-calcination, the three gold on titania structures were obtained as black powders.

3.2.3.2 Gold Characterization

The three gold on titania aerogel supports were analyzed with powder X-ray diffraction and transmission electron microscopy.

Powder X-ray Diffraction

The X-ray diffractograms of the three gold-supported titania aerogels do not seem significantly different compared to the bare supports. The gold is not detected in the diffractograms, due to the low gold loading and the fact that the peaks of gold overlap with the anatase crystal structure of titania (**Figure 27**). The powders still show an anatase crystal structure with a small brookite peak at 36° for gold-supported titania aerogels 2 and 6. Similarly, aerogel 5 had crystallite sizes of 13 nm and aerogel 6 still contained 6 nm crystallites. However, the crystallite sizes of aerogel 2 increased to some extent, from 8 nm to 9 nm. This small increase is likely caused during the reduction-calcination step after the gold ion-adsorption procedure and is negligible.

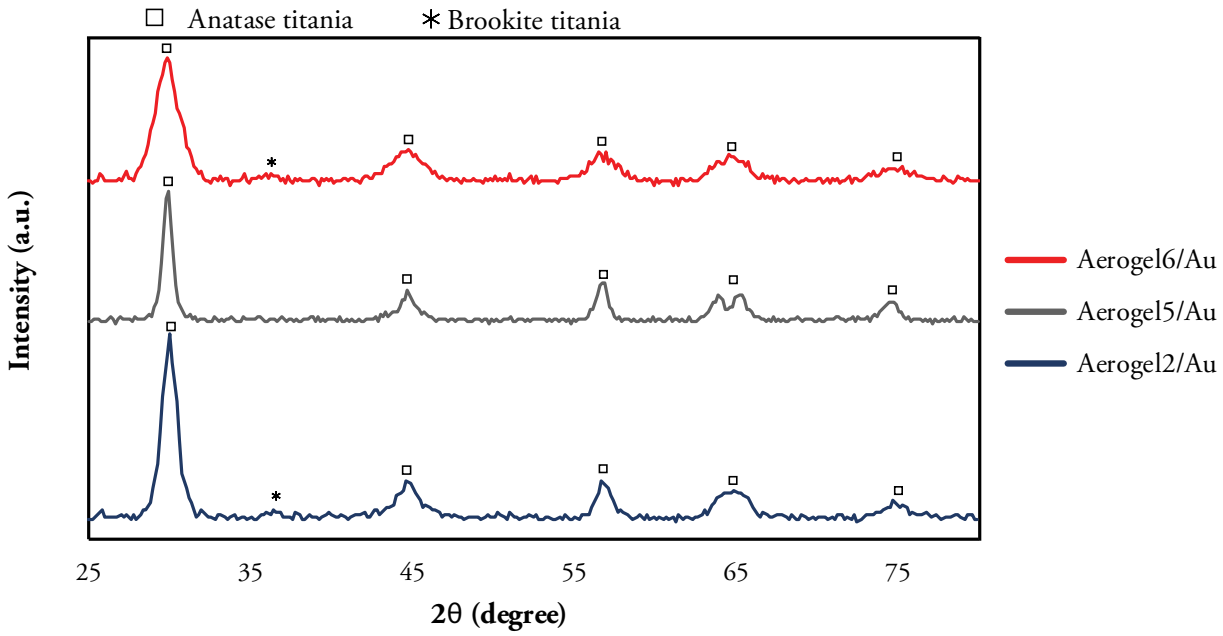

Figure 27: *The XRD diffractograms of the three gold-supported titania aerogels containing a low, intermediate and high surface area.*

Transmission Electron Microscopy

Dagan et al.[27] stated that the titania aerogels had very good adsorption capability, which can be seen in the following results. HAADF-STEM images of the three gold-supported titania aerogels were acquired (**Figure 28**). The gold nanoparticle sizes were measured with iTEM and the corresponding particle size distributions are shown in histograms (**Figure 29**). Several striking differences regarding the gold nanoparticles on these supports are observed.

The titania aerogel 5, with the lowest surface area, shows either almost no gold nanoparticles or very many gold nanoparticles on random areas throughout the support, according to **Figure 28a and b**. This may indicate that some parts of the supports contain a higher porosity than other parts, resulting in a varied distribution of the gold nanoparticles. Moreover, varying gold particle shapes are observed, including elongated and spherical particles. The gold particle size distribution histogram in **Figure 29a** shows a very broad range between 2 - 10 nm with an average around 3 - 4 nm. The larger gold nanoparticles seem to be located mostly on the external surface of the support.

The HAADF-STEM images of titania aerogels 2 and 6 show a similar gold nanoparticle distribution according to **Figure 28c and d**. The particle size distribution in **Figure 29b and c** show ranges between approximately 2 - 6 nm. However, on average slightly larger gold nanoparticles are observed on aerogel 6, which may correlate with the higher porosity in this support, still this difference is likely negligible on account of the standard deviations. Further analysis of the gold with ICP-AES on the three titania aerogels is needed in order to acquire more insight on the adsorbed amount of gold.

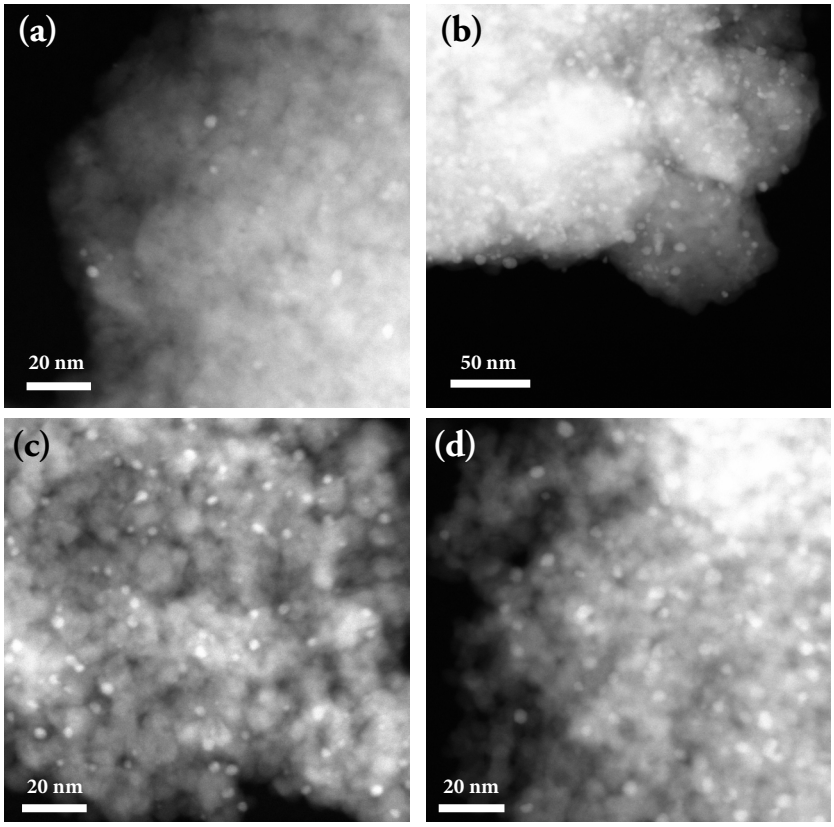

Figure 28: *The HAADF-STEM images of (a) aerogel5/Au with very little gold nanoparticles, (b) aerogel5/Au with a lot of gold nanoparticles (c) aerogel2/Au, and (d) aerogel6/Au.*

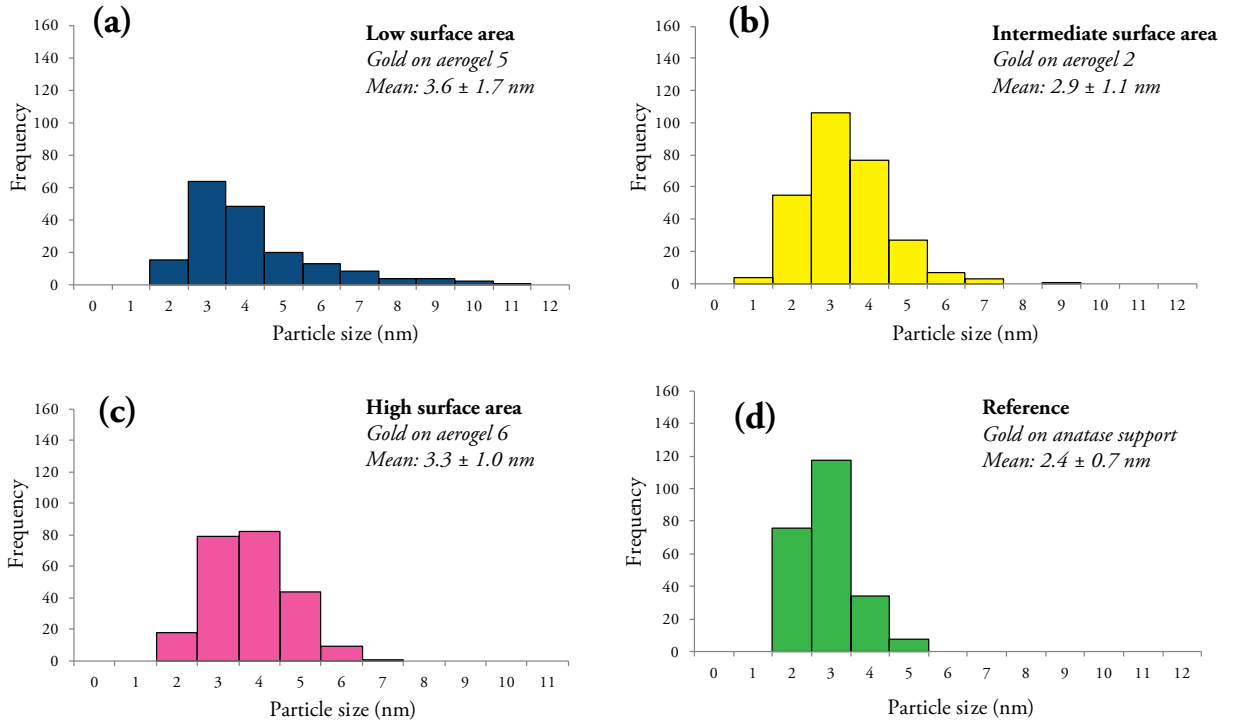

Figure 29: *Size distribution histograms of gold nanoparticles supported on titania aerogels with (a) low surface area, (b) intermediate surface area, (c) high surface area. Furthermore, the reference for gold on the anatase support is shown in (d).*

3.3 Ordered and Disordered Mesoporous Titania

3.3.1 Support Synthesis

Ordered mesoporous titania was acquired in entry 6 (aged at 40 °C) after calcination and was reproduced in entry 7 (aged at 60 °C). In previous attempts, ordered titania was already observed in uncalcined material after heat treatments, however most material had collapsed after calcination. Furthermore, both cubic and hexagonal patterns were observed, which will be further discussed in section 3.3.2.2. The disordered mesoporous titania aerogel was obtained from entry 4 of the titania aerogels (section 2.1.3). Information on the synthesis of titania aerogels specifically is described in section 3.2.

The influence of various reaction conditions were investigated in the attempts to create ordered mesoporous titania. This included the use of two different structure-directing agents, P123 and F127, also the $TiCl_4$:F127 ratio (1: 0.005 - 0.03) was investigated. Initially, the Pluronic P123 dissolved easily during the synthesis, whereas F127 only slightly dissolved in anhydrous ethanol, but upon addition of highly acidic $TiCl_4$ most of the F127 dissolved. However, some flakes were still visible in the mixture. A clear mixture was obtained when a certain amount of water was added while stirring. The dissolution of the SDAs is likely caused by the consistency, since P123 is a paste which dissolved easily, whereas some flakes of F127 were still visible in an undissolved mixture. This was especially the case when a relatively larger amount of F127 was used.

Furthermore, in most entries varying amounts of water were added to the reaction mixture. In entry 5 the influence of the amount of water was investigated, including 0.9 g and 1.83 g water, which both did not result in ordered titania. Moreover, aging temperatures around 60 °C, 40 °C and room temperature were investigated with altering the aging time and using an open or closed environment by applying a lid. This most likely influenced the condensation reaction during the synthesis. Also, vacuum evaporation was attempted in order to immediately remove the solvent and the isopropanol produced during the hydrolysis, however this did not result in ordered titania.

After the aging process, mild heat treatments were initiated to dry and stabilize the mesophase of the material. After the heat treatment, the clear samples had turned beige to dark red-brown with cracks on the surface. Furthermore, different heating rates, including 10.0, 2.0, 1.0 and 0.5 °C/min, were investigated in the calcination step. This parameter is of significant importance and it was deduced that the calcination must not proceed too fast or too slow, since the structure would collapse. The heating rate with the best outcome was 1.0 °C/min, which was used for both the heat treatments and the calcination. It may be important to note that, during the heat treatments and calcinations of entry 6 and 7, the petri dishes were placed close to the heat sensor on a plateau to obtain a stabilized and uniform removal of the organic templates and solvents.

In previous attempts with only $TiCl_4$, the precursor would violently react with ethanol and form large amounts of HCl. This resulted in an extremely low pH (< 1) in the mother liquor which is not entirely desirable, since it may cause a less ordered structural regularity.[33] In entries 6 and 7, mixed inorganic precursors TTIP and $TiCl_4$ were added, where TTIP served as the main titanium source and $TiCl_4$ regulated the acidity. The procedure accompanied a relatively short aging period for bulk titania. This modified procedure was derived from Tian et al.[33] and Zimny et al.[39]

3.3.2 Support Characterization

In this section, the results of the synthesized ordered porous titania, including the synthetic development of the ordered pore-structure in several entries, are discussed. Furthermore, the ordered mesoporous titania used for gold loading purposes is thoroughly presented, discussed and compared with the disordered porous titania aerogel from entry 4. The following sections include the comparison of the ordered and disordered pore-structure of the two titania supports.

3.3.2.1 Powder X-ray Diffraction

The mesoporous titania entries were analyzed with high angle powder X-ray diffraction, to analyze the crystal structure of the material and the crystallite sizes. The uncalcined titania, after the heat treatment, and the completely calcined titania samples were measured. Furthermore, low angle measurements were executed in order to detect the ordering of the pore sizes. The high angle measurements were performed between 25° - 80° degrees, whereas the low angle measurements were executed between 0.8° - 10° degrees (**Figure 30**).

All of the ordered titania entries obtained anatase crystal structure after complete calcination of the material (**Figure 30a**). Crystallite sizes ranging from 7 - 20 nm were obtained in several entries, where the larger crystallites were only observed in the unsuccessful attempts (App. B). In several entries, an intermediate crystal structure was observed after the stabilizing heat treatment, which is likely caused by crystalline titanium oxochloride structures, which could explain the peak around 27°. The titanium oxochlorides may be formed

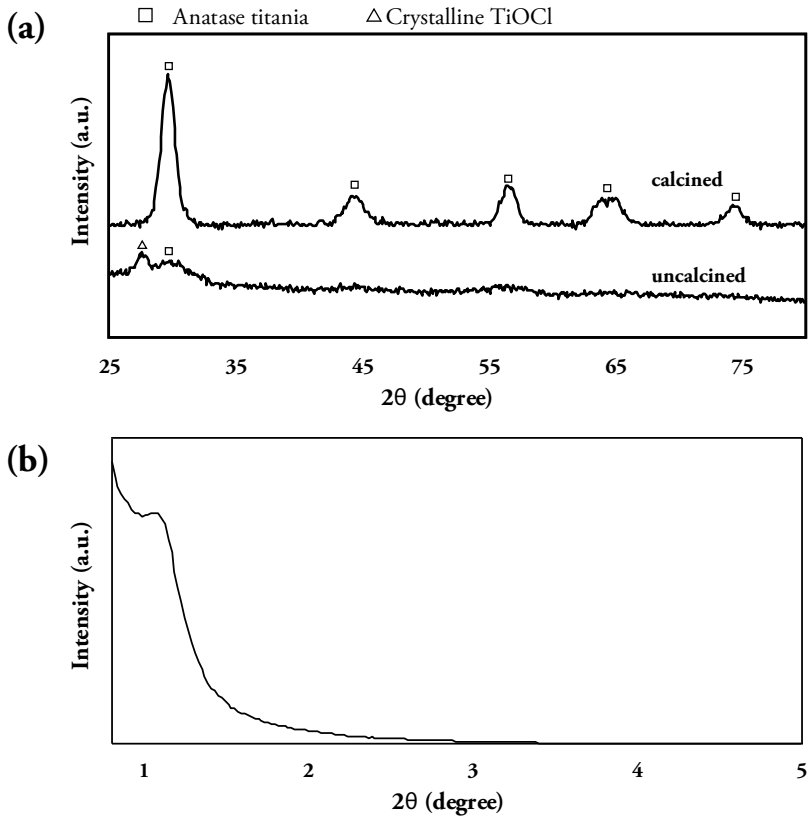

Figure 30: *The XRD diffractograms of the ordered mesoporous titania, including (a) representative high angle measurements of uncalcined and calcined titania, and (b) the low angle measurement with a peak around 1.1° degrees, corresponding with a lattice plane distance of 4.7 nm, originating from entry 7 (calcined). For convenience, a range of 0.8° - 5.0° is shown.*

due by the presence of the surfactants inside the pore-structure, since chloride ions from $TiCl_4$ are not easily removed. Furthermore, the formation of the anatase phase is observed around 29°.

The low angle measurements provided insight on the structural ordering of the titania pore-structure. In most of the titania entries, a smooth line was observed without any diffraction. In **Figure 30b** a peak is shown around 1.1° degrees, which suggests that the pores are repetitively ordered in such a fashion that the Bragg reflection is observed. It was important to begin the measurements at a 2Theta below 1.0° degrees in order to observe any reflections, since the peaks are typically seen around 1.0° degrees. Furthermore, this phenomenon was seen in the titania materials after calcination from entries 6 and 7 (App. C). The ordered titania from entry 7 had crystallite sizes of around 7 nm.

The disordered porous titania aerogel has a similar anatase crystalline structure compared to the ordered porous titania. Moreover, both supports contain crystallite sizes of approximately 7 nm. However, the titania aerogel contains a small brookite peak around 36° (**Figure 31**). The peaks of both materials are quite broad. This is easily seen according to the triplet peak, around 45° degrees, which has become one broad band. Hence, the crystallite sizes are indeed similar.

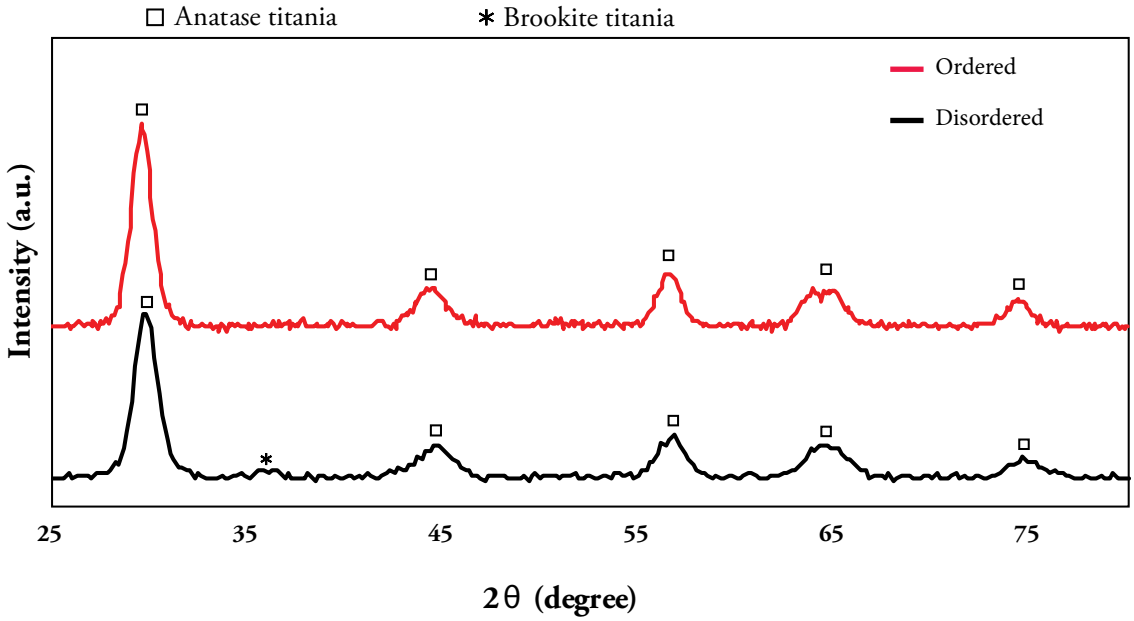

Figure 31: *The XRD diffractograms of the ordered mesoporous titania from entry 7 (red) compared to the disordered porous titania aerogel from entry 4 (black).*

3.3.2.2 Transmission Electron Microscopy

The various entries were analyzed with BF-TEM and HAADF-STEM. Images were acquired to bring the possibly ordered pore-structure in view (**Figure 32**). The organization of the pores is best viewed at the edges of the titania material, where the titania is thin. Furthermore, the organization is even better observed in the HAADF-STEM images.

Most attempts were unsuccessful and resulted in disordered mesopores throughout the titania material. A representative image is shown in **Figure 32a**. Clearly, there is no presence of ordered mesopores titania. This disorder is caused by experimental parameters, such as a fast heating rate during the calcination, causing the pore-structure to collapse when the surfactants are removed.

In entry 3, the stabilization procedure (heat treatment X) was applied for the first time. In the uncalcined titania, which was aged at 40 °C, the pore-structure is still not completely ordered. However, the material appears to contain a more intermediate pore-structure to some extent (**Figure 32b**). This intermediate pore structure was obtained with the structure-directing agent P123. This SDA contains relatively short PEO blocks, which is the place where the inorganic titania wall is built during the assembly procedure. Thin titania walls are more susceptible to collapse due to thermal instability. In order to synthesize thicker walls, template F127 is used as template for further entries. This template has PEO blocks which are five times larger compared to template P123.

In entries 4a and b, where the titania mixtures with water were aged without a cover over the petri dishes, a significant section of the titania consisted of an ordered pore-structure after the stabilizing heat treatment of the material (**Figure 32c**). A 2D-hexagonal pore structure was observed for entry 4a and b. However, in entry 4a, where a larger molar ratio of F127 was used compared to entry 4b, the ordering of the pore-structure is still mostly irregular. Most of the structure-directing agent F127 was still present in these titania structures, since the PEO-PPO-PEO polymers are typically removed at temperatures above 350 °C.[28] After the calcination of these structures around 400 °C with a rate of 2 °C/min, the organization of the pore-structure was lost due to collapsing of the titania walls. It is possible that the molar ratio of the SDA F127 also has a significant influence in the formation of ordered pores, next to the heating rate, since it was already known that different pore-structures are acquired in thin films when the molar ratio of this template is varied.[30]

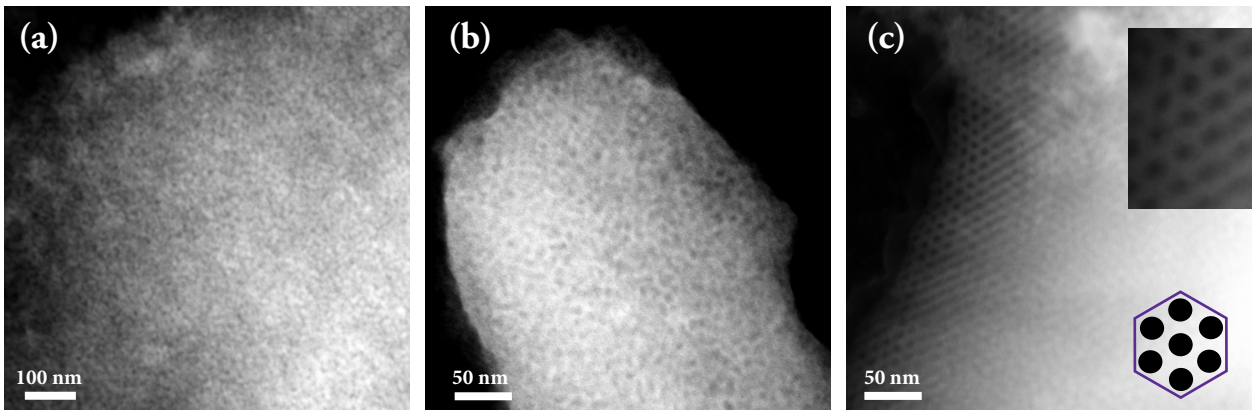

Figure 32: *HAADF-STEM images of mesoporous titania. The images are representative for (a) a disordered pore-structure (image orginates from entry 1), (b) an intermediate formation of ordered pores (entry 3), and (c) uncalcined ordered mesoporous titania with a 2D-hexagonal structure (entry 4b).*

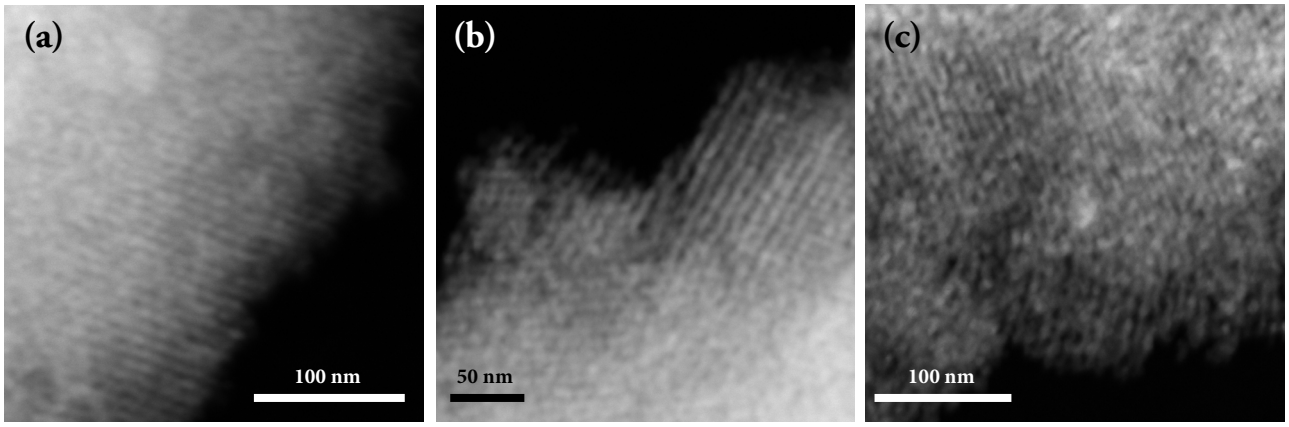

Figure 33: *HAADF-STEM images of ordered mesoporous titania, obtained from entry 7, aged at 60 °C, after calcination.*

Eventually, an ordered pore-structure was observed, even after calcination, with the use of mixed titanium precursors. The organization in entry 7 is caused by the assembly of the 7 nm sized titania crystallites in such a manner that forms the 2D-hexagonal and cubic pore-structures. Hence, both the hexagonal as cubic mesophases are observed in this material and is clearly observed in **Figure 33a and b**. Moreover, some worm-like channels are recognized (**Figure 33c**). However, the structural regularity is not reached in all parts of the ordered mesoporous titania or is slightly off. This may still be caused by the collapse of the structure during calcination. Overall, it is quite difficult to preserve such a high structural regularity in bulk mesoporous titania while removing the surfactants during the heat treatments, since the fragile pore-structure tends to collapse quite easily. This sensitivity is likely caused by strong electrostatic interactions between the surfactants and the titania walls.[39] Moreover, a non-homogeneous or fast heating program during the calcination can easily affect the internal pore-structure during the heat treatment. It is, therefore, critical to use a stabilizing heat treatment in order to prestiffen the titania network.[30]

Still, most of the material from entry 7 has acquired the mesoporous ordering. The organization of the pore-structure is reached to a high extent, even in the thicker parts of the titania material as observed in **Figure 34a**. In this HAADF-STEM image the contrast is slightly better in order to see the ordering of the pores in the thicker titania material. This confirms that ordered mesoporous titania was produced, sufficient for studies with gold ion-adsorption and the comparison with titania aerogel (entry 4). In **Figure 34b** it is clearly seen that the organization of the internal pore-structure of the disordered porous titania support differs massively.

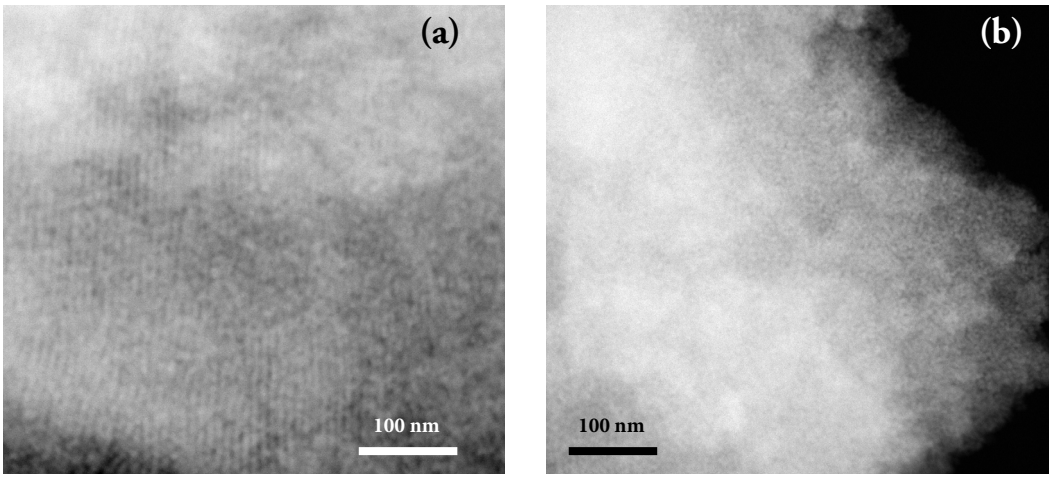

Figure 34: *Representative HAADF-STEM images of (a) the thicker part of ordered porous titania compared to (b) titania aerogel.*

All in all, the most important parameters during the synthesis of odered mesoporous titania were the specific structure-directing agent, the molar ratio of the reactants in the alkoxide mixture ($TiCl_4$, SDA and TTIP), the addition of water, the stabilizing heat treatment and the heating rates. Porous titania materials appeared to be very sensitive toward these key factors in the synthetic procedure. The block-copolymer F127 contains larger PEO blocks compared to the P123 polymer, hence thicker walls were built, which are generally less vulnerable to collapse. It also appeared that the molar ratio of the SDA could have a significant influence, although several factors were simultaneously influencing the outcome of the structure, so this is still a point of discussion. Moreover, the addition of water was generally preferred over the EISA procedure, since the humidity in the fumehood was probably not reliable or sufficient for the bulk production of ordered mesoporous titania compared to ordered mesoporous titania films.

Furthermore, the utilization of mixed inorganic precursors was very promising, since in both attempts (entries 6 and 7), ordered mesoporous titania was formed and the pore-structure remained ordered after calcination. At last, a three-day heat treatment was crucial in order to prestiffen the structure of titania and diminish the probability to collapse. The best heating rate for the heat treatment and calcination was 1 °C/min.

3.3.2.3 Nitrogen Physisorption

The N_2 physisorption technique measured the nitrogen adsorption-desorption isotherms and the BJH pore size distribution (**Figure 35**). Both supports show significant porosity, since a hysteresis is observed at intermediate relative pressures. Specific BET surface areas of 146.3 m^2/g and 131.0 m^2/g were determined for the ordered and disordered porous titania respectively. Moreover, total pore volumes of 0.20 cm^3/g and 0.16 cm^3/g respectively were measured and a micropore volume of -0.01 cm^3/g, which is 0.0 cm^3/g, was determined from the t-plots (**Table 11**).

These results suggest that no micropores are present in both the titania supports. Simultaneously, it confirms that the total pore volume originates from the presence of mesopores. Furthermore, no macropores are present, since the isotherm remains horizontal at high relative pressures (P/P_0).

The shape of the hysteresis suggests that cylindrical pores are present in the supports. Moreover, in the titania aerogel the hysteresis also suggests a larger central volume with a small end (bottle-neck). Both the hystereses are relatively wide (from 0.42 - 0.7 relative pressure) which implies the presence of a distribution in the pore size. Furthermore, the BJH size distribution plot reveals that most pores have sizes of around 5 nm with a range between 2 - 8 nm, which is still a reasonably wide range for ordered porous material.

In comparison, the ordered and disordered titania support contain a similar porosity, with matching pore sizes. However, a small difference is observed in the total pore volume and the surface areas. Also, the shape of the pores are both cylindrical, but the titania aerogel likely contains less uniform pores with a larger central volume.

Table 11: *The table shows the BET surface area's, total pore volumes, the micropore volume and the mean pore sizes of the crystalline and amorphous titania supports. The mean pore size is derived from the BJH adsorption plot.*

Support	BET surface area (m^2/g)	Total pore volume (cm^3/g)	Micropore volume (cm^3/g)	Pore size range (nm)	Mean pore size (nm)
Ordered Titania	146.3	0.20	-0.01	2 - 8	n.d.
Disordered Titania	131.0	0.16	-0.01	2 - 8	4 nm

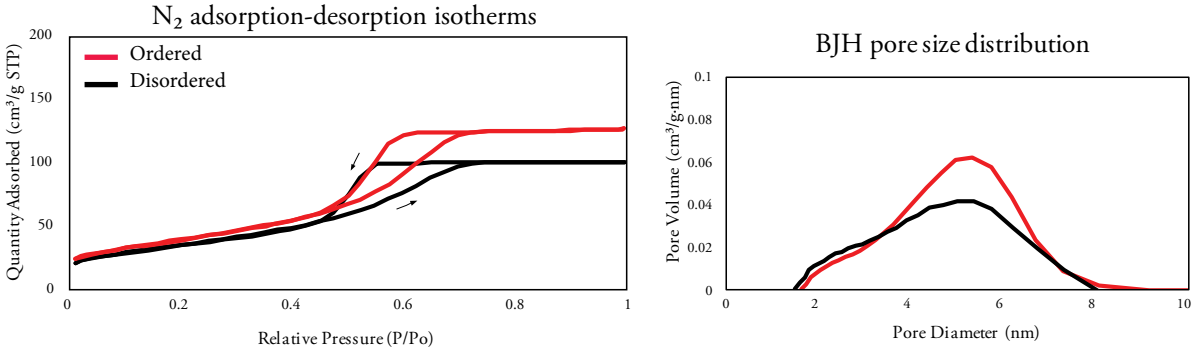

Figure 35: *The adsorption-desorption isotherms of the ordered mesoporous titania (red) and disordered titania aerogel (black). The BJH pore size distribution.*

3.3.3 Gold on Ordered and Disordered Mesoporous Titania

3.3.3.1 Synthesis

The gold on ordered and disordered mesoporous titania was deposited successfully. Interestingly, both the Au/TiO_2 powders became black after the calcination step. Furthermore, in the titania aerogel support the powder already turned black after drying at 60 °C in the oven. This phenomenon may be caused by a larger amount of Au nanoparticles on the supports, however the color change was not observed in the gold on amorphous titania support. Another explanation would be that the pores of the titania supports were filled with leftover carbon from organic species.

3.3.3.2 Gold Characterization

Powder X-ray diffraction

The gold on ordered and disordered mesoporous titania were analyzed with x-ray diffraction. The XRD results do not show a very significant difference compared to the bare supports, indicating that the amount of gold on the titania is again quite low. Moreover, the most prominent peaks corresponding to gold generally overlap with the peaks of the anatase crystal structure (**Figure 36**). However, the disordered titania aerogel shows a small peak at 31° which may originate from gold.

It is difficult to observe the gold peaks since the diffractions overlap with the crystal structures of titania. Still, these supports may show an increased signal compared to the material in the last section (3.1), since a larger amount of gold is likely adsorbed on the larger titania surfaces. The crystallite sizes after gold ion-adsorption are similar to the bare supports (7 nm), meaning that there was no significant growth of the titania crystallites during the gold loading procedure.

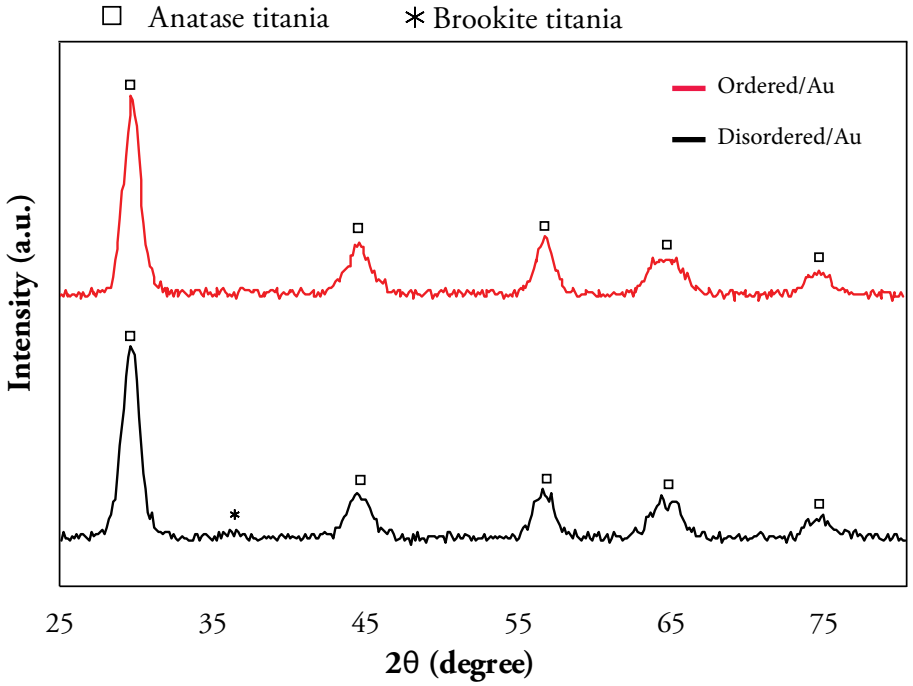

Figure 36: *The XRD diffractograms of the gold on titania supports. The ordered and disordered porous titania both contained crystallite sizes of 7 nm.*

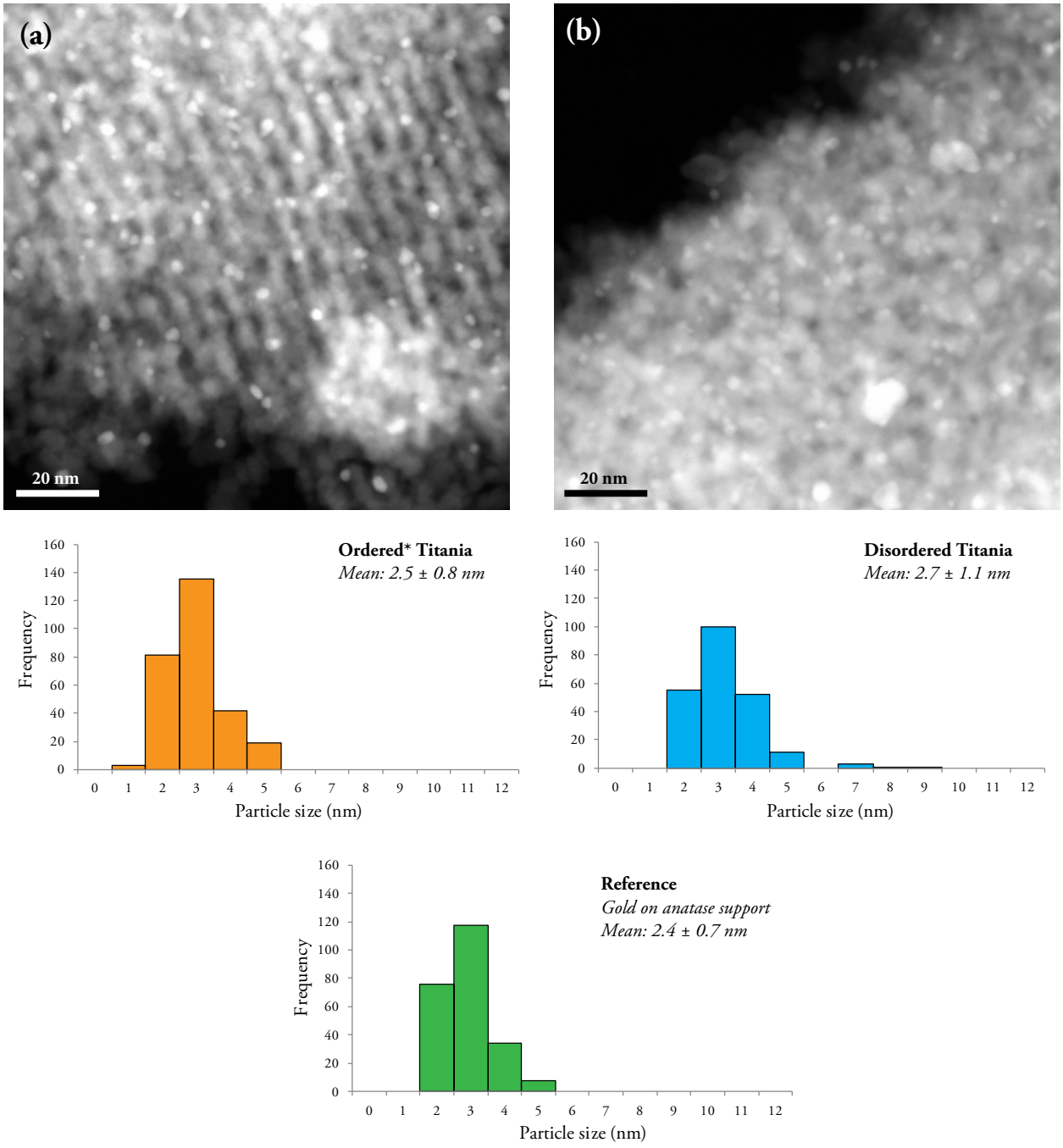

Figure 37: *The HAADF-STEM images of gold nanoparticles deposited on (a) ordered and (b) disordered mesoporous titania and their corresponding gold size distribution histograms, as well as the gold on anatase. The images both contain scale bars of 20 nm.*

Transmission Electron Microscopy

The materials were analyzed with HAADF-STEM to visualize and compare the gold nanoparticles on the ordered and disordered titania (**Figure 37**). Furthermore, histogram plots of the gold size distributions were assembled, originating from the results obtained with iTEM. It becomes apparent that a lot of smaller sized gold nanoparticles ranging from 2 - 5 nm are present on both of these materials and are localized inside the porous spaces of the titania structure. A logical explanation for this would be that the gold particles are confined inside the pores, which inhibits the particles from growing larger. It also appears that the organization of the pore structures, either ordered or disordered, is not of significant influence.

** The measured data of the Au NP's sizes of the ordered histogram mostly originates from ordered titania, however some collapsed parts of the material are taken into account as well.*

However, both the ordered and disordered titania structures have an anatase crystal structure which might simultaneously influence the gold particle formation. In section 3.1.3 it was observed that the anatase structure is accompanied with the formation of small gold nanoparticles with a particle size distribution of 2 - 5 nm. This distribution is very similar to the distributions of the ordered and disordered titania (**Figure 37**). Moreover, the gold nanoparticles present on the external surface of the titania aerogel are significantly larger than the particles inside the pore structures, resulting in a slightly broader size distribution.

ICP-AES

The amount of gold on ordered mesoporous titania and titania aerogel was detected with ICP-AES. The results were acquired from Kolbe in Germany. The percentages of gold on the two titania supports are similar (**Table 12**). A slightly higher gold amount on the ordered mesoporous titania was expected, as the surface areas are 131.0 m^2/g and 146.3 m^2/g for the disordered titania aerogel and ordered titania respectively.

Furthermore, a slightly larger amount of gold is adsorbed on the titania structures than the theoretical 2.00 wt% which was supposed to be added, similar to the gold loading on the amorphous titania support in section 3.1.3.2, where 2.48 wt% of gold was detected. In these two titania structures, it is possible that some water or organic species are still present on the titania.

Table 12: *The amount of gold on the regarding titania supports presented in wt%.*

Catalyst	Gold (wt%)	Dry (wt%)
Au/Ordered	2.18	4.4
Au/Disordered	2.06	4.0

Chapter 4 Conclusion and Outlook

The aim of this project was to investigate the influence of various titania supports on the gold nanoparticle formation. Initially, gold nanoparticles on different support crystallinities were compared, including an anatase titania support, a pure rutile titania support, a mix of the anatase and rutile crystal structure (commercially available Degussa P25) and an amorphous titania support. The crystalline titania supports were synthesized with similar porosity, surface areas (around 20 - 30 m^2/g), and particle sizes. However, TEM analysis showed that the particle sizes of the anatase and rutile supports were significantly larger than the obtained data from the Scherrer equation. Moreover, the amorphous titania support contained a rather large surface area of 293 m^2/g and a significant porosity compared to the crystalline supports.

Furthermore, the gold formation was investigated on three titania aerogel supports containing a low, intermediate, and high surface area of 27.8 m^2/g, 117.7 m^2/g and 168.7 m^2/g. The titania aerogels consisted of crystallite sizes of 13, 8 and 6 nm respectively. Furthermore, the porosity of the three aerogels differed significantly. The aerogel with the lowest porosity included pore sizes between 1 - 5 nm, whereas the other two supports with an intermediate and high surface area contained pore sizes between 2 - 10 nm and 2 - 8 nm respectively, including a larger central pore volume.

At last, the influence of the organization of the internal pore-structure of titania was observed by comparing the gold formation on an ordered mesoporous titania support versus a disordered mesoporous titania aerogel. The supports were both predominantly anatase with crystallite sizes of 7 nm. The pore size distributions of these supports had a range of 2 - 8 nm with a peak around 5 nm. Furthermore, the supports had similar surface areas of 146.3 m^2/g and 131.0 m^2/g for the ordered and disordered porous support respectively.

The titania supports described above have been synthesized successfully. Moreover, the cationic ion-adsorption of $Au(en)_2Cl_3$ was performed on these supports without complications, with a nominal amount of 2.0 wt%. However, on the supports with a large surface area: amorphous titania, ordered and disordered mesoporous titania, a larger amount of gold was adsorbed. This was caused by the assumption that dry titania was used for the ion-adsorption, however TGA-MS analysis showed that the amorphous titania support still contained a significant amount of water. This weight difference was not considered when calculating the amount of gold that was supposed to be added in order to obtain a 2.0 wt%. Similarly, in the other supports, slight amounts of water or organic species were likely present. Thus, the weight percentage of gold on the amorphous, ordered, and disordered mesoporous titania support was slightly larger than expected.

The influence of the titania supports on the formation and growth of gold nanoparticles

In conclusion, the results reveal that the crystal structure of the titania support has a significant influence on the formation of the gold nanoparticles. On the highly anatase titania support, a largely homogeneous distribution of spherical gold nanoparticles was observed. The sizes of these gold nanoparticles contained a size distribution of 2 - 5 nm, which is relatively small. However, on the highly rutile titania support, mostly larger

Au nanoparticles were observed, resulting in a broader gold size distribution with sizes between 1 - 7 nm. The rutile and anatase supports contained gold weight percentages of 0.95 wt% and 0.65 wt% respectively. The higher gold weight percentage on rutile titania was likely influenced by the slight difference in surface area between the two supports. Furthermore, on the commercial Degussa P25 support, an intermediate uniformity and size distribution was observed, caused by the mix of anatase and rutile crystallinity of the titania support. The difference in gold particles on the anatase and rutile phases could be caused by varying metal-support interactions, however more information on the specific anatase and rutile structures is needed to understand these interactions in detail.

The gold particles on the amorphous titania support were formed when the titania was simultaneously crystallizing to the anatase crystal structure with crystallite sizes up to 6 nm. This phenomenon resulted in the formation of extremely small gold particles which were caught in between growing titania crystallites. On the other hand, large chunks of gold particles were formed on the surfaces of the titania. As a result, a very broad size distribution was observed with sizes between 2 - 8 nm. Thus, the crystallinity of the titania support exhibits a striking influence on the formation of gold nanoparticles, including the particle sizes and the dispersion.

Ion-adsorption of the gold precursor on mesoporous titania aerogels with a range of low, intermediate and high surface areas resulted in a few striking differences, including differently shaped gold particles, where the titania aerogel with the lowest surface area contained either a very low amount of gold nanoparticles, or very many gold nanoparticles. This is most likely caused by the irregular, disordered mesopore-structure of the support. On the other hand, the titania aerogels with the intermediate and high surface area contained mainly a similar gold nanoparticle size distribution of approximately 2 - 6 nm. Still, more analysis of the adsorbed gold is needed with ICP-AES. In conclusion, titania aerogels containing a low porosity and surface area contain differently shaped gold nanoparticles compared to aerogels with higher porosities and surface areas.

The ordered and disordered mesoporous titania supports contained a similar gold particle size distribution of 2 - 5 nm, which is strikingly similar to the gold particle size distribution of the anatase titania support. Moreover, the adsorbed amount of gold on both titania supports was quite high and comparable, including 2.06 and 2.18 wt% for the disordered mesoporous titania aerogel and the ordered mesoporous titania respectively. Hence, the organization of the pores, either ordered or disordered, did not have a significant influence on the formation of the gold nanoparticles.

Synthesis strategies to obtain titania structures

The highly anatase crystal phase was reached in the titania support with the sol-gel precipitation procedure. A specific water-alkoxide ratio (20:1) was derived from previous methods described by Wang et al.[14] The calcination was carried out in a fluidized-bed in N_2/O_2 flow, instead of the usual calcination in a stagnant-air oven, in order to diminish the amount of agglomeration between the titania crystals. The highly rutile crystal phase was evenso obtained with the sol-gel precipitation procedure, containing a significantly higher water-alkoxide ratio (165:1). Furthermore, the hydrothermal treatment with 1 M HNO_3 around 180 °C was performed for no longer than three days to obtain the rutile structure successfully. Amorphous titania was synthesized with a significantly lower water-alkoxide ratio (5:1).

Titania Aerogels were successfully obtained containing various porosities and surface areas. The highest porosity and surface areas were obtained when the aerogels were additionally washed with water. Moreover,

the acid-water ratio of the HNO_3 concentrations affected the rate of hydrolysis and condensation during the formation of the aerogels. The best results were obtained with acid concentrations of 0.05 M or higher.

Ordered mesoporous titania was successfully obtained and reproduced via mixed inorganic precursors, including $TiCl_4$ and TTIP, structure-directing agent Pluronic F127 and the addition of water, which was preferred over the EISA method. Moreover, the stabilization of the structure with a three-day heat treatment (60 - 100 - 130 °C) was essential to preserve the stability of the pore-structure during calcination. The heating rate during the stabilization and calcination is of great importance, since a large heating rate removes the surfactants too quickly, making the structure more liable to collapse due to capillary tension. The best results were obtained with heating rates of 1 °C/min in a homogeneously heated muffle furnace.

4.1 Outlook

Influence of alternative titania supports on the gold nanoparticle formation

Based on the findings from this study, it might be interesting to see how the gold nanoparticles are formed on titania supports with either a larger or smaller pore size distribution. The confinement of the gold nanoparticles can be studied with micro- and macroporous titania supports. Furthermore, it might be interesting to investigate even differently shaped pore sizes, such as titania nanotubes.

Aside form the porous material, it could be interesting to investigate differently shaped titania structures to acquire more insight on the localization of the gold nanoparticles. For instance, titania nanorods, nanowires or nanosheets can be used as a support.

Catalytic tests with the synthesized Au/TiO_2 catalysts on the oxidation of CO

The sizes of the gold nanoparticles are strongly influence the catalytic activity of the oxidation reaction of CO to CO_2. Catalytic tests with the synthesized Au/TiO_2 catalysts can be done in future studies. The gold on anatase titania will probably give the best results due the small gold nanoparticles of 2 - 5 nm. This is based on the fact that the supported gold catalysts are only catalytically active when the particles are smaller than 5 nm. However, the anatase titania phase is metastable and a phase transition of anatase to rutile titania could occur.[43] As a result, this phase transition might cause coalescence of the gold nanoparticles, which is highly undesirable as the catalytic activity will decrease when larger gold particles are formed.

The mesoporous supports may be excellent candidates for catalytic experiments, since the gold nanoparticles are confined, so the growth is inhibited. This results in gold nanoparticles of approximately the same sizes, which also will not sinter easily due to the pore-structure. However, the pore-structure can still collapse so a strong, thermally stable structure needs to be obtained.

Stability tests on Au/TiO_2 catalysts

The stability of the synthesized gold on titania catalysts is critical in further studies, for instance during the catalytic oxidation of CO. In order to see if the Au/TiO_2 catalysts are stable during industrial processes, stability tests can be performed on the Au/TiO_2 catalysts.

Acknowledgements

First, I would like to thank Mark Meijerink for being my daily supervisor. He provided guidance and support throughout the project and stimulated me to think of new ideas.

Also, I want to thank Jovana Zecevic and Petra de Jongh for the advice and discussions about the obtained results. Furthermore, my appreciation goes out to the Inorganic Chemistry & Catalysis group for allowing me to do research on an exciting project. The following people have helped me significantly during my studies at the group:

Renée van Alst
Iris Teune
Jochem Wijten
Remco Dalebout (N_2 physisorption)
Lennart Weber (N_2 physisorption)
Marjan Versluijs-Helder (XRD / TGA-MS)
Chris Schneijdenberg (CPD)
Patrick Springer from Kolbe (ICP-AES)

Bibliography

1. Jong, K. P. de, *et al*, (**2016**), MSc Course Synthesis of Heterogeneous Catalysts & Related Materials part 1 – Synthesis of Supported Catalysts.

2. Watanabe, R. and Masuda, Y., (**1975**), Sintering and Catalysis, G. C. Kuczynski, ed., Plenum Press, New York, 389 - 398.

3. Haruta, M., (**2005**), Gold Rush., Nature, 437, 1098 - 1099.

4. Hutchings, G. J., (**2005**), Catalysis by gold, Catalysis Today, 100 (1–2), 55 - 61.

5. Haruta, M. *et al*, (**1989**), Gold catalysts prepared by co-precipitation for low-temperature oxidation of hydrogen and of carbon monoxide, Journal of Catalysis, 115, 301 - 309.

6. Haruta, M. *et al*, (**1993**), Low-Temperature Oxidation of CO over Gold Supported on TiO_2, alpha-Fe_2O_3, and Co_3O_4, Journal of Catalysis, 144, 175 - 192.

7. Hutchings, G. J., (**1985**), Vapor phase hydrochlorination of acetylene: Correlation of catalytic activity of supported metal chloride catalysts, Journal of Catalysis, 96 (1), 292 - 295.

8. Hashmi, A. S. K. and Hutchings, G.J., (**2006**), Gold Catalysis, Angewandte Chemie - International Edition, 45 (47), 7896 - 7936.

9. a) Boccuzzi, F. *et al*, (**1996**), FTIR Study of Carbon Monoxide Oxidation and Scrambling at Room Temperature over Gold Supported on ZnO and TiO_2 . 2, The Journal of Physical Chemistry, 100 (9), 3625 - 3631. b) Hayashi, T. *et al*, (**1998**), Selective Vapor-Phase Epoxidation of Propylene over Au/TiO_2 Catalysts in the Presence of Oxygen and Hydrogen, Journal of Catalysis, 178 (2), 566 - 575.

10. Delannoy, L. *et al*, (**2014**), Selective hydrogenation of butadiene over TiO_2 supported copper, gold and gold-copper catalysts prepared by deposition-precipitation, Phys. Chem. Chem. Phys., 16, 26514 - 26527.

11. Haruta, M., (**2002**), Catalysis of Gold Nanoparticles Deposited on Metal Oxides, Cattech, 6 (3), 102 - 115.

12. Haruta, M. and Daté, M., (**2001**), Advances in the catalysis of Au nanoparticles, Applied Catalysis A: General, 222 (1–2), 427 - 437.

13. Meijerink, M. J. *et al*, (**2017**), Stability of Silicon Dioxide in Liquid Phase TEM, Microscopy and Microanalysis, 23 (Suppl 1), 868.

14. Wang, C.-C. and Ying, J. Y., (**1999**), Sol–Gel Synthesis and Hydrothermal Processing of Anatase and Rutile Titania Nanocrystals, Chemistry of Materials, 11 (11), 3113 - 3120.

15. a) Chen, X. and Mao, S. S., (**2007**), Titanium Dioxide Nanomaterials: Synthesis, Properties, Modifications, and Applications, Chem. Rev., 107 (7), 2891 - 2959. b) Claudionico, **(2013)**, Sol-Gel, URL: https://en.wikipedia.org/wiki/Sol-gel

16. Brinker, C. J. and Scherer, G.W., (**1990**), Sol-Gel Science: The Physics and Chemistry of Sol-Gel Processing, Academic Press London, 8.

17. Danks, A. E. *et al*, (**2016**), The Evolution of "Sol–Gel" Chemistry as a Technique for Materials Synthesis, Materials Horizons, 3, 91 - 112.

18. Malinowska, B. *et al*, (**2003**), Titania aerogels: Preparation and photocatalytic tests, International Journal of Photoenergy, 5 (3), 147 - 152.

19. Loryuenyong, V. *et al*, (**2012**), The synthesis of microporous and mesoporous titania with high specific surface area using sol-gel method and activated carbon templates, Materials Letters, 87, 47 - 50.

20. Barbé, C. J. *et al*, (**1997**), Nanocrystalline titanium oxide electrodes for photovoltaic applications, J. Amer. Ceramic Soc, 80 (12), 3157 - 3171.

21. Woodley, S. M. and Catlow, C. R. A., (**2009**), Structure prediction of titania phases: Implementation of Darwinian versus Lamarckian concepts in an Evolutionary Algorithm, Computational Materials Science, 45 (1), 84 - 95.

22. Watson, J. M. *et al*, (**2005**), Nanoglued titanium dioxide aerogels for photocatalysis, Environmental Engineering Science, 22 (5), 666 - 675.

23. Teichner, S. J. *et al*, (**1976**), Inorganic oxide aerogels, Advances in Colloid and Interface Science, 5 (3), 245 - 273.

24. Aguado-Serrano, J. and Rojas-Cervantes, M. L., (**2006**), Titania aerogels: Influence of synthesis parameters on textural, crystalline, and surface acid properties, Microporous and Mesoporous Materials, 88 (1–3), 205 - 213.

25. Schneider, M. and Baiker, A., (**1992**), High-surface-area Titania Aerogels: Preparation and Structural Properties, J. Mater. Chem., 2 (6), 587 - 589.

26. Dagan, G. and Tomkiewicz, M., (**1994**), Preparation and characterization of TiO_2 photocatalysts aerogels for use as photocatalyst, Journal of Non-Crystalline Solids, 175, 294 - 302.

27. Dagan, G. and Tomkiewicz, M., (**1993**), Titanium dioxide aerogels for photocatalytic decontamination of aquatic environments, The Journal of Physical Chemistry, 97 (49), 12651 - 12655.

28. Zhao, D. *et al*, (**2013**), Ordered Mesoporous Materials, Wiley-VCH Verlag GmbH & Co.

29. Brinker, J. C. *et al*, (**1999**), Evaporation-Induced Self-Assembly: Nanostructures Made Easy, Advanced Materials, 11 (7), 579 - 585.

30. Crepaldi, E. L. *et al*, (**2003**), Controlled formation of highly organized mesoporous titania thin films: From mesostructured hybrids to mesoporous nanoantase TiO_2, Journal of American Chemical Society, 125 (32), 9770 - 9786.

31. Yang, P. *et al*, (**1999**), Block copolymer templating syntheses of mesoporous Metal Oxides with large ordering lengths and semicrystalline framework, Chem. Mater., 11 (10), 2813 - 2826.

32. Uchida, H. *et al*, (**2010**), Highly-ordered mesoporous titania thin films prepared via surfactant assembly on conductive indium-tin-oxide/glass substrate and its optical properties, Thin Solid Films, 518 (12), 3169 - 3176.

33. Tian, B. *et al*, (**2002**), Fast preparation of highly ordered nonsiliceous mesoporous materials via mixed inorganic precursors, Chemical communications (Cambridge, England), No. 17, 1824 - 1825.

34. Li, H. *et al*, (**2008**), Synthesis of well-ordered mesoporous titania powder with crystallized framework, Materials Letters, 62 (8–9), 1410 - 1413.

35. Grosso, D. *et al*, (**2001**), Highly organized mesoporous titania thin films showing mono-oriented 2D hexagonal channels, Advanced Materials, 13 (14), 1085 - 1090.

36. Kipkemboi, P. *et al*, (**2001**), Triblock copolymers as templates in mesoporous silica formation: Structural dependence on polymer chain length and synthesis temperature, Langmuir, 17 (17), 5398 - 5402.

37. Alberius, P. C. A. *et al*, (**2002**), General predictive syntheses of cubic, hexagonal, and lamellar silica and titania mesostructured thin films, Chemistry of Materials, 14 (8), 3284 - 3294.

38. Liu, K. *et al*, (**2005**), Preparation of large-pore mesoporous nanocrystalline TiO_2 thin films with tailored pore diameters, Journal of Physical Chemistry B, 109 (40), 18719 - 18722.

39. Zimny, K. *et al*, (**2010**), Highly ordered mesoporous titania with semi crystalline framework templated by large or small nonionic surfactants, New Journal of Chemistry, 34 (10), 2113 - 2117.

40. Porta, F. *et al*, (**2000**), Metal sols as a useful tool for heterogeneous gold catalyst preparation: Reinvestigation of a liquid phase oxidation, Catalysis Today, 61 (1), 165 - 172.

41. Thompson, D. T. *et al*, (**2007**), Using Gold Nanoparticles for catalysis, Nanotoday, 2 (4), 40 - 43.

42. Hiemstra, T. and Riemsdijk, W. H. van, (**1996**), A Surface Structural Approach to Ion Adsorption: The Charge Distribution (CD) Model, Journal of Colloid and Interface Science, 179 (2), 488.

43. Hadjiivanov, K. I. *et al*, (**1996**), Surface chemistry of titania (anatase) and titania-supported catalysts, Chemical Society Reviews, 25 (1), 61.

44. Zanella, R. *et al*, (**2002**), Alternative Methods for the Preparation of Gold Nanoparticles Supported on TiO_2, J. Phys. Chem., 106 (31), 7634 - 7642.

45. Zanella, R. *et al*, (**2005**), Mechanism of deposition of gold precursors onto TiO_2 during the preparation by cation adsorption and deposition-precipitation with NaOH and urea, Applied Catalysis A: General, 291 (1–2), 62 - 72.

46. Block, B. P. and Bailar, J. C., (**1951**), The Reaction of Gold(III) with Some Bidentate Coordinating Groups, 73, 4722 - 4725.

47. Guillemot, D. *et al*, (**1996**), Preparation of nanometeric gold particles on NaHY, Catalysis letters, 41, 143 - 148.

48. Zhu, H. *et al*, (**2006**), Preparation of Highly Active Silica-Supported Au Catalysts for CO Oxidation by a Solution-Based Technique, Society, No. 1, 10842 - 10848.

49. Zhu, H. *et al*, (**2007**), Low-temperature CO oxidation on Au/fumed SiO2-based catalysts prepared from Au(en)2Cl3 precursor, Applied Catalysis A: General, 326 (1), 89 - 99.

50. McCafferty, E. and Wrightman, J.P., (**1998**), Determination of the Concentration of Surface Hydroxyl Groups on Metal Oxide Films by a Quantitative XPS Method, Surface and Interface Analysis, No. 26, 549 - 564.

51. a) Dinnebier, R.E. and Billinge, S. J. L., (**2008**), Powder diffraction: theory and practice, Royal Society of Chemistry, RSC Publishing. b) Patterson, A. L. (**1939**), The scherrer formula for X-ray particle size determination, Physical Review, 56 (10), 978 - 982.

52. Brunauer, S., *et al*, (**1938**), Adsorption of Gases in Multimolecular Layers. J. Am. Chem. Soc. 60, 309 - 319.

53. Jongh, P.E. de. *et al*, (**2017**), MSc Course Adsorption, Kinetics and Catalysis - Part 3: Physisorption.

54. Moulijn, J. A., *et al*, (**2006**), Heterogeneous Catalysis for chemical engineers, DelftChemTech, Section R&CE.

55. Harris, D. C., *et al*, (**2010**), Quantitative chemical analysis. Eighth edition, W. H. Freeman and Company.

56. Concordia College, Simultaneous Determination of Manganese and Nickel in Steel by Inductively Coupled Plasma Atomic Emission Spectrometry. URL: http://sites.cord.edu/chem-330-lab-manual/experiments/icp-aes, Accessed December 5th, 2017.

57. Tauster, S. J., (**1987**), Strong Metal-Support Interactions, Accounts of Chemical Research, 20 (11), 389 - 394.

58. Comotti, M. *et al*, (**2006**), Support effect in high activity gold catalysts for CO oxidation, Journal of the American Chemical Society, 128 (3), 917 - 924.

59. Titanium(IV) oxide nanopowder, Sigma-Aldrich, URL: https://www.sigmaaldrich.com/catalog/product/aldrich/718467?lang=en&region=NL, last accessed 11 January 2018.

60. Science Media group, A Phase Diagram for Carbon Dioxide, URL: https://www.learner.org/courses/chemistry/text/text.html?dis=U&num=Ym5WdElUQS9NeW89&sec=YzJWaklUQS9PU289, last accessed 15 January 2018.

Appendix

A Shrinkage caused by drying

Shrinkage of the titania material can originate from the drying step (**Figure I**). When the tiania gels are dried, the pores start to shrink and follow the three stages stated below:

I. Initial condition: The pores are filled with solvent, there is a flat meniscus with a large radius. Moreover the capillary tension is low.

II. Constant rate period: Shrinkage of the material starts to occur. There is a rise in tension until a certain critical point.

III. Falling rate period: The solvent in the pores starts to retract and the pores become empty. This is accompanied with a large meniscus and the radius of the meniscus is equal to the pore radius. At this point, the pores are likely to collapse.

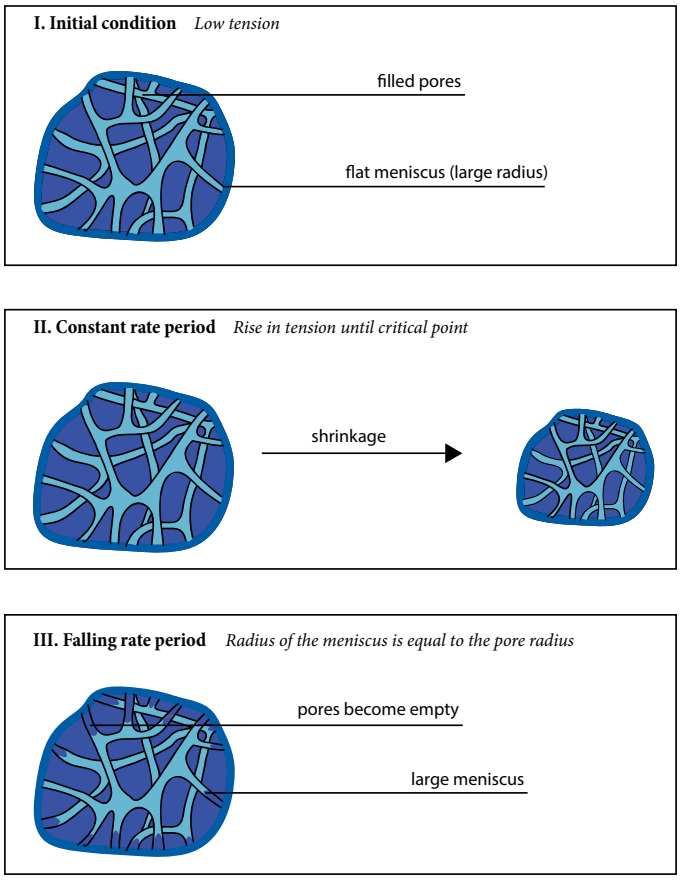

Figure I: *A schematic representation of shrinkage caused by drying.*[29]

B Crystalline and Amorphous titania supports

The following calculations were done to determine the amount of reagents which should be used per titania support.

Anatase Titania
Molar ratio TTIP:Ethanol:water (1:10:20) and water-ethanol (1:2)

4 g TTIP / 284.22 g/mol = 14.07 mmol TTIP
14.07 mmol · 20 = 0.28 mol H_2O
0.28 mol · 18.016 = 5.07 g H_2O

14.07 mmol · 10 = 0.14 mol ethanol
0.14 mol · 46.07 g/mol = 6.48 g ethanol

Water-ethanol mixture:
0.28 mol · 2 = 0.56 mol ethanol
0.56 mol · 46.07 g/mol = 25.8 g ethanol

Rutile Titania
Molar ratio TTIP:Ethanol:water (1:10:165) and water-ethanol (2:1)

4 g TTIP / 284.22 g/mol = 14.07 mmol TTIP
14.07 mmol · 165 = 2.32 mol H_2O
2.32 mol · 18.016 = 41.83 g H_2O

14.07 mmol · 10 = 0.14 mol ethanol
0.14 mol · 46.07 g/mol = 6.48 g ethanol

Water-ethanol mixture:
2.32 mol / 2 = 1.16 mol ethanol
1.16 mol · 46.07 g/mol = 53.44 g ethanol

Amorphous Titania
Molar ratio TTIP:Ethanol:water (1:10:5) and water-ethanol (1:2)

2 g TTIP / 284.22 g/mol = 7.04 mmol TTIP
7.04 mmol · 5 = 0.035 mol H_2O
0.035 mol · 18.016 = 0.63 g H_2O

7.04 mmol · 10 = 0.07 mol ethanol
0.07 mol · 46.07 g/mol = 3.24 g ethanol

Water-ethanol mixture:
0.035 mol · 2 = 0.07 mol ethanol
0.07 mol · 46.07 g/mol = 3.22 g ethanol

Powder X-ray Diffraction

A large overview of the XRD diffractograms obtained from the EVA program are shown below. The images include the (a) anatase and (b) rutile titania support, (c) the amorphous titania support, and (d) a representative diffractogram of the commercial P25 Degussa.

(a)

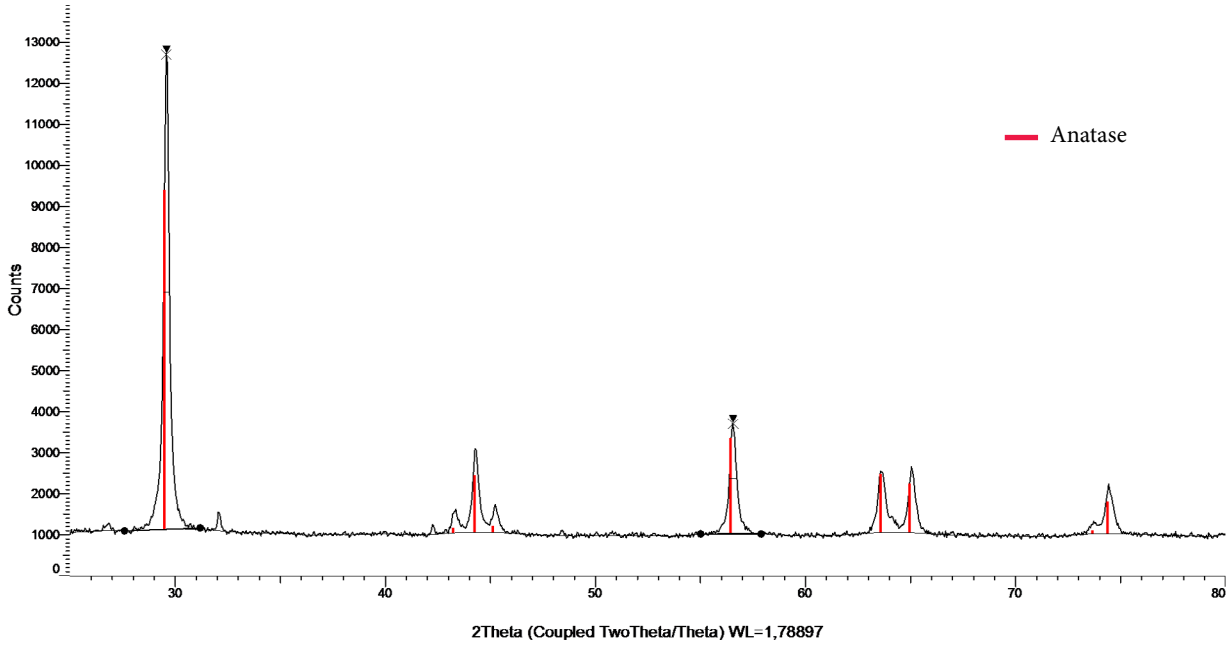

(b)

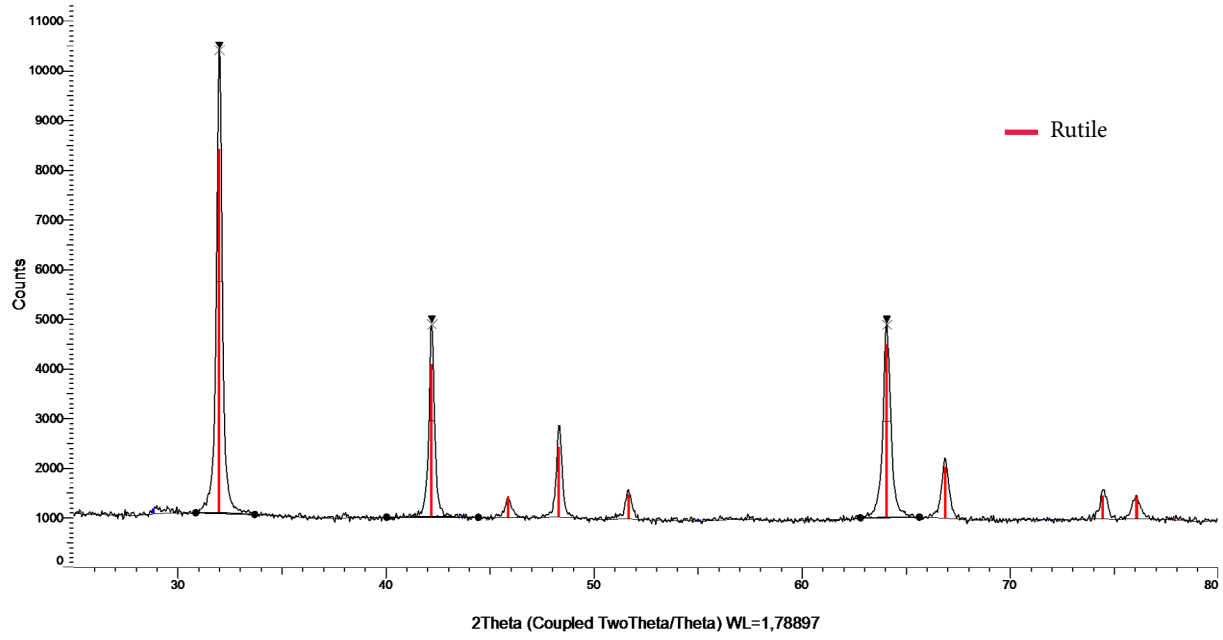

(c)

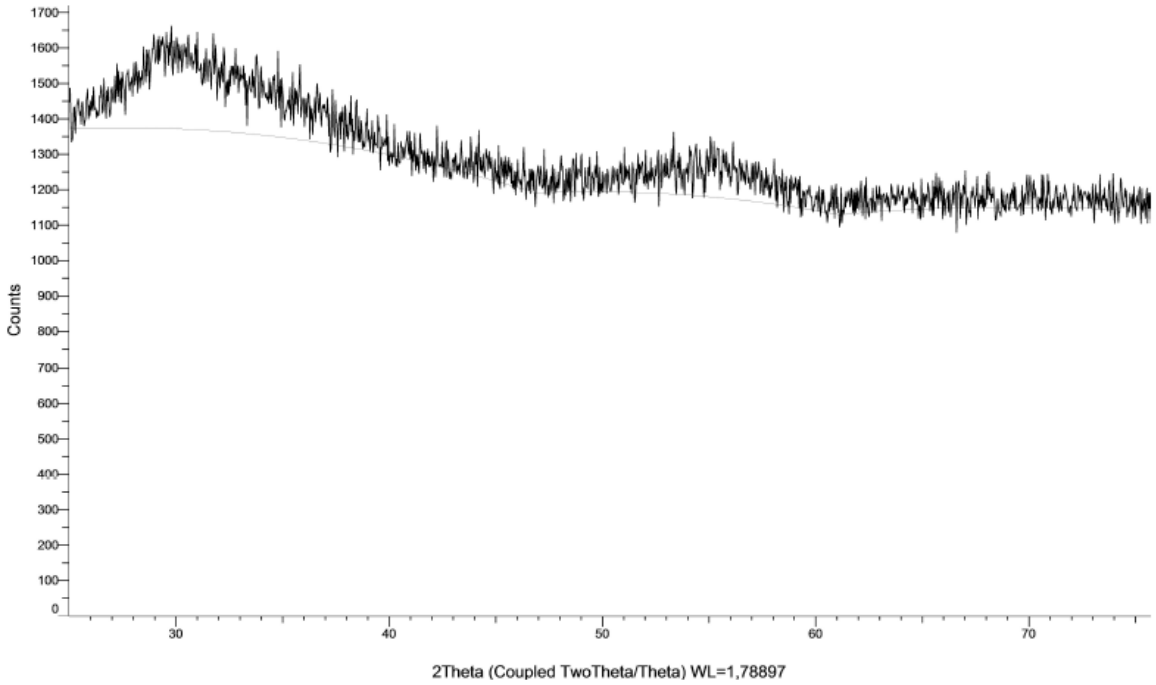
Counts
2Theta (Coupled TwoTheta/Theta) WL=1,78897

(d)

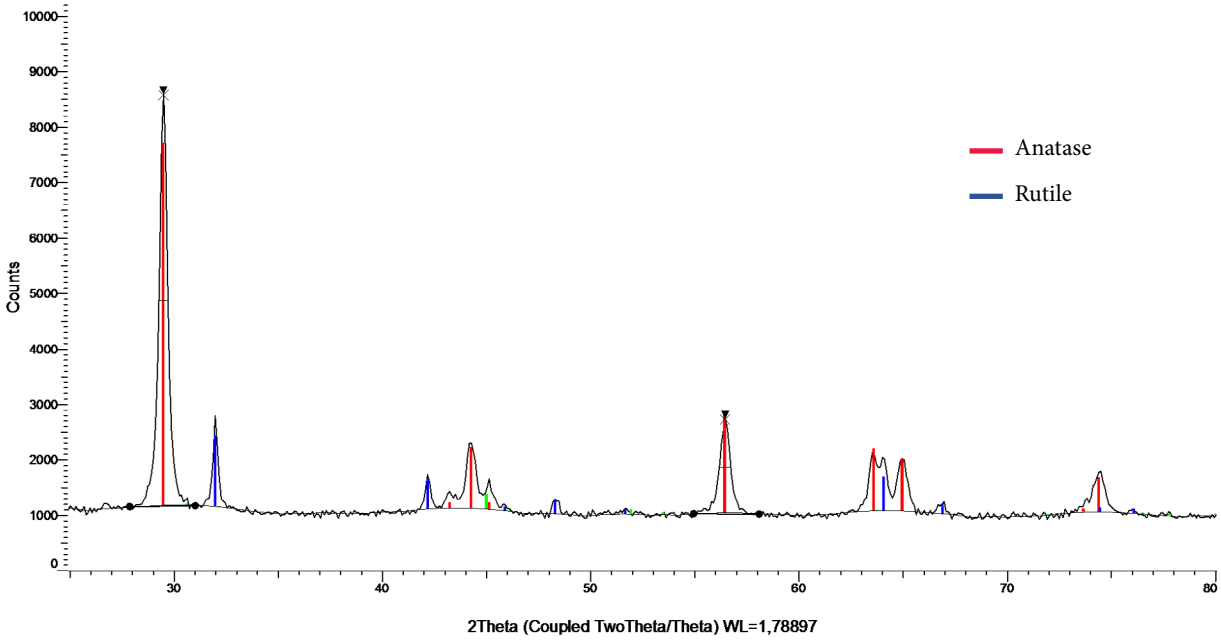
Anatase
Rutile
Counts
2Theta (Coupled TwoTheta/Theta) WL=1,78897

C Ordered Mesoporous Titania

Detailed synthesis procedures of the attempts to synthesize OMT are described below.

Entry 1 - Inside a glovebox, 1.0 g of Pluronic P123 was dissolved in 13 mL anhydrous Ethanol. To this solution 1.9 g $TiCl_4$ was added dropwise. The solution was brought into a petri-dish. The dish was covered with aluminum foil and it was aged in an oven at 60 °C for 5 days. A brown color was observed on the edges of the sample and in the middle cracks were seen. The precipitate was transferred to a ceramic dish and it was dried at room temperature for 6 days. The precipitate was calcined at 400 °C for four hours with a heating rate of 10 °C/min. The final powder was light yellow/white of color and contained some dark grains.

Entry 2 - An amount of 1.16 g of Pluronic P123 was dissolved in 10.0 g anhydrous ethanol. To this solution 1.9 g $TiCl_4$ was added dropwise. The solution was brought into a petri-dish. The dish was covered with parafilm and it was aged at room temperature for 6 days. The parafilm was removed and the gel was dried for another 5 days. The gel was clear with no cracks and it was transferred to a ceramic dish for calcination. The precipitate was calcined at 400 °C for four hours with a heating rate of 2 °C/min. The final powder was white with a brittle, needle-like texture.

Entry 3 - Again, 1.16 g of Pluronic P123 was dissolved in 10.0 g anhydrous Ethanol. To this solution 1.9 g $TiCl_4$ was added dropwise. The solution was split in two fractions and were both brought into open petri-dishes. One fraction was aged at 40 °C on a heater for 5 days. The other fraction was aged at room temperature. Both fractions were aged for a total of 21 days. The fractions were stabilized using heat treatment X. Next, the fractions were devided and calcined at 400 °C for four hours with a heating rate of 2 °C/min. The samples were characterized after the heat treatment and after calcination.

Entry 4 (a) - A solution of 18.33 g anhydrous ethanol, 1.36 g Pluronic F127 and 1.90 g $TiCl_4$ was prepared. To this solution, 1.86 g demi-water was slowly added with a pipette. The clear and slightly viscous solution was poured into two petri dishes. One petri dish with lid and one without lid. The solutions were aged at room temperature for 11 days. The two samples were stabilized using the heat treatment X. Approximately half of each sample was calcined at 400 °C for four hours with a heating rate of 2 °C/min.

Entry 4 (b) - A mixture of 18.3 anhydrous ethanol, 0.65 g Pluronic F127, 1.8 g $TiCl_4$ and 1.79 g demi-water was prepared similar to entry 4 (a) and was aged for 8 days at room temperature. (Difference: a lower F127 concentration was used)

Entry 5 - A solution of 18.30 g anhydrous ethanol, 0.69 g Pluronic F127 and 1.96 g $TiCl_4$ was prepared. To this mixture, 1.8 g demi-water was slowly added with a pipette. The clear and slightly viscous solution was poured into two petri dishes. An additional amount of 0.93 g demi-water was added to one of the petri dishes, thus it contained twice as much water compared to the previous samples, and was aged at room temperature. The other petri dish was aged on a heating plate at 40 °C. The solutions were aged for one week. The two samples were stabilized in an oven using the heat treatment X. Approximately half of each sample was calcined at 400 °C for four hours with a heating rate of 0.5 °C/min.

Entry 6 - A mixture of 1.17 g F127, 20.0 g anhydrous ethanol, 0.6 g $TiCl_4$ and 2.50 g TTIP was prepared. A pH of ~1 was measured. Demi-water was added dropwise to the mixture while stirring (20 drops

was equal to 0.63 g H_2O). The mixture was stirred for two hours. The pH was measured again (~2). The clear solution was devided over a petri dish and a round bottom flask. The solution in the petri dish was put in the oven to age at 40 °C for 24 hours. The solution in the round bottom flask was vacuum dried to remove the solvent instantly and was left overnight. The next morning, the round bottom flask was brought inside the oven at 40 °C to age for eight hours before the stabilizing heat treatment (X) inside the same oven. The samples in the oven had become brown-red and were split in half. Half of each sample was calcined at 400 °C for four hours with a heating rate of 1 °C/min.

Entry 7 - Initially, 3.63 g Pluronic F127 was weighed in a beaker and 60.1 g anhydrous ethanol, 1.70 g $TiCl_4$ and 4.7 g TTIP were added in that order. The titanium precursors were added dropwise and with caution. Afterwards, water was added dropwise while stirring until a clear mixture was observed. The mixture was stirred for two hours. The solvent was transferred to three petri dishes, (1) was aged at 60 °C and was stabilized according to heat treatment X, (2) was aged at 40 °C and followed the same heat treatment (X), and (3) was aged at 40 °C and was stabilized according to heat treatment Y. After heat treatment the clear samples had turned beige/brown and cracks were seen on the surface. Parts of each sample was retrieved for TEM and XRD characterization. The three samples were eventually calcined at 400 °C for four hours with a heating ramp of 1 °C/min.

Table I: *The above table shows an overview of the results of the attempts to acquire ordered mesoporous titania. [a] The uncalcined titania was starting to show ordering (intermediate), [b] Ordering was observed in the uncalcined titania. n.d. not determined.*

Entry	Aging T (°C)	Crystallite sizes (size)	TEM	BET surface area	BJH pore size range	Total pore volume
1	60	Anatase (13 nm)	Disordered	74.2 m^2/g	2 - 40 nm	0.16 cm^3/g
2	RT	Anatase (12 nm)	Disordered	n.d.	n.d.	n.d.
3	RT	Anatase (20 nm)	n.d.	n.d.	n.d.	n.d.
	40	Anatase (16 - 20 nm)	[a]Disordered	n.d.	n.d.	n.d.
4a	RT	Anatase (17 nm)	[b]Disordered	n.d.	n.d.	n.d.
	RT	Anatase (15 nm)	Disordered	n.d.	n.d.	n.d.
4b	RT	Anatase (10 nm)	[b]Disordered	n.d.	n.d.	n.d.
	RT	Anatase (10 nm)	Disordered	46.0 m^2/g	2 - 14 nm	0.06 cm^3/g
5	40	Anatase (11 nm)	Disordered	n.d.	n.d.	n.d.
	RT	Anatase (14 nm)	Disordered	n.d.	n.d.	n.d.
6	40	Anatase (n.d.)	Ordered	138.5 m^2/g	n.d.	n.d.
	[c] RT / 40	Anatase (n.d.)	Disordered	n.d.	n.d.	n.d.
7	40	Anatase (8 nm)	n.d.	n.d.	n.d.	n.d.
	40	Anatase (9 nm)	n.d.	n.d.	n.d.	n.d.
	60	Anatase (7 nm)	Ordered	146.3 m^2/g	2 - 8 nm	0.20 cm^3/g

Powder X-ray Diffraction

In entries 6 and 7, several samples showed some diffraction around 1.1° - 1.2° degrees (**Figure IIa and b**). Titania from entry 6, aged at 40 °C, contained a light and darker part after stabilization, where the dark material contained a significant peak around 1.1° degrees after calcination, even after calcination. The titania samples from entry 7 also showed a slight peak around 1.1°, however the sample which was aged at 60 °C contained the sharpest peak, indicating that this material had a higher ordering of the pore-structure. The results of the other two samples aged at 40 °C are merely based on the low-angle XRD analysis and were not verified with HAADF-STEM.

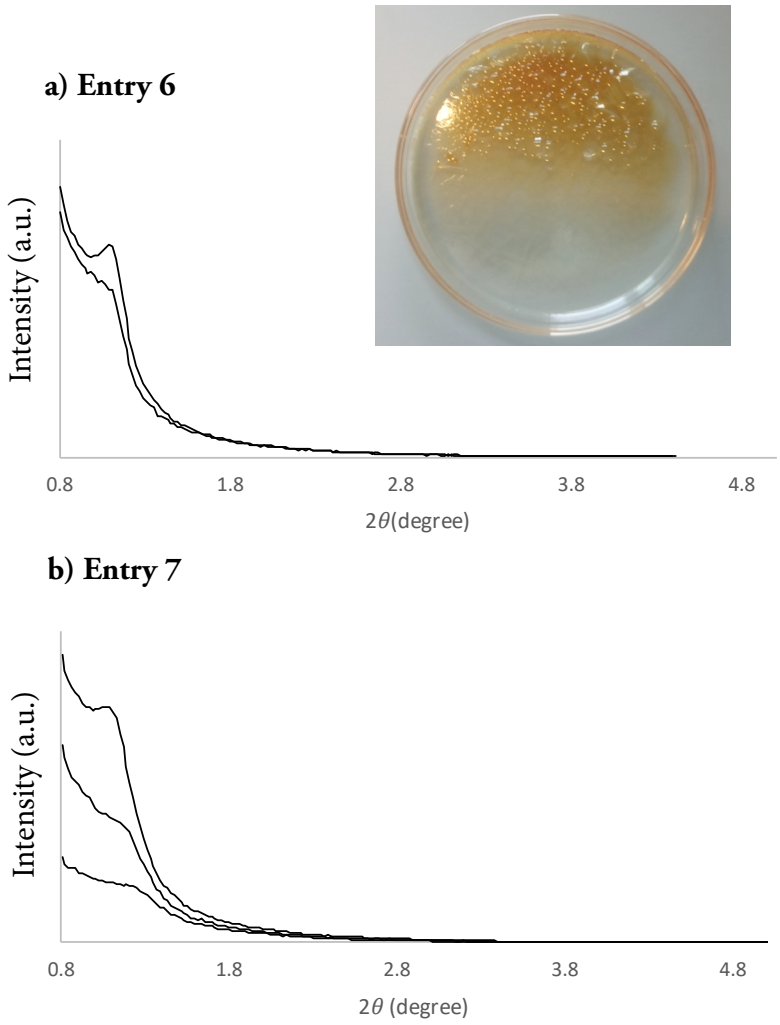

Figure II: *Low angle XRD diffractograms of the samples from (a) entry 6 and (b) entry 7. The best ordering of the pore-structure was observed at an aging temperature at 40 °C for entry 6 and 60 °C for entry 7.*

D Titania Aerogels

Calculations of HNO_3 concentrations:

2.5 mL HNO_3 (70%) + 22.5 mL water = 25 mL in total
2.5 mL · 0.7 · 1.413 g/mL= 2.47 g
2.47/63.01 = 0.04 mol
0.04/0.025 = 1.57 M

2.15 mL HNO_3 (70%) + 22.85 mL water = 25 mL in total
2.15 mL · 0.7 · 1.413 g/mL= 2.13 g
2.13/63.01 = 0.03 mol
0.03/0.025 = 1.35 M

3.10 mL HNO_3 (70%) + 21.9 mL water = 25 mL in total
2.5 mL · 0.7 · 1.413 g/mL= 3.07 g
3.07/63.01 = 0.05 mol
0.05/0.025 = 1.95 M

Critical point drying (CPD)

The critical point for CO_2 is around 31 °C and 73 atm.

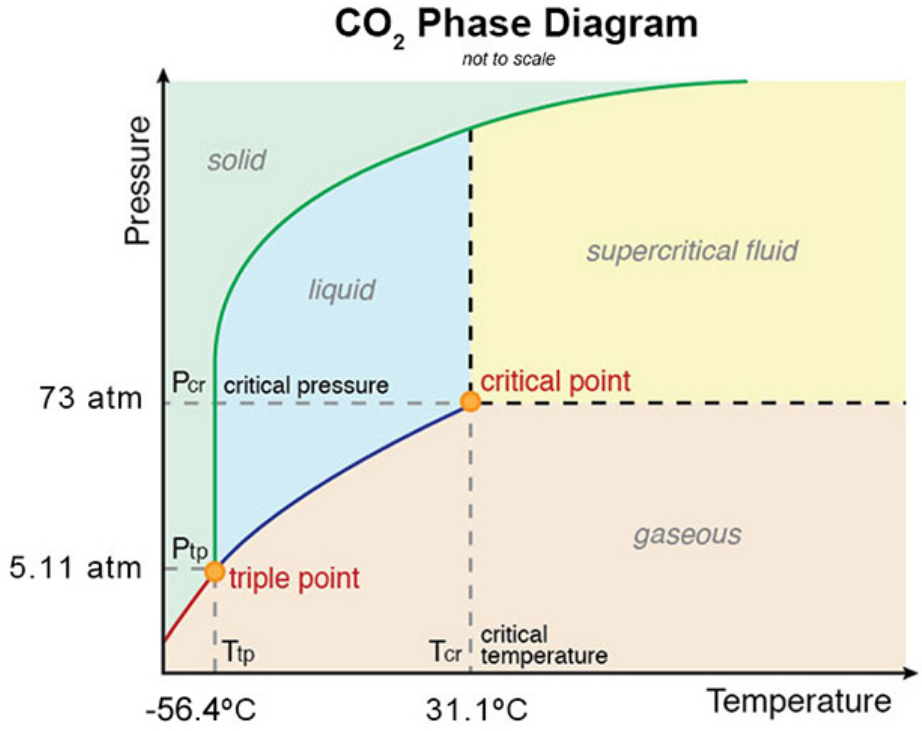

Figure III: *A phase diagram of carbon dioxide with pressure against temperature. A supercritical fluid is formed around the critical point.*[60]

Results overview

An overview of the results of all the aerogel entries is presented in **Table II**. Aerogel D was not additionally washed with water, however it was aged for a significantly longer period (4 months), which might be the cause of the higher surface area compared titania aerogels 3 and 5. Titania aerogels of entries 1, 3, D, 7 and 8 were not used for gold loading purposes, because a low yield was obtained or there was no time. The XRD diffractogram is presented in **Figure III**.

Table II: *The above table shows an overview of the results of the titania aerogel samples.*

Entry	Crystallinity (size)	TEM	BET surface area	BJH pore size range	Total pore volume	Micropore volume
1	Anatase (5 nm)	Disorder	182.4 m^2/g	1 - 5 nm	0.13 cm^3/g	-0.01 cm^3/g
2	Anatase/brookite (8 nm)	Disorder	117.7 m^2/g	2 - 8 nm	0.17 cm^3/g	0.00 cm^3/g
3	Anatase (15 nm)	Disorder	44.4 m^2/g	2 - 6 nm	0.04 cm^3/g	0.00 cm^3/g
D	Anatase (7 nm)	n.d.	123.4 m^2/g	1 - 6 nm	0.11 cm^3/g	-0.01 cm^3/g
4	Anatase/brookite (7 nm)	n.d.	131.0 m^2/g	2 - 7 nm	0.16 cm^3/g	-0.01 cm^3/g
[b]5	Anatase (13 nm)	Disorder	27.8 m^2/g	1 - 5 nm	0.02 cm^3/g	0.00 cm^3/g
[b]6	Anatase/brookite (7 nm)	Disorder	168.7 m^2/g	2 - 8 nm	0.21 cm^3/g	-0.01 cm^3/g
[c]7	Anatase/brookite (8 nm)	n.d.	n.d.	n.d.	n.d.	n.d.
[c]8	Anatase/brookite (8 nm)	n.d.	n.d.	n.d.	n.d.	n.d.

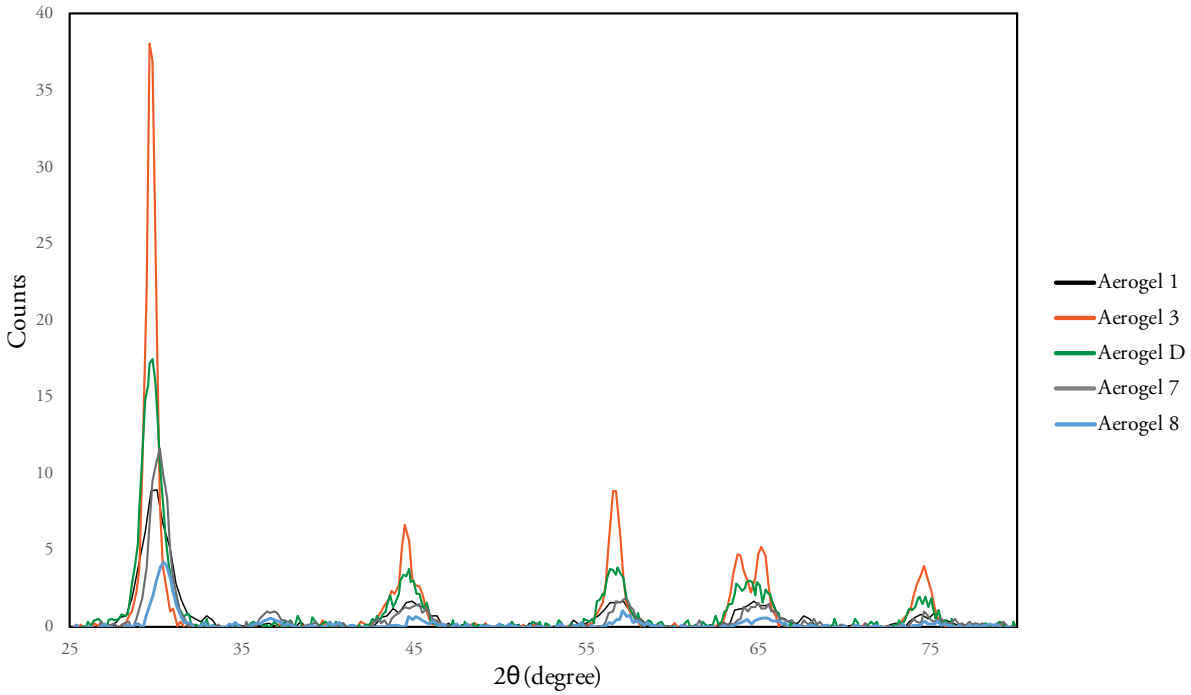

Figure III: *The XRD diffractograms of the other titanium aerogels, entries 1, 3, D, 7 and 8.*

Nitrogen physisorption overview

All titania aerogels were analyzed with N_2 physisorption, with exception of aerogels 7 and 8 due to lack of time. The nitrogen isotherms and BJH pore size distributions of the other titania aerogels, entry 1, 3 and D, are presented in **Figure IV**. These aerogels were not suitable for the gold-loading process due their low yields.

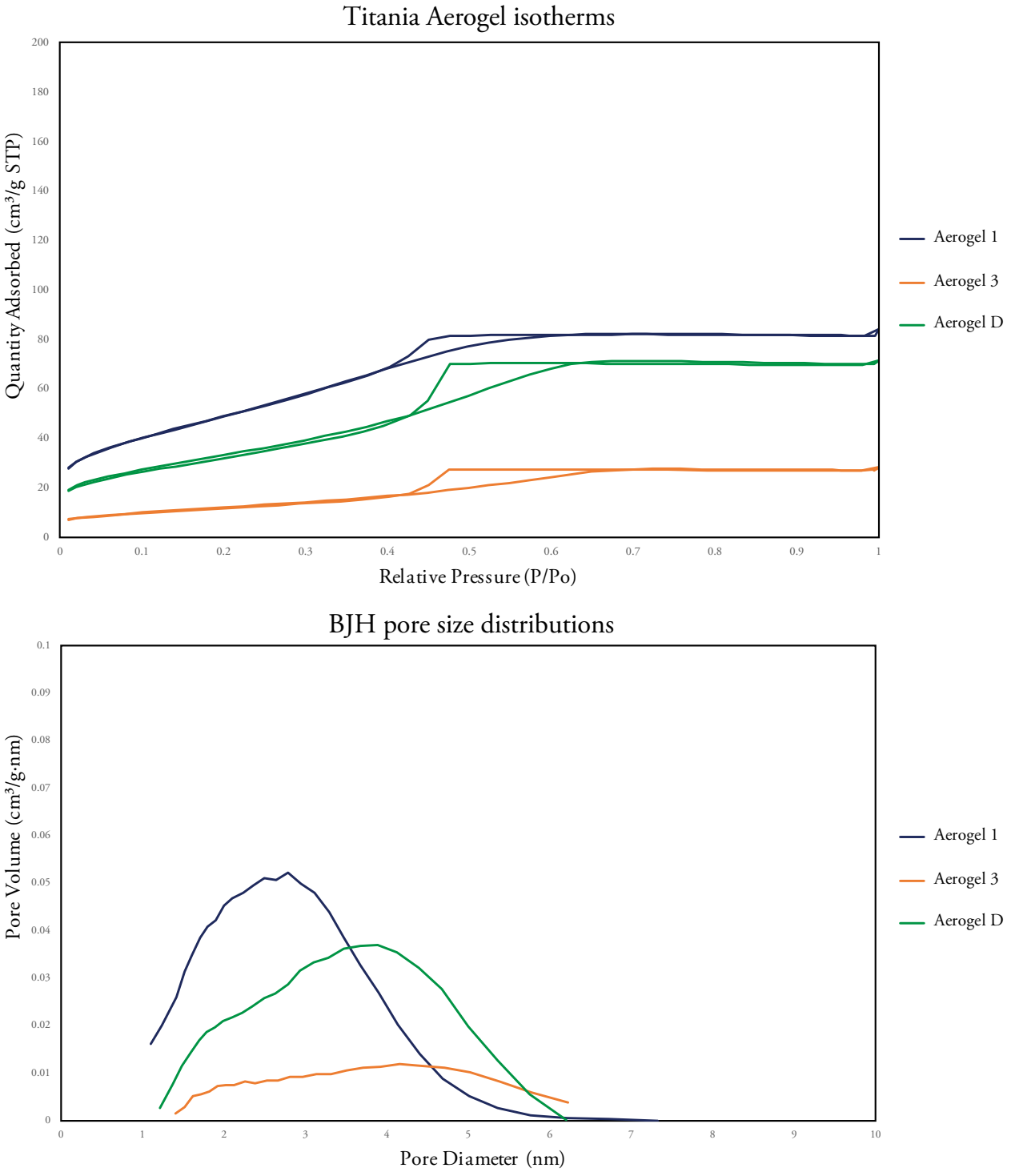

Figure IV: *The nitrogen adsorption-desorption isotherms and BJH pore size distributions of titania aerogel entries 1, 3 and D are depicted in the figures above.*

E Gold Ion-adsorption

Gold weight percentage calculation

The wt% of 2.00 was calculated as follows:

A stock solution contained 0.865 g $HAuCl_4 \cdot 3H_2O$

0.865 g / 393.826 mol/g = 0.002196 mol $HAuCl_4 \cdot 3H_2O$
So, 0.002196 mol gold is present in the solution.

Approximately 90% of the gold is obtained as $Au(en)_2Cl_3$ after the procedure:

0.002196 * 0.90 = 0.001977 mol $Au(en)_2Cl_3$
This was diluted in a 100 mL flask, so 0.001977 / 0.1 = 0.020 M $Au(en)_2Cl_3$

The weight percentage is calculated with the formula:

$$\frac{\text{Au (g)}}{\text{Au (g)} + \text{TiO}_2\text{ (g)}}$$

On the 600 mg amorphous titania support 3.15 mL of the stock-solution was added.
0.00315 * 0.020 M = 0.062 mmol $Au(en)_2Cl_3$
0.062 mmol * 196.97 g/mol = 12.3 mg $Au(en)_2Cl_3$

When 12.3 mg gold is filled in the formula, a weight percentage of 2.0 is calculated. However, TiO_2 (g) was experimentally (TiO_2 (g) + H_2O (l)), since some water was still present in the material. Thus, when the titania supports were dried, the mass of the titania decreased and simultaneously the gold weight percentage was increased.